August 2015

Engineering Novel Detection and Treatment Strategies for Bacterial Therapy of Cancer

Jan T. Panteli
University of Massachusetts - Amherst

ENGINEERING NOVEL DETECTION AND TREATMENT STRATEGIES FOR BACTERIAL THERAPY OF CANCER

A Dissertation Presented

by

JAN T. PANTELI

Submitted to the Graduate School of the

University of Massachusetts Amherst in partial fulfillment

of the requirements for the degree of

DOCTOR OF PHILOSOPHY

May 2015

Department of Chemical Engineering

ENGINEERING NOVEL DETECTION AND TREATMENT STRATEGIES FOR BACTERIAL THERAPY OF CANCER

A Dissertation Presented

by

JAN T. PANTELI

Approved as to style and content by:

_____
Neil. S. Forbes, Chair

_____
Shelly Peyton, Member

_____
Joseph Jerry, Member

_____

John Collura - Interim Department Head
Department of Chemical Engineering

DEDICATION

To my grandfathers who are not here to share in my accomplishments.

ACKNOWLEDGMENTS

I would like to thank my advisor, Neil Forbes, for giving me the opportunity to work on this project, and providing guidance and support throughout my research. I could not have accomplished much without his mentorship and guidance. I would also like to thank members of my dissertation committee, Shelly Peyton and Joe Jerry, for their timely advice about focusing my work towards well-defined goals. I would like to thank my academic family who taught me and provided an enjoyable work environment: Bhushan Toley, Adam St. Jean, Miaomin Zhang, Charles Swofford, Yumei Dai, and especially Nele Van Dessel without whom the mouse studies would not have been possible. I would also like to thank the chemical engineering community at the University of Massachusetts Amherst who created an amazing environment to do great research.

I want to thank all the animal facility staff and professors who taught and guided me in performing mouse experiments: at BACF/PVLSI: Alexandre Dufresne, for the numerous lesson in tail-vein injections and cardiac punctures which do not always go according to plan, Sally Schneider for her lab's assistance in cutting my tissues, the animal care staff at UMass: Dr. Paul Spurlock, Allison Bardwell, and Christie Hart, for getting me set up here at UMass and last minute training.

I gratefully acknowledge financial support from the National Institutes of Health (Grant No. R01CA120825), the National Science Foundation, (Grant No. 1159689), and the Friends for Earlier Breast Cancer Test (Grant No. 1140866) who provided funding for this work.

I am eternally grateful to my friends and family who, through their love and support made this all possible. I want to thank all the friends who put me up for the night, or week, as the situation required, to completed experiments. I want to thank my girlfriend, Bobby, who has supported me emotionally and financially while I completed my writing and for guiding me while I struggled through the process. I want to thank my parents who have always put my needs before their own; their love and encouragement has shaped me into who I am today.

ABSTRACT

ENGINEERING NOVEL DETECTION AND TREATMENT STRATEGIES FOR BACTERIAL THERAPY OF CANCER

MAY 2015

JAN T. PANTELI

B.S. CHEMICAL ENGINEERING, STATE UNIVERSITY OF NEWYORK AT BUFFALO

Ph.D. CHEMICAL ENGINEERING, UNIVERSITY OF MASSACHUSETTS AMHERST

Directed by: Professor Neil S. Forbes

Finding and treating cancer is difficult due to limited sensitivity and specificity of current detection and treatment strategies. Many chemotherapeutic drugs are small molecules that are limited by diffusion, making it difficult to reach cancer sites requiring high doses that lead to systemic toxicity and off-target effects. Tomographic detection techniques, like PET, MRI and CT, are good at identifying macroscopic lesions in the body but are limited in their ability to detect microscopic lesions. Biomarker detection strategies are extremely sensitive and able to identify ng/ml concentrations of protein, but are poor at discriminating between healthy and disease state levels due to patient-to-patient variance, often leading to misdiagnosis. Gram negative bacteria, specifically *Salmonella typhimurium* and *Escherichia coli*, are potential

anticancer agents because of their preferential accumulation and growth within tumors. This tumor specificity allows these bacteria to reduce off-target effects and it enables production of recombinant proteins directly at the tumor site. This thesis presents, three strategies for improving cancer therapy and detection using engineered bacteria.

The first part of this thesis discusses a tumor detection strategy that combines the specificity of tumor-targeting bacteria with the sensitivity of biomarker assays. Attenuated bacteria were engineered to release an exogenous reporter protein, ZsGreen, using a remotely inducible genetic switch. *In vitro* administration of these bacteria to a tumor-on-a-chip microfluidic device showed ZsGreen was able to diffuse through malignant tissue and release from a 0.12 mg spheroids at a rate of 23.9 μg/h. *In vivo* administration of tumor-detecting bacteria to subcutaneous murine tumor models identified tumors larger than 0.2 g through systemic measurement of released ZsGreen. Tumor-detecting bacteria could provide a sensitive, minimally invasive method to detect tumor recurrence, monitor treatment efficacy, and identify the onset of metastatic disease.

The second part of this thesis discusses how bacteria can be engineered to sense sugar concentration the tumor microenvironment and how this might be useful to hone bacterial therapies to viable cancer tissue. A plasmid system was created that utilized a fusion protein between two transmembrane receptors, Trg, a chemotaxis receptor for Ribose and Glucose, and EnvZ, an osmolarity sensor, which enabled visualization of sugar gradients *in vitro* through expression of green fluorescent protein. Sugar sensing bacteria were administered to tumor spheroids in a microfluidic device that mimics tumor tissue adjacent to a blood vessel, and identified gradients in glucose as a function of distance from vasculature. Drop in sugar concentration with tissue depth was shown to correlate with the extent of apoptosis in the tumor

environment. These sugar-sensing bacteria could benefit treatment by producing more protein drug in areas of higher nutrient availability, increasing dose where tumors are likely to be more active. In addition, these bacteria can serve as a platform for future work on enabling bacteria to sense other metabolites through modification of the receptors' binding proteins to recognize other cancer specific compounds.

The last part of this thesis, discusses a project to discover new proteins for anti-cancer bacterial therapy that can overcome the limitations of traditional therapeutic strategies. Extremely toxic proteins could be potential drug candidates as dosing would be restricted to tumors owing to the targeting capabilities of the bacteria. Several protein toxins were cloned into bacteria and tested for protein secretion and efficacy on monolayer. Two toxins were identified as possible therapeutics, *Staphylococcus aureus* α hemolysin (SAH) and *Pseudomonas exotoxin* A (PEA). SAH is a pore former and as such would be able to target all malignant cells not just the proliferating region because it is indiscriminant of cell metabolism or cell cycle. Efficacy of SAH producing bacteria were tested in tumor spheroids in a microfluidic device and in murine tumor models. These studies showed significant tumor cell death and regression. This strategy enables targeting very cytotoxic proteins directly to the tumor site where systemic administration would fail.

TABLE OF CONTENTS

Page

LIST OF TABLES

Page

LIST OF FIGURES

Page

CHAPTER I

INTRODUCTION AND BACKGROUND

1.1 Cancer growth, development, and transport

Cancer is a malignant growth of cells that arises from disruption of normal cell division. This rapid and uncontrolled growth is typically caused by mutation in the cell cycle and other key metabolic pathways. As we develop from an embryo, our cells divide and differentiate into the tissues and organs that make up the human body. In normal development and growth there are precise mechanisms that allow individual cells to replicate and differentiate into organ-specific cells. These mechanisms are controlled by growth factors, stimulatory or inhibitory molecules, which are produced by the cells to control the balance of growth and development. When a cell receives signals that stimulate the growth process, cell division is initiated and two daughter cells are formed (Alberts et al., 2002a). Just as growth is controlled, so is cell death. Apoptosis, or programmed cell death, occurs as a result of stimuli such as heat, nutrient depravation, infection, and hypoxia causing apoptotic signals to be released intracellularly leading to activation of the apoptotic pathways and eventual cell death. The balance of growth, differentiation, and cell death are all rigorously controlled in the human body to provide necessary functions such as the generation of new blood cells, regrowth of damaged tissue after an injury, and synthesis of lymphocytes to fight off infection (Alberts et al., 2002b).

Cancer arises when significant DNA damage occurs that disrupts this balance of normal cell division, differentiation, and death. Tumor growth differs from normal growth in that many malignant cells do not respond to the growth inhibitors and stimulators that control the cell cycle or apoptotic pathways, resulting in rapidly uncontrolled cell division. Cancer cells have been

shown to stimulate their own growth, resist inhibitory signals that would normally stop growth, evade apoptosis, replicate indefinitely, and promote the growth of new blood vessels (Hanahan and Weinberg, 2000; Hanahan and Weinberg, 2011). As malignant cells replicate uncontrollably, they begin to cause damage by increasing local pressure and exhausting local nutrient supply. This stimulates production of angiogenic factors that stimulate the development of new blood vessels, in a process called neoangiogenesis. Several oncogenes including ras, raf, myc, EFR, and HER-2 are known to directly trigger these proangiogenic properties in cancer cells (Rak et al., 2000). These new vessels are chaotic and not well formed leading to regions of cells at large distances from vessels (Minchinton and Tannock, 2006). Chaotic vasculature arises from an imbalance in the rate at which neoplastic cells divide and the rate at which angiogenesis occurs (Folkman et al., 1989). In addition, the tumor interstitium that forms is collagen rich and characterized by large interstitial distances which inhibit macromolecule diffusion and convection (Chary and Jain, 1989; Jain, 1999). As a result, nutrients supplied through these vessels are unable to reach the distant regions from vessels leading to hypoxia, hypoglycemia, and acid environments which facilitate metastasis formation (Gillies et al., 1999). Metastasis occurs when a primary tumor cell breaks off from the primary cell mass and relocates, through the lymphatic or circulatory system to another location in the body. For a tumor cell to disseminate it must undergo invasion of surrounding tissue, intravasation into the blood vessel, survive in circulation, extravasation from the blood stream and then proliferate at the secondary foreign tumor site (Egesten et al., 2011). It has been shown that renormalization of blood vessels in tumors has been shown to promote tissue oxygenation and decrease metastasis formation in mice (Agrawal et al., 2014).

1.2 Cancer detection and treatment

Current strategies to find and treat cancer have allowed physicians to fight this debilitating disease and reduce patient mortality. Cancer is diagnosed using several different methods, typically a lump is identified via palpation or imaging and then a biopsy is taken to identify whether the cell mass is malignant. Several imaging techniques exist today that enable identification of malignant cell masses down to a few millimeters in diameter (Ernst and Roukema, 2002; Rakheja et al., 2013; Schöder and Gönen, 2007). These imaging techniques identify cancer based on tumor size, morphology, and metabolism. Positron emission tomography (PET) utilizes uptake of a fluorinated glucose molecule (FDG), to identify highly metabolically active cells in the body. Many cancer cells upregulate glycolysis to fuel rapid cell division (Altenberg and Greulich, 2004; Gillies et al., 2008). When FDG is injected, cancer cells typically uptake more of the radioactive glucose than surrounding normal tissue identifying the region of malignant cells (Bos et al., 2002; Fogelman et al., 2005; Veronesi et al., 2007; Yasuda et al., 1999). Magnetic resonance imaging (MRI) uses radio waves to identify diseased tissue from healthy tissue (Behjatnia et al., 2010; Belião et al., 2012; Brismar et al., 2012). MRI enables identification of cancer tissue with contrasting agent by highlighting areas of increased angiogenesis and high vascular permeability associated with these vessels (Barrett et al., 2006; Schima, 2005). Computed tomography (CT) uses x-rays to map the three dimensional structures of the body identifying tumors by edema, the swelling and distortion they cause to their neighboring tissues (Hasegawa et al., 2000; Vansteenkiste et al., 2012). Combined PET/CT enables improved imaging and identifies smaller malignant cell masses (Goldsmith, 2004; Griffeth, 2005; Lim et al., 2007; Schöder and Gönen, 2007).

Several diagnostic assays are also used to identify cancer from blood and urine samples. Circulating tumor cells (ctc) and cell free DNA (cfDNA) are identified from blood samples and sequenced to identify mutations in the DNA that may indicate oncogene mutations (Kulemann et al., 2015; Mok et al., 2015; Xu et al., 2015). Several cancers over express specific proteins, biomarkers, that are used to identify and diagnose their disease: prostate specific antigen (prostate cancer), AFP (liver cancer), BRCA1+2, (breast and ovarian cancer), CA-125 (ovarian cancer), HER-2 (breast cancer), EGFR (non-small-cell lung carcinoma)(Chatterjee and Zetter, 2005; Lutz et al., 2008; Mizejewski, 2002; Mok et al., 2015; Rak et al., 2000; Thompson et al., 2005; Zhang et al., 2012). These biomarkers are detected in tissue biopsies, serum or the urine at the ng/ml to pg/ml and lower concentrations (Rusling et al., 2010) and depending on their baseline levels, indicate the presence of cancer (Chatterjee and Zetter, 2005; Franci et al., 2013; Ludwig and Weinstein, 2005; Xue et al., 2010).

1.3 Limitations in cancer detection

Finding small malignant lesions is necessary to treat the primary causes of cancer mortality. Secondary metastatic tumors, for example, are often not discovered until pathological symptoms have manifested and the lesions are large (Nguyen and Massagué, 2007). Imaging techniques such as positron emission tomography (PET), magnetic resonance imaging (MRI), and computed tomography (CT) are good at identifying macroscopic tumors but are limited in their ability to detect microscopic lesions (Behjatnia et al., 2010; Griffeth, 2005). These techniques lack the spatial resolution needed to detect tumors and metastases less than 6-8 millimeters in diameter (Behjatnia et al., 2010; Belião et al., 2012; Brismar et al., 2012; Cook et al., 1998; Czernin and Phelps, 2002; Fukumura and Jain, 2008; Schöder and Gönen, 2007; Takalkar et al., 2008). Endogenous biomarkers can be used in conjunction with imaging techniques to identify

cancer, but they are sub-type specific and highly variable (Chatterjee and Zetter, 2005; Thompson et al., 2005). Healthy biomarker concentration levels often vary from patient-to-patient making it difficult to establish a baseline for disease diagnosis (Brooks, 2012; Ludwig and Weinstein, 2005). Detecting small cancer masses could improve patient survival by identifying recurrence earlier and enabling more effective treatment. Small tumors have less chance of spreading making them easier to treat, whereas large tumors have an increased chance for metastatic disease making treatment more difficult (Koscielny et al., 1984). Identifying smaller malignant masses earlier will reduce patient mortality.

1.4 Tumor heterogeneity limits cancer treatment

Once diagnosed, cancer treatment encounters its own limitations with systemic toxicity, barriers in transport, drug specificity and selectivity, and tumor drug resistance. Blood-born therapeutics must first make their way through chaotic tumor vasculature to the site of the malignant cells (Carmeliet and Jain, 2000; Jain, 1999). For small molecule therapeutics, the high interstitial fluid pressure, poor blood flow, and slow diffusive transport of tumor interstitium, creates a transport barrier for diffusion deep within tumors. For radiation therapy, hypoxia limits efficacy because it is dependent upon oxygen radical formation (Milosevic et al., 2012). Gradients in nutrients and oxygen also cause a change in cancer cell metabolism creating three observed cell growth regions: proliferative regions closest to vessels, quiescent regions farther from vasculature at the nutrient diffusion limit, and necrotic regions farthest from vessels where nutrients have been exhausted (Sutherland and Durand, 1984). Treating all cell regimes in tumors can be difficult because cell behavior changes dependent upon nutrient availability. Many chemotherapeutic drugs target cell cycle replication effectively treating the proliferating region of malignant cells but are unable to eradicate quiescent cells. In addition, drugs targeting cell

division cause systemic toxicity, seen with hair and nail loss. Cancers can also develop drug resistance by mutation; increasing drug efflux, activating DNA repair mechanisms, and evading drug-induced apoptosis (Gillet and Gottesman, 2010). For example, acquired drug resistance limits one of the most widely used cancer drugs on the market, Taxol. Taxol is an antimitotic agent that works by stabilizing microtubules and inhibiting tubulin polymer assembly (Horwitz, 1994). Cancer drug resistance to Taxol has been attributed to over expression of multidrug transporters, altered metabolism of the drug, reduced sensitivity to cell death-inducing stimuli, and altered microtubule dynamics and binding to Taxol(Orr et al., 2003). Development of a targeted therapy that is able to reach all regions of the tumor and that utilizes a mechanism-of-action that is indiscriminate of cancer cell metabolism and can avoid drug resistance pathways, would improve upon many of the current small molecule therapeutics used in the clinic today.

1.5 Anti-cancer bacterial vectors

Bacterial infections have been shown to localize and thrive in the tumor microenvironment. In the late 1800s, Dr. William Coley discovered that after operating multiple times to remove a tumor only to have it regrow; after the patient suffered an infection of *Streptococcus pyogenes* during the final surgery, the tumor regressed completely (Hoption Cann et al., 2003). Since then, several pathogenic strains of bacteria have been identified to localize in tumors after infection. Obligate anaerobes like *Clostridium* localize in the necrotic core of tumors where facultative anaerobes such as, *Vibrio cholera*, *Listeria monocytogenes*, *Escherichia Coli, and Salmonella* localize throughout (Bolhassani and Zahedifard, 2012; Cronin et al., 2012; Dang et al., 2001; Forbes, 2010; Nemunaitis et al., 2003; Pawelek et al., 2003; Swofford et al., 2014). In a study to identify bacterial infections in tumors, surgically removed lung cancer samples were screened for bacterial and fungal infection and several strains of bacteria were identified:

Staphylococcus epidermidis, Streptococcus mitis, Bacillus, Chlamydia, Cadida, Listeria, and Haemophilus influenza, Legionella pneumonia and *Candida tropicalis* (Apostolou et al., 2011).

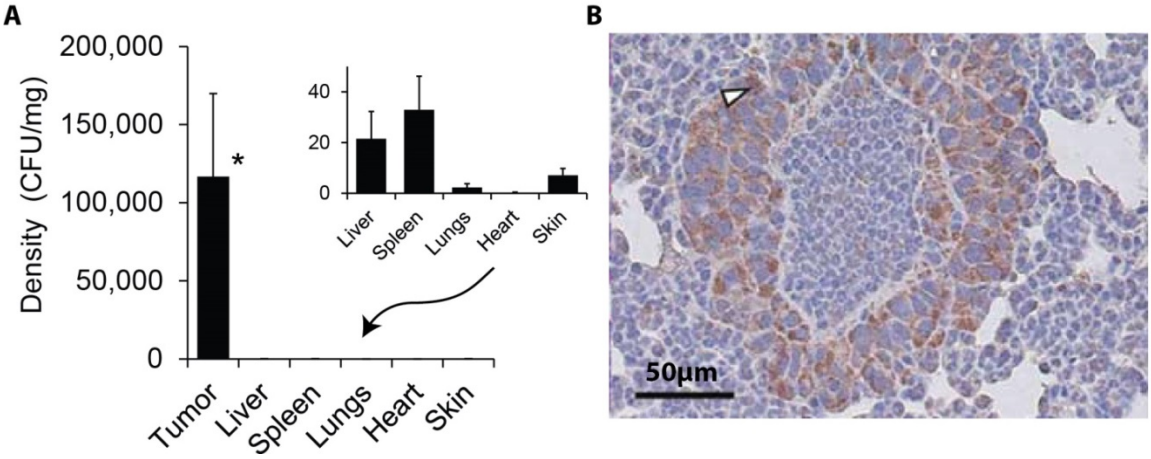

Figure **1**. Salmonella preferentially accumulate in tumors
A) Biodistribution in the organs of tumor-bearing mice, one week after systemic tail-vein injection of 2 million CFU/mouse (strain VNP20009). Significantly (*, $P<0.05$) more bacteria accumulated in tumors than the liver and spleen, the major clearance organs (adapted from, Forbes et al., 2003). **B)** Salmonella colonies (arrows, brown) in 4T1 pulmonary micro-metastases in a BALB/c mouse; identified using an anti-Salmonella polyclonal antibody. Scale bars is 50 µm (Ganai et al., 2011).

Salmonella and specifically are very favorable candidates for anti-cancer vectors due to their high tumor penetration and ease of genetic manipulation. Both *Salmonella* and *E. coli* selectively accumulate and replicate in tumors (Kasinskas and Forbes, 2006). The specific affinity of *Salmonella* to tumors over normal tissue has been demonstrated in many studies (Clairmont et al., 2000; Low et al., 1999; Pawelek et al., 1997; Platt et al., 2000; Zheng et al., 2000). After systemic administration with *S. typhimurium*, the bacterial density in tumors is typically 2,000 times more than other organs (Figure 1A), and once colonized, bacteria are seen to spread throughout tumor tissue (Forbes et al., 2003). *Salmonella* have also been shown to accumulate in hepatic and pulmonary metastases as small as five cell layers thick (Figure 1B; Ganai et al.,

2011). Due to the ease of genetic manipulation, *Salmonella* can also express numerous reporter peptides. These bacteria can also release non-native proteins in the human body, increasing the reporter sensitivity because there would be no biomarker background. A non-pathogenic, attenuated *Salmonella* strain (VNP20009) has been created for clinical purposes. The strain has a partial deletion of the *msbB* gene which diminishes the TNF immune response to bacterial lipopolysaccharides and prevents septic shock. It also has a partial deletion of the *purI* gene. This deletion makes the bacteria dependent on external sources of purines and speeds clearance from non-cancerous tissues (Low et al., 1999). In mice, the virulence (LD_{50}) of this therapeutic strain is 10,000-fold less than wild-type *Salmonella* (C. Lee, 2000; Clairmont et al., 2000). In pre-clinical trials, attenuated *Salmonella* have been administered systemically into mice and dogs without toxic side effects (Luo et al., 2001; Thamm et al., 2005). In human trials with metastatic melanoma patients, the attenuated *Salmonella* strain was safely administered (Toso et al., 2002).

1.6 Synopsis

In this dissertation, I describe several strategies to genetically engineer *Salmonella* and *E. coli* for cancer detection, sensing, and treatment. Each strategy was tested in a microfluidic model that simulates the transport limitations within the tumor microenvironment of hypoxia, hypoglycemia and poor diffusion into the tumor site and two strategies were further evaluated in murine tumor models. Specifically I describe:

i. Creation of diagnostic bacteria to identify solid tumor masses by release of a recombinant biomarker A) within a microfluidic device and B) in a murine tumor model.

ii. Creation of bacteria to sense ribose and glucose concentrations within the tumor environment to identify regions of tumor cell viability

iii. Evaluation of novel recombinant protein toxins for bacterial therapy A) within a microfluidic device and B) in a murine tumor model.

CHAPTER II

DETECTION OF MURINE TUMORS WITH GENETICALLY MODIFIED BACTERIA

PART A: IN A TUMOR MIMIC MICROFLUIDIC DEVICE

2.1 Introduction

Previously, several strategies have been described using bacteria for tumor detection. *Escherichia coli* expressing ferritin enhance magnetic resonance imaging (MRI) by increasing iron uptake and improving signal to background ratio (Hill et al., 2011). *Escherichia coli* have also been used to enhance positron emission tomography (PET) through innate uptake of FDG (Brader et al., 2008). Combined with the native uptake of malignant tissue, these bacteria amplified FDG uptake producing a higher radiologic signal. *Escherichia coli*, *Salmonella typhimurium, Vibrio cholera,* and *Listeria monocytogenes* have also been used to visualize bacterial colonization of different tumor models via expression of bioluminescent proteins (Cronin et al., 2012; Min et al., 2008a; Min et al., 2008b; Yu et al., 2004). Bioluminescence performs well in small animals but translation to the clinic is difficult because light cannot penetrate through tissue. Bioluminescent signal decreases approximately 10-fold for every 1 cm of tissue depth (Contag et al., 1995). Using bacteria with PET and MRI would still be limited by the resolution of tomographic techniques.

Combining the sensitivity of biomarker detection with the specificity of tumor-targeting bacteria has the potential to detect microscopic tumors smaller than the current resolution of tomography. Figure 2 describes a concept of how bacteria could be used to detect cancerous lesions. Bacteria would be injected systemically and preferentially accumulate in tumors (*step 1*). After growth in tumor tissue (*step 2*) and clearance from the rest of the body, expression of a

biomarker would be triggered by a small inducing molecule (*step 3*). A protein biomarker would be released by the bacteria (*step 4*) and diffuse through tumor interstitium into the blood stream (*step 5*) where it could be detected (*step 6*). The presence of biomarker molecules in the blood would indicate bacterial colonization of malignant tissue. For this conceptual strategy to be possible, bacteria must produce the biomarker at sufficient rates. This production is dependent on the rate of protein expression, the efficiency of secretion, the bacterial density, and the limit of detection.

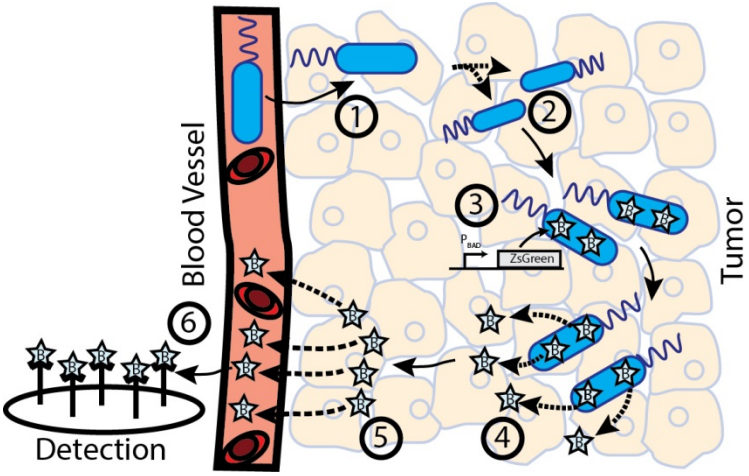

Figure 2. Concept of bacterial tumor detection
This illustration shows how bacterial detection would function *in* vivo. The method combines biomarker detection with bacterial selectivity for tumors. After intravenous delivery, engineered *Salmonella* would preferentially accumulate in tumor tissue (1) and proliferate (2). Expression of a biomarker (stars, here ZsGreen) would be triggered by a small inducing molecule (3). The biomarker would be released from the bacteria (4) and diffuse into the blood stream (5). Biomarker molecules would be measured using specific antibodies (6) and the concentration would indicate the presence and size of tumor masses. These mechanisms were quantified by administering tumor-detecting bacteria to a microfluidic tumor-on-a-chip device that mimics tissue surrounding blood vessels in tumors (Panteli et al., 2015).

To create tumor detecting bacteria, an attenuated strain of *Salmonella* was engineered to express and release the fluorescent protein ZsGreen under control of the L-arabinose inducible promoter. A single-layer antibody method was developed to measure low concentrations of ZsGreen. In liquid culture, half of produced ZsGreen was released by viable bacteria at a rate of

87.6 fg·bacterium^{-1}·h^{-1}. A new technique, Single-layer antibody dot was created to detect ZsGreen by pull down to nitrocellulose membrane. Bacteria colonization and release of ZsGreen was tested in microfluidic device that mimics systemic delivery and the transport limitations found in the tumor microenvironment (Figure 3; Walsh et al., 2009). Mathematical analysis was used to predict the efficacy of tumor detection using a two compartment pharmacokinetic model with first order elimination. Tumor-detecting bacteria could provide a sensitive, minimally invasive method to detect tumor recurrence, monitor treatment efficacy, and identify the onset of metastatic disease.

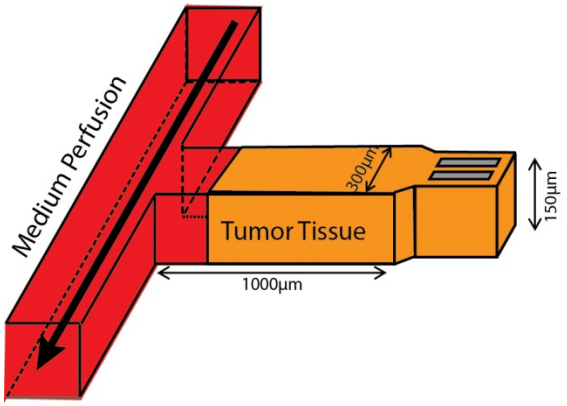

Figure 3. Schematic of a tumor-on-a-chip microfluidic device
The device mimics tumor tissue adjacent to a blood vessel. The device chip consists of six of these individual chambers in series off a single main flow channel. Each chamber for each tissue has an individual packing outlet used to insert tumor spheroids into the chamber. All tumors share the main flow channel to receive the same treatment for replicate tumor spheroids (Walsh et al., 2009).

2.2 Materials and Methods

2.2.1 Plasmids and bacterial strains

Bacteria were grown in LB broth at 37°C and 225 rpm. Two bacterial strains were used: attenuated *Salmonella enterica* serovar Typhimurium, strain VNP20009 ($purI^-$, msb^-, and xly^-), and *Escherichia coli*, strain DH5α, (Invitrogen, Carlsbad, CA). ZsGreen expression was controlled by transformation with plasmid pDF02, which contains the *ZsGreen* gene under control of the L-arabinose inducible promoter, P_{BAD} (Dai et al., 2013). This plasmid contains the puc19 origin of replication and ampicillin resistance. To produce purified ZsGreen, a 6x histidine tag was added to the n-terminus of *ZsGreen* in pDF02, creating plasmid pZsG-His, which was transformed into *E. coli* DH5α. All transformed cultures were supplemented with 100 µg/ml ampicillin. ZsGreen expression was induced with 0.2% w/v (2 mg/ml) L-arabinose.

2.2.2 ZsGreen release

ZsGreen release was determined by measuring the concentration in the extracellular and intracellular fractions of liquid cultures. *Salmonella* were inoculated into LB from single colonies, grown overnight at 37˚C, subcultured, and grown to an optical density (at 600 nm) of 0.4. ZsGreen expression was induced with 0.2% L-arabinose, and fluorescence was measured for 40 hours. Bacterial density was measured turbidimetrically at 600 nm (BioTek Instruments, Winooski, VT) and converted with factor of 5×10^8 $CFU\cdot ml^{-1}\cdot OD_{600}^{-1}$. Extracellular samples were acquired by centrifuging 1 ml of culture and collecting 200 µl of supernatant. Intracellular fractions were acquired by resuspending cell pellets in 1 ml of fresh LB broth to equalize volumes with supernatant samples. Fluorescence of 200 µl samples was measured in a microtiter plate

reader with 460 nm excitation and 505 nm emission filters (Molecular Devices, Sunnyvale, CA). Background fluorescence of LB broth was subtracted from all measurements.

Fluorescence measurements were converted to concentration units by determining the fluorescence of pure ZsGreen. Cultures of *E. coli* containing pZsG-His were induced with 0.2% w/v L-arabinose and grown overnight. Bacteria were lysed with lysozyme and vortexed on ice with glass beads for 20 minutes. ZsGreen was purified from the lysate by immobilized-metal-ion (nickel) affinity chromatography. The ZsGreen concentration in the eluent was determined by colorimetric Bradford assay. Fluorescence of the eluent was determined by spectrometry as above. Serial dilutions were used to determine a conversion factor between fluorescence units and concentration. The average rate of ZsGreen release was determined by linear fitting to the measurements from 0 to 40 hrs.

2.2.3 ZsGreen detection in blood

ZsGreen was diluted in bovine blood to determine the detectable limit of the fluorescence signal. Cultures of *Salmonella* with pDF02 were induced at 0.4 OD_{600} with 0.2% L-arabinose, and grown for 24 hours. Supernatant fractions from these cultures were sterile filtered through a 0.22 µm filter and serially diluted in bovine blood or plasma (Hemostat Laboratories, Dixon, CA) in ten-fold increments. Plasma was isolated from whole blood by centrifugation for 10 min. Fluorescence was measured in a plate reader with 460 nm excitation and 505 nm emission filters. Intensities were normalized to the auto-fluorescence of blood and plasma, respectively.

2.2.4 Viability of ZsGreen-releasing bacteria

Bacterial viability was measured to determine the relationship between ZsGreen release and cell integrity. *Salmonella* and *E. coli* were induced with 0.2% L-arabinose at an optical density OD_{600} of 0.4 and grown for 24 hours, as described above. Cultures were centrifuged. The fluorescence of the supernatant and cell pellet, at equalized volumes, was determined and normalized by the density.

To determine the ratio of ZsGreen released by live and dead bacteria, ZsGreen-expressing bacteria were grown for 24 hours in LB and induced with 0.2% L-arabinose. At 24 hours, 1 ml of culture was centrifuged and resuspended in an equal volume of PBS. Suspension in PBS halted growth, because PBS contains only salts and no carbon source. Preventing growth enabled determination of release from one generation of bacteria. Resuspended bacteria were stained by adding an equal volume of a PBS solution containing 20 µM ethidium homodimer-1 (ThermoFisher, Waltham, MA) and 25 µM 4',6-diamidino-2-phenylindole (DAPI). Ethidium homodimer-1 stains dead cells and DAPI stains cell nuclei and identifies all bacteria. Ten µl of the stained cell suspension was applied to glass slides and covered with a coverslip to prevent evaporation. For 11 hours, fluorescence from the bacteria on the slide was observed by microscopy (Olympus, Center Valley, PA) at 10X magnification. Three fluorescence filter sets (Chroma, Rockingham, VT) were used: DAPI (EX, 358 nm; EM, 461nm), ZsGreen (EX, 496 nm; EM, 506 nm), and ethidium homodimer-1 (EX, 528 nm; EM, 617 nm). Acquired images were overlaid to determine the location of individual bacteria from the DAPI stain. Red and green fluorescence intensities were determined for each bacterium. Background fluorescence was subtracted from these intensities. The viability threshold was determined by starving bacteria of all nutrients for 48 hours and staining with ethidium homodimer-1. ZsGreen fluorescence

intensity was normalized by the brightest bacterium in all images. The fraction released from viable and dead bacteria was determined by comparing the integral of green fluorescence (ZsGreen content) over the 11 hours of observation.

2.2.5 Single-layer antibody dots

An antibody-based method was developed to improve detection of ZsGreen. Small circles of nitrocellulose membrane were cut using a 1.5 mm diameter biopsy punch. Antibody dots were prepared by coating with a pan-polyclonal antibody against α-reef coral fluorescent proteins (RCFP; Clontech, Madison, WI) that was diluted 1:10 in PBS, and stirring overnight at 4˚C. To test sensitivity, supernatant was isolated from a 24-hour culture of ZsGreen-producing *Salmonella*. The supernatant was serially diluted in PBS at ratios of 1:1; 1:10; 1:100; 1:1,000; 1:10,000; $1:10^5$, $1:10^6$, $1:10^7$; $1:10^8$ and $1:10^9$. These solutions (200 µl) were added to antibody dots in 96 well plates, which were incubated and rocked overnight at 4°C. The fluorescence of the antibody dots was acquired by microscopy (Olympus) and the fluorescence of diluted solutions was measured using a spectroscopic plate reader (Molecular Devices). The fluorescence intensity of each dot was quantified by averaging the intensity over the entire area. Images were acquired at three exposure times, 100, 400, and 1000 ms, to accommodate the range of the CCD camera (Hamamatsu, Shizuoka, Japan). The background fluorescence of antibody dots treated with PBS was subtracted from all measured intensities. The detection limit was defined as the intensity at which fluorescence measurements did not change with decreasing concentration. All antibody-dot fluorescence measurements values were normalized by this value. Spectroscopy measurements were background subtracted and similarly normalized.

2.2.6 Plasmid stability of pDF02

Two groups of liquid LB cultures were inoculated with *Salmonella* transformed with pDF02. Both groups were grown at 37°C and 225 rpm in media supplemented with received 2 mg/ml L-arabinose and 100 µg/ml ampicillin for 12 hours. After this period, two groups of cultures were inoculated with 5,000 bacteria. The antibiotic-free group (No Amp, n=4) was resuspended in media with only L-arabinose, and the control group (Amp, n=4) received both L-arabinose and ampicillin. Resuspension was repeated approximately every 12 hours. Fluorescence and bacterial density (at 600 nm) were measured periodically throughout. Background fluorescence was subtracted from all measurements. Expression ratios were determined by normalizing fluorescence intensities by culture density and the maximum measured intensity.

2.2.7 ZsGreen release from bacteria colonized in tumor masses *in vitro*

A microfluidic tumor-on-a-chip device was used to determine the release rate of ZsGreen release from bacteria colonized in solid tumor masses. Devices were fabricated using soft lithography techniques described previously.(Toley and Forbes, 2012; Walsh et al., 2009) The device pattern consisted of a flow channel bordering six chambers with filters at the rear end to trap injected spheroids (Figure 3,8A). Molds of the microfluidic pattern were formed on silicon wafers coated with SU-8 polymer by photolithography. A 1:10 mixture of Sylgard 184 polydimethylsiloxane (PDMS; Dow Corning, Midland MI), was cast onto the molds, vacuum pumped to remove bubbles, and heated overnight at 55˚C. Holes were punched for the inlets and outlet channels using a 1.5 mm diameter biopsy punch. PDMS reliefs were cleaned with ethanol and treated with oxygen plasma to adhere to glass slides. Prior to inserting cells, devices were sterilized and degassed by flushing with 70% ethanol and PBS.

LS174T human colon adenocarcinoma cells were grown in Dulbecco's modified Eagles medium (DMEM) with 10 % fetal bovine serum (FBS), and incubated at 37 °C and 5% CO_2. To form spheroids, cells were suspended in flasks coated with poly(2-hydroxyethyl methacrylate), and fed every two days for three weeks. Spheroids were inserted into device chambers through flow channels, and were incubated at 37°C in an enclosed environment on the microscope stage. The medium flow rate through the device was 3.0 µl/min and pH was maintained with 25 mM HEPES.

ZsGreen-expressing *Salmonella* at were administered to the microfluidic devices for one hour at a density of $2x10^6$ CFU/ml in DMEM with 10% FBS, 25 mM HEPES and 100 µg/ml ampicillin. Bacteria were administered to devices with empty chambers to serve as tumor-free negative controls. Chambers filled with normal cells would not have been suitable controls because they would have accumulated bacteria. Three-dimensional tissue grown from normal cells contains necrotic tissue, which would promote colonization, and has no immune system to clear bacteria. An empty chamber, where there is no environment for growth, was more representative of bacterial accumulation in normal tissue *in vivo*. After bacterial addition, devices were supplied with bacteria-free medium for eight hours to mimic systemic clearance. After this clearance period, medium containing 0.2% L-arabinose was administered to induce ZsGreen expression. Effluent from the devices was collected every four hours, immediately placed on ice, and sterile filtered to remove bacteria.

Images of tumor cell masses were acquired throughout by fluorescence microscopy (Olympus). To capture an entire chamber, two images were stitched together using a macro in IPLab (*BD Bioscience*, Rockville, MD). Transmitted light and fluorescence images were captured at1 hour intervals and analyzed with ImageJ (NIH Research Services Branch). Fluorescence

intensities were calibrated by flowing a 279.5 µg/ml solution of ZsGreen in PBS through the device. For each chamber, the total tissue area and the area with a ZsGreen concentration greater than 100 µg/ml was determined from transmitted and fluorescence images, respectively. The ZsGreen concentration in the effluent medium was determined by incubating 200 µl with antibody dots in 96-well plates overnight as described above. The fluorescence intensity of each dot was measured at an exposure of 400 ms and the background fluorescence of dots treated with fresh medium was subtracted.

The ZsGreen production rate was determined from a mass balance around the device. $FC_Z = K_p C_B V_T$

(1)

Where, F is the flow rate in the channel, C_Z is the concentration of ZsGreen, K_P is the per-bacterium production rate, C_B is the bacterial density, and the V_T is the volume of the cell mass. The per-tissue ZsGreen production rate is given by $K_P \cdot C_B$. Bacterial density in the device was estimated from previously measured profiles of bacterial growth (Toley and Forbes, 2012). A Gompertz expression (Zwietering et al., 1990) was used to model bacterial growth in devices based on previous measurements (Toley and Forbes, 2012).

$$C_B = C_{B,max} exp\left[-exp\left(\frac{\mu_m exp(1)}{C_{B,max}}(\lambda - t) + 1\right)\right] \quad (2)$$

Two Gompertz parameters were calculated by least squares regression analysis: the maximum growth rate, μ_m (CFU·ml^{-1}·h^{-1}); and the lag time, λ (h). Maximum bacterial density, $C_{B,max}$ (CFU·ml^{-1}) was determined by simultaneously solving equations (1) and (2) for $C_{B,max}$ and production rate, $K_{P,}$ using least squares regression to the experimental ZsGreen production data.

2.2.8 Mathematical prediction of minimum detectable tumor volume

A two-compartment pharmacokinetic model was used to predict the detection limits *in vivo*. In this model, ZsGreen accumulation is equal to the amount produced in tumor tissue minus the amount cleared from the plasma.

$$V_p \frac{dC_Z}{dt} = K_P C_B V_T - K_e V_p C_Z \quad (3)$$

The concentration of ZsGreen, C_Z (μg·ml^{-1}), depends upon the bacterial production rate, K_P (μg·CFU^{-1}·h^{-1}); the bacterial density, C_B (CFU·ml^{-1}); the tumor volume, V_T (ml); the elimination rate, K_e (h^{-1}); and the plasma volume, V_p (ml). This ordinary differential equation was solved using a 4th order Runge-Kutta approximation. The rate of ZsGreen production, K_P, was determined from the microfluidic experiments and bacterial density, C_B, was determined from previous measurements in the microfluidic device (Toley and Forbes, 2012). The minimum detectable tumor volume was determined by calculating the volume that would produce the minimum detectable ZsGreen concentration with the antibody dot technique. The effects of clearance and measurement time on detection were determined by calculating the tumor volume that would produce the minimum detectable ZsGreen concentration over a 72 hour period for four half-lives. Clearance rate is inversely proportional to half-life: $K_e = \ln(2)/t_{1/2}$. The effect of increasing bacterial density or ZsGreen production was determined by increasing the production term, $K_P \cdot C_B$, in Eq. 3 and determining the minimum detectable volume as a function of time.

2.3 Results

2.3.1 *Salmonella* secreted ZsGreen in liquid culture

In liquid culture, *Salmonella* released ZsGreen, which was detectable when suspended in blood (Figure 4). A plasmid that expressed ZsGreen, pDF02, was transformed into *Salmonella* and grown in liquid culture. ZsGreen expression increased for 24 hours after induction with L-arabinose (Figure 4A). Over the first 10 hours, a majority of the ZsGreen, 83%, was found in the intracellular fraction of the culture. Between 10 and 41 hours, ZsGreen levels increased in the extracellular fraction ($P<0.05$), while intracellular ZsGreen decreased ($P<0.05$). These changes in concentration indicate that ZsGreen was released from the bacteria. At 41 hours, over half of the protein was released, which was greater than the intracellular ZsGreen concentration ($P<0.05$). The release rate of ZsGreen was 87.6 $fg \cdot bacterium^{-1} \cdot h^{-1}$.

To determine the threshold for fluorescence detection in blood, ZsGreen from liquid culture was diluted in whole blood and plasma (Figure 4B). Extracellular ZsGreen, at a concentration of 528 µg/ml, was diluted at ratios of 1:1, 1:10, 1:100 and 1:1000. In whole blood, ZsGreen fluorescence was detected down to a 1:10 fold dilution (52.8 µg/ml), 3.2 times brighter than the background fluorescence of the blood ($P<0.05$). Erythrocytes and leukocytes have unique optical properties which can interfere with fluorescence molecule detection in blood (Friebel et al., 1999). Removal of these red and white blood cells by centrifugation increased detection sensitivity of extracellular ZsGreen. Identical concentrations of recombinant ZsGreen in plasma enabled detection down to a ratio of 1:1000 (0.528 µg/ml). At this dilution (100-fold less), fluorescence from ZsGreen was 1.8 times brighter than the background fluorescence of the plasma ($P<0.05$, Figure 4B).

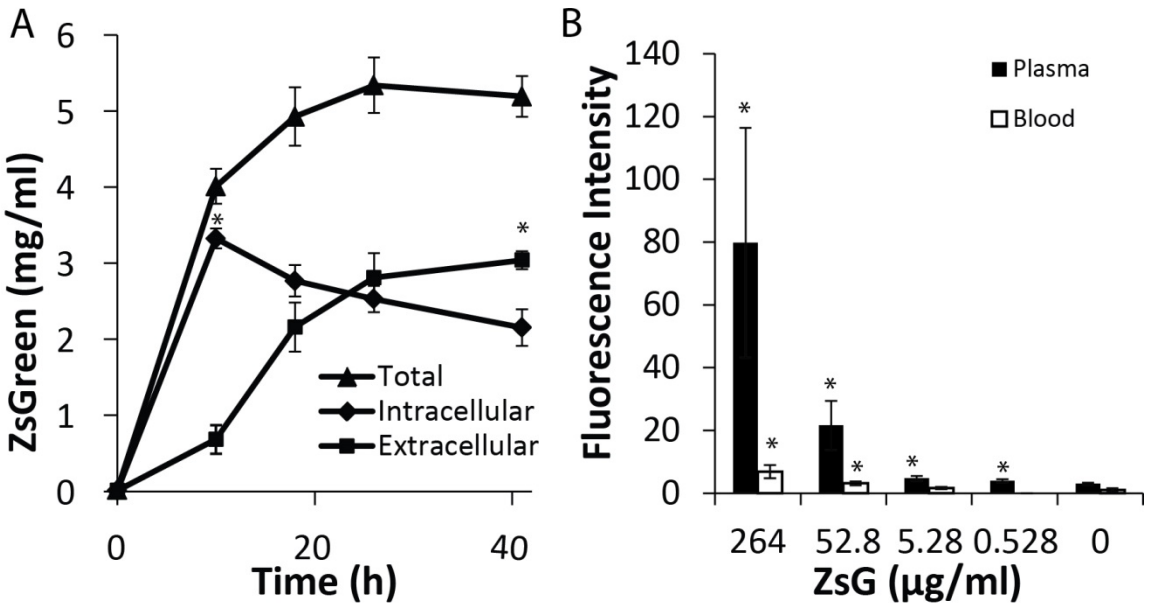

Figure 4. ZsGreen was released by *Salmonella* and was detectable when suspended in blood
A) After induction (time 0), transformed *Salmonella* produced ZsGreen. At 10 h, the intracellular concentration was greater than the extracellular concentration (*, P<0.05; *n*=3). At 40 h, the extracellular concentration was greater (*, P<0.05). The total concentration is the sum of the intracellular and extracellular concentrations. **B)** ZsGreen was isolated from liquid culture supernatant and serially diluted in bovine blood and plasma. The fluorescence intensity was greater than background fluorescence at concentrations of 0.528 µg/ml in plasma and 52.8 µg/ml in whole blood (*, P<0.05). Intensity values were normalized by the autofluorescence of whole blood (Panteli et al., 2015).

2.3.2 ZsGreen release from viable *Salmonella*

Recombinant ZsGreen was released from living *Salmonella,* but was not released from *E. coli* (Figure 5). ZsGreen fluorescence intensity was measured in the intracellular and extracellular fractions of *Salmonella* and *E. coli* liquid cultures at 26 hours (Figure 5A). Bacteria density was described in colony forming units (CFU). *Salmonella* utilize type I, type III, type VI, sec and twin-arginine (Tat) secretion systems for protein export, whereas *E. coli* primarily utilize type I, type II, Sec and Tat mediated secretion systems (Kanehisa, 2000). *Salmonella* expressed 3 times more ZsGreen (2.6 mg/ml; P<0.05) and released 40 times more (1.4 mg/ml; P<0.05) than *E. coli*. Intracellular ZsGreen intensities in both species were approximately equal (Figure 5A). ZsGreen was primarily secreted from living *Salmonella* indicating that an active secretion mechanism was

responsible for its release (Figure 5). Transformed *Salmonella* were grown in LB and transferred to phosphate buffered saline (PBS) to prevent replication and observe a single bacterial generation (Figure 5B). The PBS-suspended bacteria were labeled with 4',6-diamidino-2-phenylindole (DAPI) to identify all bacteria (blue) and ethidium homodimer-I to identify dead bacteria (red). Images of these bacteria were acquired for 11 hours to determine changes in ZsGreen content (green) and viability (Figure 5B). Overlay of fluorescent images enabled classification of individual bacterium as live or dead (Figure 5B,C). The ZsGreen content and cell viability of 255 individual bacteria were measured (Figure 5C). Cells were classified as live or dead based on a red intensity threshold determined from a dead cell control stained with ethidium homodimer-I (solid vertical line; Figure 5C). Suspension in nutrient-free PBS halted growth. For the 11 hours of observation, the number of bacteria did not increase and cell viability remained above 85% (Figure 5D). On average, live cells contained more intracellular ZsGreen compared to dead cells ($P<0.05$; Figure 5E). Over time, both live and dead *Salmonella* lost intracellular ZsGreen, indicating protein release. Living *Salmonella* released ZsGreen 1.475 times faster than dead bacteria ($P<0.05$, Figure 5E). Integration of ZsGreen release from viable and dead cells over time showed that 91% of released ZsGreen was from live cells (Figure 5F). Faster ZsGreen release from live cells than dead cells indicates that active secretion was the dominant mechanism of release and that ZsGreen was not released after cell lysis.

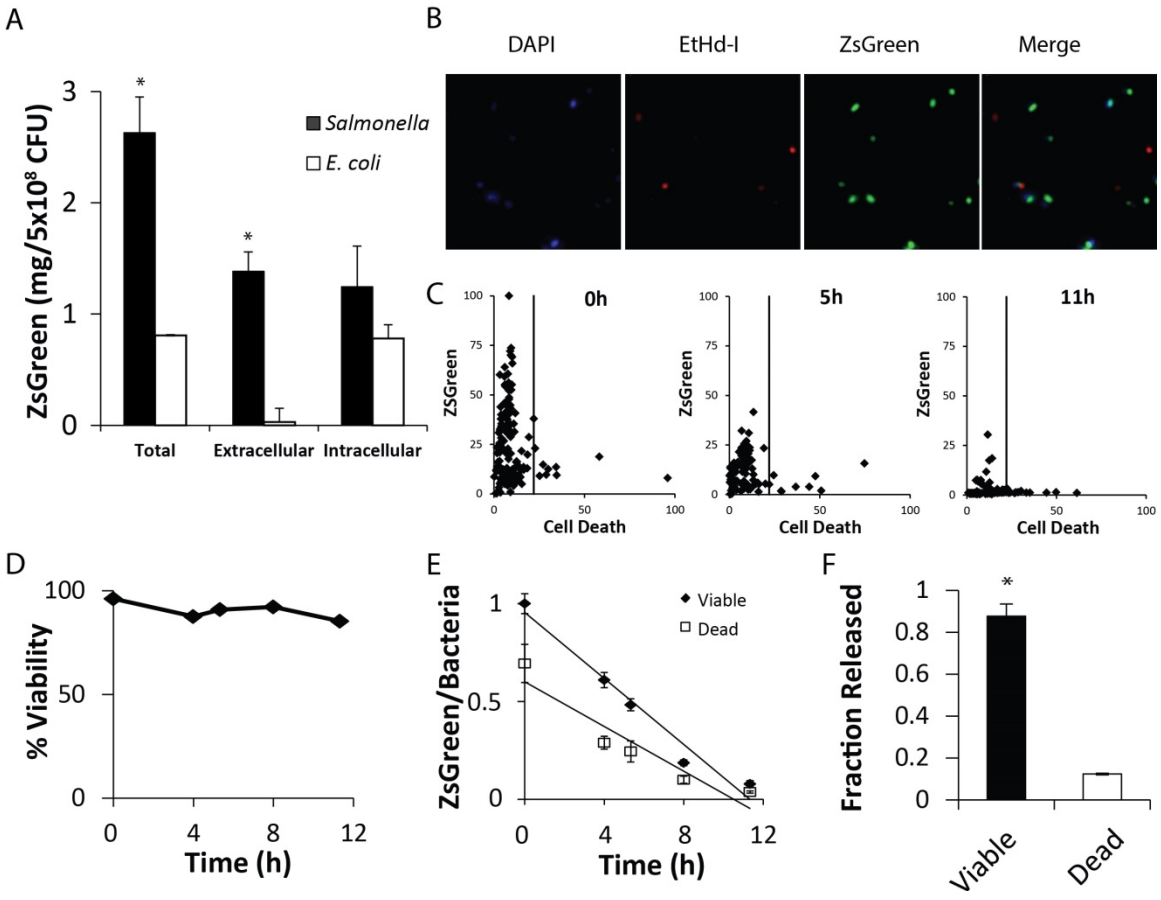

Figure 5. ZsGreen was released from viable *Salmonella.*
A) In liquid culture, *Salmonella* expressed (total) and released (extracellular) more ZsGreen than *E. coli* (*, P<0.05). **B)** *Salmonella* were stained with DAPI (blue) and ethidium homodimer (EtHd-1, red) to identify viable (blue only) and dead (both red and blue) bacteria. In the merged image, most ZsGreen expressing bacteria (green) are viable (not red). **C)** Fluorescence from ZsGreen and EtHd-1 (cell death) of individual *Salmonella* in microscopy images (*B*). Bacteria were grouped into viable and dead (solid vertical line) based on control measurements. ZsGreen fluorescence was normalized by the greatest intensity measured in an individual bacterium and multiplied by 100. Cell death was normalized by the fluorescence of positive-control bacteria. **D)** Bacterial viability was greater than 85% for 11 hours of incubation in PBS. **E)** Over time, ZsGreen fluorescence decreased in all bacteria. This rate of ZsGreen release was greater from viable compared to dead cells (P<0.05). **F)** More ZsGreen was released by viable cells (*, P<0.05) (Panteli et al., 2015).

2.3.3 Detection of ZsGreen with single-layer antibody dots

ZsGreen measurement with a single-layer antibody technique improved sensitivity over direct fluorescent spectroscopy almost 1000 fold (Figure 6). To measure ZsGreen fluorescence,

nitrocellulose membranes were cut into 1.5 mm diameter circles and coated with anti-ZsGreen antibody (Figure 6A). ZsGreen was applied to antibody dots in 96-well plates and measured by epifluorescent microscopy. The ability to measure extended fluorescent exposure of a surface with a CCD camera provided a greater range of detection compared to spectroscopy with a microtiter plate reader (Figures 6B,C). For each measurement method, the fluorescence signal intensity was normalized to a value of one at the lowest detectable ZsGreen concentration. The detection limit was defined as the concentration that produced a signal that was statistically greater than background fluorescence. The lowest detectable concentration of ZsGreen with single-layer antibody dots (4.5 ng/ml) was significantly lower than the limit with direct spectroscopy (4,500 ng/ml; $P<0.05$; Figure 6C). To improve dynamic range, exposure times were increased for lower concentrations (Figure 6B,C). Increasing exposure time of the CCD camera enabled detection of lower concentrations of ZsGreen (Figure 6B). The dot fluorescence intensity from a 100 ms exposure equaled 10 and 2.5 times the intensities produced by 1000 and 400 ms exposure times, respectively. Fluorescence intensity on dots had a linear relationship with ZsGreen concentrations between 4.5 and 10,000 ng/ml (Figure 6C). At concentrations greater than 10,000 ng/ml, little change in fluorescence intensity was observed indicating saturation of antibody binding sites on the surface of the dots (Figure 6C). Fluorescence intensity of spectroscopic measurements was less sensitive than measurement on antibody dots, with a linear range of detectable concentrations between 1,000 and $1x10^6$ ng/ml (Figure 6C).

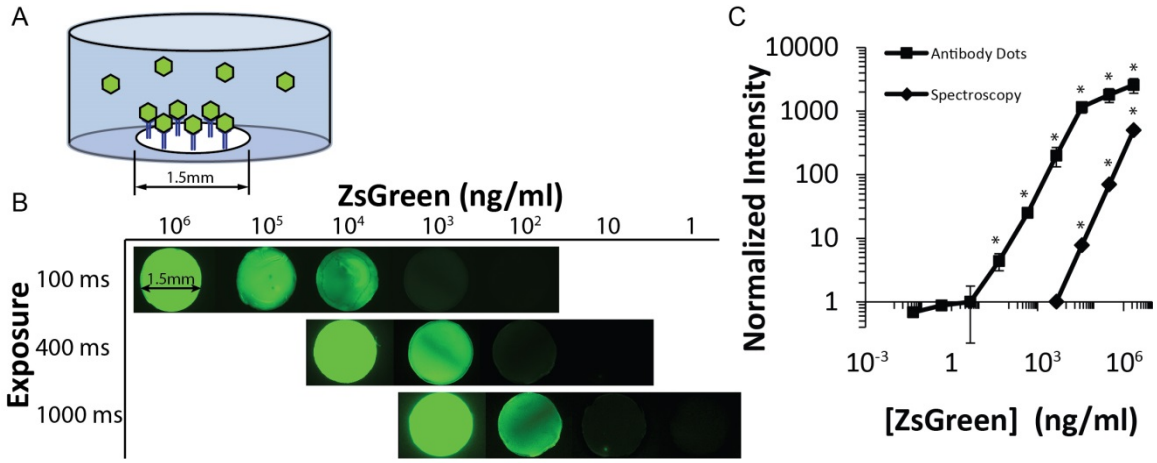

Figure 6. Single-layer antibody dots
A) Antibody dots were formed by binding anti-ZsGreen antibodies to 1.5 mm diameter circles of nitrocellulose membrane. ZsGreen concentrations were measured by incubating solutions overnight and measuring dot fluorescence. **B)** The fluorescence of antibody dots decreased with decreasing ZsGreen concentration. Higher camera exposure times were used to detect lower concentrations of ZsGreen. **C)** Fluorescence increased for increasing concentrations of ZsGreen. Intensities were normalized by the lowest detectable value. Dot measurements greater than 4.5 ng/ml and spectroscopic measurements greater than 1,000 ng/ml were significantly greater than auto-fluorescent values (*, $P<0.05$) (Panteli et al., 2015).

2.3.4 ZsGreen plasmid stability

Plasmid stability is an important consideration for future *in vivo* experiments. Maintenance of plasmid pDF02 was determined by culturing transformed bacteria in the presence and absence of the antibiotic Ampicillin, the resistance gene incorporated into the plasmid. The control set (n=4) was maintained with 100 µg/ml ampicillin (Amp), and the other set (n=4) was not (No Amp). Cultures were diluted approximately every 12 hours back down to 5,000 cells to inoculate the next cycle. Fluorescence intensities were normalized by culture density and by the maximum intensity measured. Cultures without ampicillin maintained the same expression as cultures with ampicillin. There was no significant difference in expression levels over 58 hours (average $P=0.54$), and the average relative difference between the intensities of the two groups

was 2.6%. Although the plasmid contained resistance to ampicillin, antibiotic was not needed to maintain expression for up to 58 hours (Figure 7).

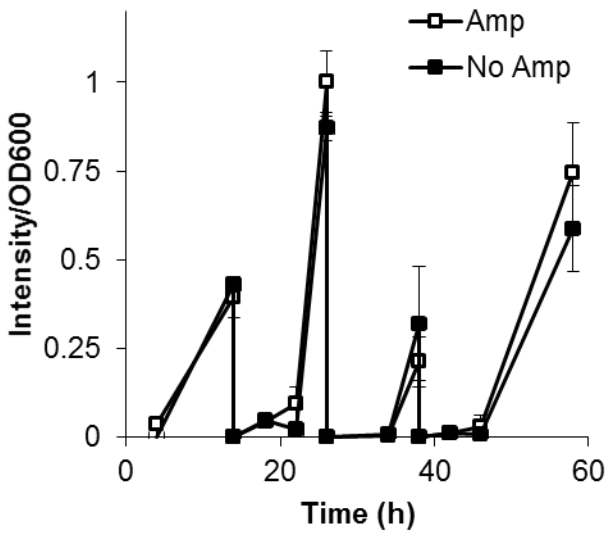

Figure 7. Plasmid stability of pDF02
Fluorescence ratio of *Salmonella* cultures transformed with pDF02, and cultured with and without antibiotic (ampicillin). The control set (*n*=4) was maintained with 100 µg/ml ampicillin (Amp), and the other set (*n*=4) was not (No Amp). Cultures were diluted approximately every 12 hours. Fluorescence intensities were normalized by culture density and by the maximum intensity measured. Cultures without ampicillin maintained the same expression as cultures with ampicillin. There was no significant difference in expression levels over 58 hours (average P=0.54), and the average relative difference between the intensities of the two groups was 2.6% (Panteli et al., 2015).

2.3.5 Released ZsGreen was detected from small *in vitro* tumor cell masses

Tumor detecting *Salmonella* produced ZsGreen in microscopic tumor masses and was released into the flow channel of a microfluidic device (Figure 8). The device mimics tumor tissue adjacent to a blood vessel (Figure 8A). Ten chambers containing tumor cell masses were analyzed across three replicate experiments (A: *n*=3, B: *n*=4, C: *n*=3). In each run, the chambers are connected in series. The total volume for each run (A, B, and C) was the sum of the volumes of each cell mass in the device chambers. The average volume was 0.12 ± 0.02 mm^3 (*n*=3; Figure

8B). Empty tumor-on-a-chip devices were used as negative controls (*n*=3), because they mimic healthy organs where bacteria are cleared by the immune system. Chambers filled with normal cells accumulate bacteria and would not be appropriate controls. Tumor detecting *Salmonella*

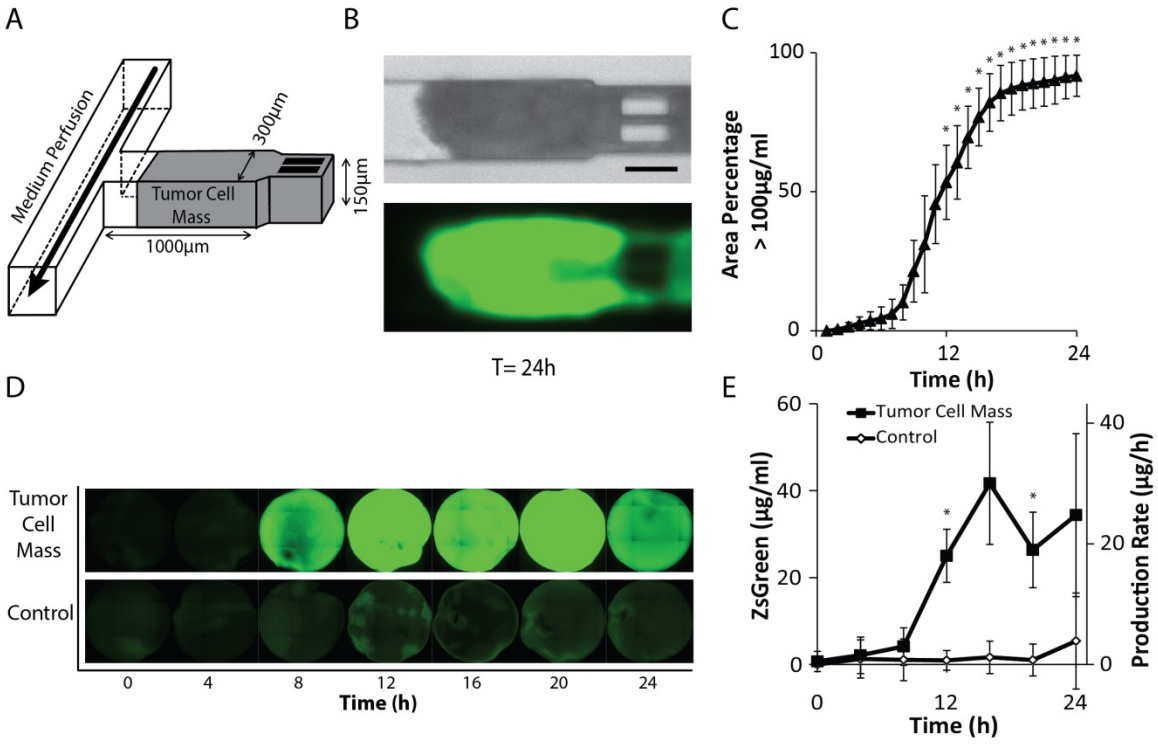

Figure 8. ZsGreen production by tumor-colonized bacteria
A) Tumor-on-a-chip device used to measure ZsGreen production. Tumor cell masses were contained within a 1000×300×150 µm chamber that borders a flow channel from which ZsGreen was collected. **B)** A cell mass composed of LS174T colon carcinoma cells in a device chamber (top) that was colonized by ZsGreen-producing bacteria (bottom, green). Scale bar is 200 µm. **C)** The area of a cell mass with a local ZsGreen concentration greater than 100 µg/ml increased rapidly and was significantly greater than zero,12 hours after induction (*, P<0.05; *n*=10). **D)** Fluorescence images of antibody dots incubated with device effluent, collected every four hours after induction (time = 0). **E)** The average concentration of ZsGreen in the effluent streams (*n*=3) was greater than controls, 12 hours after induction (*, P<0.05). The average effluent concentration of 33.3 ± 6.3 µg/ml was equivalent to a production rate of 23.9 ± 2.5 µg/h (Panteli et al., 2015).

were administered to the devices for one hour and flushed from flow channels with an additional eight hours of media flow. After the eight hours, ZsGreen expression was induced with the addition of L-arabinose (time zero, Figure 8C). Eight hours after induction, fluorescence in the tumor cell masses quickly increased (Figure 8C). By 20 hours, more than 90% of the cell

masses contained over 100 µg/ml ZsGreen (*n*=10; Figure 8B, C). Effluent samples were averaged over three runs to determine the release of ZsGreen. ZsGreen concentration was determined with antibody dots (Figure 8D). Little ZsGreen was seen in the controls. At 12 hours after induction, the concentration of ZsGreen in the effluent stream was greater than in controls ($P<0.05$, Figure 8E). Measurements ceased at 24 hours, when bacteria flooded both systems. After 12 hours, ZsGreen was steadily released at an average rate of 23.9 ± 2.5 µg/h, which is equivalent to 200. ± 21 µg/h per mm^{-3} of tissue (Figure 8E). Based on measurements of bacterial growth in tumor cell masses, (Toley and Forbes, 2012) (Figure 6), the *per-bacterium* ZsGreen production rate was 1.48×10^{-5} µg·CFU^{-1}·h^{-1}.

2.4 Discussion

A bacterial cancer detection system has been created that could identify microscopic tumors by releasing a fluorescent reporter protein and was tested in a tumor-mimic microfluidic device. It has previously been shown that *Salmonella* target tumor tissue with high specificity and replicate within the tumor microenvironment (Ganai et al., 2009; Ganai et al., 2011; Kasinskas and Forbes, 2006; Swofford et al., 2014; Toley and Forbes, 2012). In this study, we engineered an attenuated strain of *Salmonella*, VNP20009, to express and release a fluorescent reporter protein after induction with an external inducer molecule (Figure 5). Protein release was found to be predominantly from living *Salmonella* (Figure 5), which is essential for continual production and release of the biomarker from tumors. A method was developed to detect the released protein that was able measure concentrations in the ng/ml range (Figure 6). The engineered bacteria colonized microscopic tumor cell masses in a microfluidic device (Figure 8). After induction, they produced and released the reporter protein, which diffused through tissue into the flow channel *in vitro*, where it was detected in the flow channel. In the cell masses, bacteria released ZsGreen at a rate

of 8.5 $\mu g \cdot ml^{-1} \cdot h^{-1}$ per 0.12 mm^3 of tumor tissue. Detecting microscopic lesions could enable earlier treatment, which could reduce patient mortality rates. Release of ZsGreen indicates that bacteria could detect small tumors in humans (Figure 9). At ZsGreen production rate determine in the microfluidic device (Figure 8E,9D) a two compartment pharmacokinetic model (Figure 9A) predicts how blood concentration would depend on tumor size (Figure 6E).

ZsGreen accumulation is equal to the amount produced in tumor tissue minus the amount cleared from the plasma. Based on this model, ZsGreen from a 0.043 mm^3 tumor would be detectable after 24 hours, at a clearance half-life of 24 h (Figure 9E). At 24 h, the ZsGreen in the blood would be greater than the detectable limit with antibody dots of 4.5 ng/ml (Figure 6C). This volume is 2,600 to 6,200 times smaller than the current limits of tomographic imaging (6-8 mm in diameter) (Behjatnia et al., 2010; Belião et al., 2012; Schöder and Gönen, 2007). A larger tumor would have a higher rate of ZsGreen production and would be detectable earlier (Figure 9E). A larger tumor would support a greater number of bacteria, which would, in turn, produce more ZsGreen.

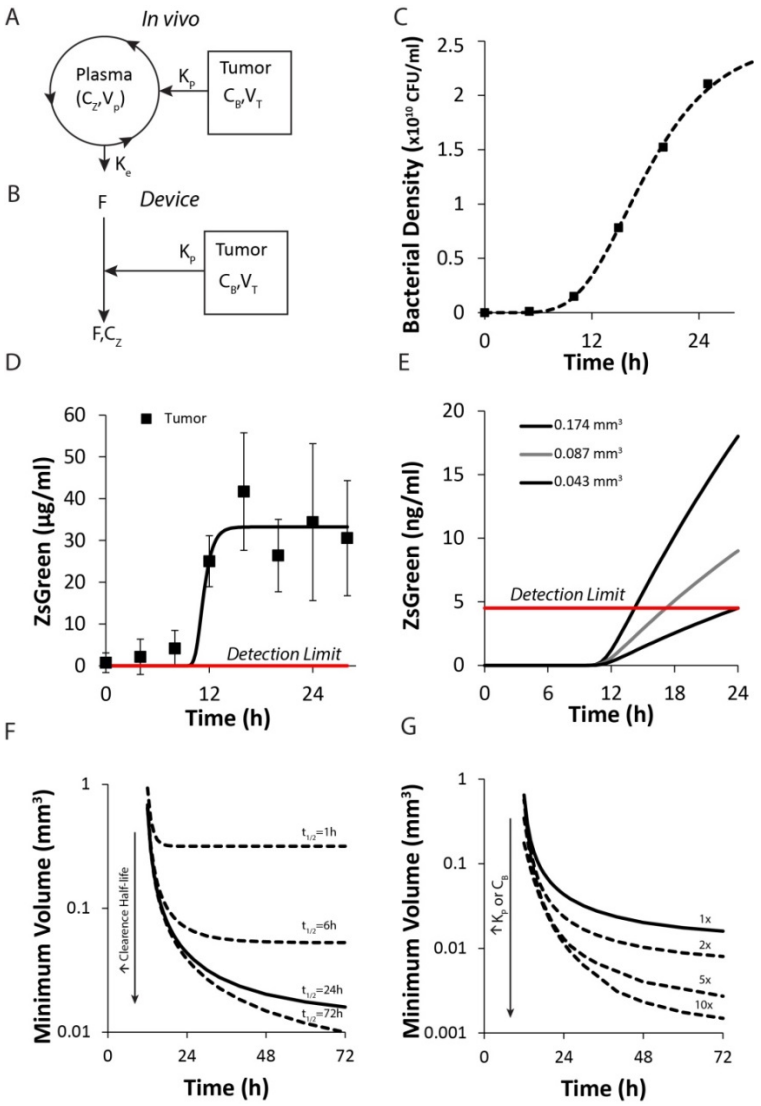

Figure 9. Mathematical predictions of detection efficacy

A) Two compartment model of ZsGreen production and clearance. ZsGreen is produced at rate KP by bacteria at density CB in a tumor of volume VT. The concentration of ZsGreen CZ in the plasma, with volume VP, decreases by clearance rate Ke. **B)** Compartment model of ZsGreen production in a tumor-on-a-chip-device. ZsGreen is produced at rate KP, and enters the flow channel with flow rate F and concentration CZ. **C)** Bacteria density in tumor devices fit to a Gompertz function with growth rate of 1.65x109 CFU·ml-1·h-1 and lag time of 10.3 h. **D)** ZsGreen release from the device experiment was fit to the compartment model in (B). Steady-state production of ZsGreen from 0.12 mg tumor mass of 23.9 ± 2.5 µg/h was found by solving C and D simultaneously (see equations (1) and (2)). **E)** Predictions of ZsGreen concentrations in human plasma using parameters derived from device measurements and the two compartment pharmacokinetic model in (A). A 0.043 mm3 tumor, with a nominal clearance half-life of 24 h, would produce the limiting ZsGreen concentration by 24 h. Larger tumors, 0.087 and 0.174 mm3, would produce more ZsGreen and be detectable by 14.2 and 17.2 h. The lag in ZsGreen production is caused by the predicted delay in bacterial growth (C, λ=10.3 h). **F)** The volume of the smallest detectable tumor decreases as the time of measurement is increased and the when the clearance half-life (t1/2) is longer. **G)** Increasing the production rate of ZsGreen (KP) or the bacterial density in tumors (CB) would reduce the volume of the minimum detectable tumor (Panteli et al., 2015).

Waiting longer to measure the concentration would allow more time for ZsGreen to accumulate in the bloodstream and enable detection of smaller tumors (Figure 9F). If ZsGreen was measured at 72 hours and the clearance half-life was 24 h, the minimum detectable volume would be 0.016 mm^3. This benefit is dependent on the clearance rate. For fast rates, e.g. $t_{1/2}$=1 h, waiting would not affect detectable tumor size (Figure 9F). At times greater than 24 h, the elimination rate and the production rate equalize and the minimum detectable volume limit becomes time independent (Figure 9F). For slow clearance rates, e.g. $t_{1/2}$=72 h, the minimum detectable tumor volume at 72 h would be 0.010 mm^3.

The efficacy of detecting microscopic tumor lesions in the clinic will depend upon 1) the rate of biomarker production, 2) the number of bacteria colonizing neoplastic sites, 3) the tumor volume, and 4) the clearance rate of the biomarker reporter. Increasing the ZsGreen production rate or the maximum bacterial density would enable detection of smaller tumors (Figure 9G). Increasing either of these 10-fold would decrease the detectable tumor volume from 0.016 to 0.0015 mm^3 at a measurement time of 72 hours (Figure 9G). The rate of ZsGreen expression and release could be increased by increasing plasmid copy number or promoter strength. Eliminating rare codons in the ZsGreen DNA sequence would also increase production rates. To increase bacterial density, lipid A could be concurrently administering with the bacteria. Lipid A increases bacterial dispersion throughout tumor tissue by causing a temporary inflammatory response (Zhang et al., 2014).

In animal models, detecting bacteria would have to stably express ZsGreen. For long studies in animals, stable expression could be maintained by continual administration of ampicillin (Bakker-Woudenberg et al., 1981; Corpet et al., 1989). Similarly, L-arabinose has been administered to animals to induce protein expression from injected bacteria (Brader et al., 2008;

Stritzker et al., 2007). For short studies, ZsGreen from cultures without ampicillin would maintain the same expression as cultures with ampicillin (Figure 7). In humans, antibiotics could not be used, and the ZsGreen construct would have to be maintained with a balanced lethal system or be incorporated into the *Salmonella* genome (Dai et al., 2013; St Jean et al., 2014).

Active release of ZsGreen by *Salmonella* will greatly enhance the sensitivity of tumor detection. Continuous production would cause ZsGreen to build up in the circulation system until the eliminate rate balances the production rate (Figure 9F; Eq. 1). Waiting longer to measure the blood concentration would enable detection of smaller lesions (Figure 6F, G). In culture, over 90% of ZsGreen was actively secreted by living *Salmonella* (Figure 5). Release from dead bacteria would not be continuous and would limit efficacy. If bacteria produce ZsGreen in a single batch after injection, only a pulse of ZsGreen would appear in the blood and it would be more difficult to detect.

The difference in release rates between *Salmonella* and *E. coli* (Figure 5A), indicates that *Salmonella* actively secrete ZsGreen. Some of the major differences between these two organisms are their secretion mechanisms. Gram negative bacteria have seven classes of secretion systems that are activated in different environments to transport proteins across the cell envelope (Filloux, 2004; Francetic et al., 2000; Kerr, 2000; Natale et al., 2008; Thanassi and Hultgren, 2000). *Salmonella* and *E. coli* contain many of the same secretion genes, although not all are functional (Tseng et al., 2009). For example, *Salmonella* and K-12 *E. coli* both activate type III secretion systems when quorum sensing is activated (Choi et al., 2007; Sperandio et al., 1999). However, DH5α *E. coli* (a K-12 sub-strain), have a quorum sensing deficiency and are unable to synthesize autoinducer-2 (Surette and Bassler, 1998). As a result, DH5α *E. coli* cannot activate quorum-sensing-related secretion machinery (Li et al., 2007; Sperandio et al., 1999; Surette et al., 1999).

This difference suggests that type III secretion, or another quorum-sensing-related mechanism, is used by *Salmonella* to secrete ZsGreen. This difference in active secretion also shows that *Salmonella* would be superior to DH5α *E. coli* for tumor detection.

Efficient molecular transport through tumor tissue is necessary for effective intravenous detection (Figure 2). For the biomarker to be present in the blood or the device effluent, it must diffuse through tissue and not be sequestered by cancer cells. Similarly, if the gene inducer does not diffuse through tissue, gene expression would not be activated. Appearance of ZsGreen in the effluent of the microfluidic device (Figure 8E) shows that both ZsGreen and L-arabinose diffuse through tumor cell mass. It also shows that *Salmonella* can both produce and release the protein when colonized in a tumor mass. The increase of ZsGreen throughout the chambers (Figure 8B-C) shows that L-arabinose was rapidly delivered. We have previously shown with another system that L-arabinose can activate gene expression throughout tumor tissue (Dai et al., 2013). In this system, over 90% of the cell mass in the device contained at least 100 μg/ml of ZsGreen after 24 hours (Figure 8C).

The inclusion of a triggered gene expression system is essential for bacterial detection. Systemic administration of the inducer molecule (L-arabinose) is necessary to activate protein production after bacteria have cleared from normal tissue. It is critical that tumor-detecting bacteria are not making the protein biomarker when they are injected into the body. After systemic injection of *Salmonella*, it takes approximately three days for them to clear from healthy organs (Clairmont et al., 2000). If a biomarker was constitutive produced, bacteria in healthy organs would express it during this period and obscure detection of malignant lesions. To prevent expression in normal tissue, the tightly regulated P_{BAD} promoter would not express the biomarker until administration of L-arabinose.

Using these engineered bacteria after resection of a primary tumor could provide a fast and easy method to detect tumor recurrence or the onset of metastatic disease. Detecting tumors with bacteria would be minimally invasive. Measurement would require injection of bacteria followed by a single blood draw three days later. How the system is used will depend on whether it can be administered repeatedly. An immune response that produces anti-ZsGreen antibodies could induce adverse side effects and could be detrimental to the single-layer dot technique. In mice, it takes at least one week to develop antibodies, suggesting that a single administration would be possible (Dittmer et al., 1999). Patients could receive a screening dose at a set period of time after surgery to detect recurrence or metastatic spread.

If repeated doses are possible, the utility of the technique would be greater. We envision that after surgery to remove a primary tumor, patients would receive an initial dose of tumor-detecting bacteria to establish a baseline plasma level of ZsGreen. Patients would then receive periodic screenings with bacteria. Signal increases would indicate recurrence or formation of secondary cancers. This system could also be used to determine the aggressiveness of a malignant mass or monitor tumor growth in response to treatment. The mathematical model predicts that the magnitude of ZsGreen signal is indicative of the volume of a malignant cell mass (Figure 9E). If a tumor were to grow, the number of bacteria would increase proportionally. Similarly, if a tumor shrinks in response to therapy, the number of colonized bacteria would decrease. In this way, monitoring tumor growth with bacteria could determine if a therapy is effective.

2.5 Conclusions

Here I showed development of a bacterial diagnostic tool to detect microscopic tumor masses. Genetically modified tumor-targeting bacteria were engineered to release a reporter

protein for detection. An *in vitro* tumor model was used to test tumor targeting and production of the reporter molecule in 3D tumor cell masses. Production of ZsGreen from tumor-targeting *Salmonella* detected microscopic 0.12 mm^3 tumor masses from a microfluidic device. At the estimated parameters, mathematical analysis of these results predicts detection of tumor masses as small as 0.043 mm^3 in humans, more than 2,600 fold smaller than the current limits of tomography. These results suggest the possibility of a bacterial detection in humans. This method has the potential to non-invasively monitor treatment, detect tumor masses that are invisible to current techniques, and increase life expectancy.

CHAPTER III

DETECTION OF MURINE TUMORS WITH GENETICALLY MODIFIED BACTERIA

PART B: IN MURINE TUMOR MODELS

3.1 Introduction

Detecting microscopic tumor lesions in the clinic with tumor-targeting bacteria depends upon 1) the rate of biomarker production, 2) the number of bacteria colonizing neoplastic sites, 3) the tumor volume, and 4) the stability of the biomarker reporter. ZsGreen stability will determine the retention time in circulation. ZsGreen clearance rate was measured in mice by systemic injection and subsequent blood collection. A stable protein half-life will enable detection of smaller malignant cell masses. To determine the efficacy of *in vivo* tumor detection, a tumor model experiment was performed to identify subcutaneous tumors of various sizes.

3.2 Materials and Methods

3.2.1 ZsGreen purification and quantification

Recombinant ZsGreen was purified from bacterial lysate of liquid cultures of pHis-ZsGreen with nickel column chromatography. Solvent exchange was performed to concentrate and solubilize the purified protein into an excipient solution suitable for injection. Excipient solution consisted of: 200 mM glycine, 8 mM L-histidine, 40 mM sodium chloride, and 0.8% sucrose in sterile water for injection. This composition is necessary to maintain ZsGreen solubility in purified state and prevent protein precipitation. The excipient composition is an accepted known excipient formulation for an intravenous protein drug on the market (BeneFIX, coagulation factor IX, Pfizer).

Bradford assay was used to measure concentration of ZsGreen. ZsGreen was diluted to a final concentration of 10 micrograms/ 100 microliter. ZsGreen solution was sterile filtered through a 0.2 micron filter prior to injection for the half-life study. Sterilized ZsGreen solution administered to murine models via tail vein injection of 100 microliters (1 µg/ml) with a 30 gauge needle.

3.2.2 Pharmacokinetic study of the half-life of ZsGreen

ZsGreen was purified by column chromatography and buffer exchanged into an excipient formula suitable for intravenous injection into animals. Ten µg of ZsGreen in 100 µl of excipient formula was injected into the tail vein of 20 mice, 8-10 week old female BALB/c (The Jackson Laboratory, Bar Harbor, Maine). In groups of five, blood samples were collected at 1, 3, 9 and 24 hours and compared to a negative control group, injected only with equal volume saline (n=5). Blood samples were collected by cardiac puncture upon euthanasia with CO_2.

3.2.3 Tumor models

Two groups of 8-10 week old female BALB/c mice (The Jackson Laboratory, Bar Harbor, Maine) (Large group, n=8 and Small group, n=10) were subcutaneously injected with 50,000 cells of 4T1 mammary carcinoma cells at two separate inoculation times day 0, and day 11. A third group of mice (n=9) cancer free mice served as a negative control. At day 27 all mice received intravenous injections with ZsGreen expressing *Salmonella*. The bacteria were allowed 48 hours to grow in the tumors and clear from healthy organs, with subcutaneous injections of Ampicillin every 8 hours to maintain plasmid. After the 48 hour growth period, 100µl 0.2% L-

arabinose was injected subcutaneously with 10mg/100µl ampicillin every 8 hours for the next 24 hours, to induce ZsGreen expression. At 72 hours after bacterial injection, all mice were then euthanized and tumor, liver, spleen and blood were harvested.

3.2.4 Immunofluorescent staining and image acquisition

Immunofluorescent staining was used to identify locations of bacteria and ZsGreen throughout tumors. Paraffin embedded sections were blocked after 20 min antigen retrieval at 65C in citrate buffer, with Dako protein block (Dako). Sections were stained with two primary antibodies, 1:100 anti-rabbit α-RCFP polyclonal antibody (Clontech) and 1:10 FITC-conjugated-anti-salmonella-antibody (Abcam, Cambridge, MA). Washes were performed in TBS-T and a secondary Alexa Fluor 546-donkey-antirabbit IgG (Life technologies) was applied at 1:100.

An Olympus IX71 Inverted Epi-fluorescence Microscope (Olympus America, Center Valley, PA) equipped with 10X Plan-APO objective, a LudI Motorized Z-stage (LudI Electronic Products, Hawethorne, NY), and a monochromatic Hamamatsu cooled-CCD Digital Camera (Hamamatsu Photonics K. K., Hamamatsu City, Japan) was used to acquire images from immunofluorescent labeled slides. A script in IPLab (BD Biosciences, Rockville, MD) was used to automate image acquisition and assemble a tiled montage of individual images comprising of three fluorescent filters: D350/50x UV: ~300-400nm, D546/10x Blue:~ 415-500nm, D455/70x Green:~537-557nm (Chroma Technologies Corporation, Bellows Falls, VT). ImageJ/Fiji (Schindelin et al., 2012) was used to perform image analysis and threshold red and green images to enable quantification of *Salmonella* and ZsGreen.

3.2.5 Colony counting via plating

A fraction of each harvested tumor, liver, and spleen were weighed, minced, suspended in equal volumes of phosphate buffered saline (PBS), and applied to LB agar plates with ampicillin. Four dilutions of each tissue in PBS were plated on antibiotic plates. For livers and spleens, dilutions of 1, 1:10, 1:100, and 1:100 were used and for tumors $1:10^3$, $1:10^4$, $1:10^5$, and $1:10^6$ were plated. After overnight incubation at 37°C, plates were imaged using a black and white camera and colonies were counted using Fiji/ImageJ particle analyzer plugin.

3.2.6 Tumor transition boundary analysis

Whole tumors at 25% image quality were analyzed for the transition boundary analysis. The boundary between necrotic and viable tissue was determined by the size and density of nuclei from DAPI staining. Necrotic and apoptotic tissue has small dispersed and fragmented nuclei, termed pyknosis. The boundary between viable, large well distributed nuclei, and pyknosis was drawn on tumors with necrotic tissue (n=5). A Euclidean distance map to this boundary into necrosis (positive x axis) and out to viable tissue (negative x-axis). The distance map was multiplied by the thresholded bacterial and ZsGreen to determine the abundance of pixels of each color as a function of distance from this boundary. Raw bacteria and ZsGreen were background subtracted by rolling ball 50 pixel, to eliminate autofluorescence from tissue. Individual *Salmonella* threshold was set to 550 and ZsGreen to 850 based on negative control autofluorescence.

3.2.7 Colony characteristics image analysis

Six images from the tumors were randomly picked using a random number generator, excluding tissue edges, images with tissue folds, and over 75% black space, i.e. broken tissue within the main body of a tumor (n=5). Small tumors and large tumors, with no necrotic regions showed little to no detectable *Salmonella* or ZsGreen via immunofluorescent staining and were not analyzed. In Fiji/Imagej, individual images, at 100% image quality, were background subtracted using 25 pixel rolling ball method, thresholded and converted to binary. Red and green binary images were then aligned by maximizing the area of overlap through sequential rigid transformations. The maximum overlap was assumed to be the best alignment. Using Fiji/ImageJ particle analyzer the number of bacteria and the size were measured in binary red images. The ZsGreen binary images were multiplied by the aligned red images to identify regions of co-localization. Only co-localized ZsGreen regions of interest were analyzed for diffusion distance. Sequential dilations around each colony identified the average ZsGreen distance from the colony and concentration. Scripts for binary image alignment and measuring ZsGreen diffusion distance from a colony by sequential dilations and unions can be found in Appendix C.

3.2.8 Mathematical model of diffusion from a colony

ZsGreen production from bacteria was modeled as a continuous point source production from the edge of a colony with a constant rate of production. ZsGreen expression from a colony can be described by 1-D diffusion from a spherical particle:

$$\frac{\partial C}{\partial t} = \frac{D}{r^2}\frac{\partial}{\partial r}\left(r^2\frac{\partial C}{\partial r}\right),\ \frac{\partial C}{\partial t} = \dot{m}|_{r=r0}\ ,\ C = 0|_{r\to\infty}\ ,\ C = 0|_{t=0} \quad (4)$$

Where C is the extracellular concentration of ZsGreen, t is time, in hours, r, is the radial distance from the edge of the colony with radius r_0, and $\dot{m}$ (moles/time) is the production rate of ZsGreen.

The steady state solution to equation (4) is:

$$t \to \infty, \overline{C}(r) = \frac{M}{\bar{r}} \frac{\dot{m}}{4\pi D r_0 C_0 \bar{r}} \quad (5)$$

With dimensionless concentration, $\overline{C}$ = C/C_0, radius, $\overline{r}$ =r/r_0, and time, $\overline{t}$ = $\frac{Dt}{{r_0}^2}$, where C_0 is the minimum detectable ZsGreen concentration by indirect immunofluorescence, estimated from reported measured values for several different paraffin embedded proteins (Davis et al., 2003). The diffusion coefficient for ZsGreen was estimated from the molecular weight of the protein assuming a hydrodynamic radius of ZsGreen similar to that of a globular protein (Narang et al., 2005) at the molecular weight of the tetrameric form of ZsGreen (104.2 g/mol) and calculating the estimated effective diffusion coefficient and the respective tumor interstitium diffusion coefficient (Pluen et al., 2001). From least squares regression of concentration to the model in equation (5), the M value was determined for the average concentration of ZsGreen released from all colonies. The colony level production rate of ZsGreen, $\dot{m}$, was then calculated, based on the minimum concentration, C_0, and diffusion coefficient, D.

The relationship between tumor size and ZsGreen production rate based on $\dot{m}$ was compared to the actual production rate measured in tumors, K_p. K_p and $\dot{m}$ share the same units [ng/ CFU/ h]. The K_p was determined by solving equation (3) at t= 24 hours, given the measured ZsGreen concentrations and tumor weights, a constant bacterial density of 485 CFU/mg, a plasma volume in mice of 2 ml, and the measured half-life of ZsGreen, 2.7 h. The minimum tumor size detected in humans was then calculated based on the measured K_p. Increasing bacterial

density in equation (3) from 485 CFU/mg to 100,000 CFU/mg allowed calculation of minimum tumor size based on previously recorded bacterial densities in tumors. Tumor weight was converted to diameter assuming perfect spherical masses and a density of 1g/ml.

3.3 Results

3.3.1 ZsGreen half-life was determined in mice

To determine if biomarker elimination would be a limitation for detection, the half-life of ZsGreen was measured in mice (Figure 10). Blood samples were applied to single layer antibody dots and quantified. Over 24 hours ZsGreen concentration decreased with time. Half-life was determined by fitting the measured data points to the equation for exponential decay: $C = C_0 \cdot e^{-kt}$, where $k = \ln(2)/t_{1/2}$, t is time, C is concentration, and C_0 is the starting concentration. The half-life in circulation for ZsGreen was found to be 2.7 ± 0.44 hours (Figure 10). ZsGreen in the blood was detectable to 1ng/ml with confidence compared to saline injected controls (*, $P<0.05$).

3.3.2 *Salmonella* detect subcutaneous murine tumors by triggered release of ZsGreen

The capability of bacterial tumor detection was evaluated in murine tumor models to determine if subcutaneous tumor could be detected and if tumor size affected the concentration of ZsGreen found in blood samples. Three groups of mice were used to test this hypothesis: a large

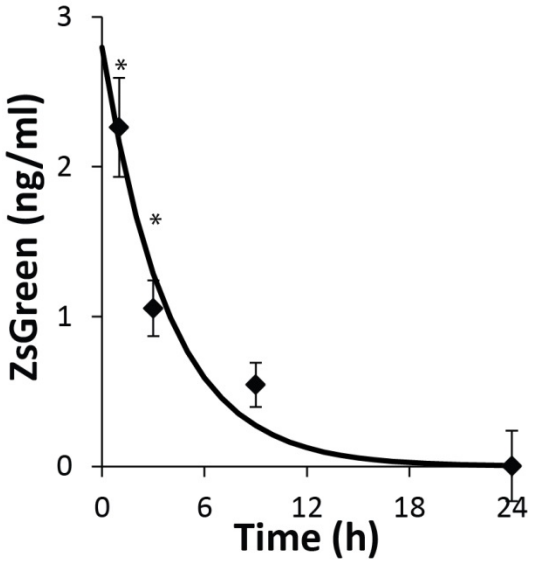

Figure 10. Half-life of ZsGreen in circulation in mice
The half-life for ZsGreen in circulation was found to be 2.7 ± 0.44 hours, measured by plasma application to single-layer antibody dots.

tumor group (A, n=8), small tumor group (B, n=10) and a no tumor control group (C, n=9). At time zero all three groups of mice were injected with ZsGreen producing bacteria. After 48 hours the mice received 3 subcutaneous doses (every 8 hours) of L-arabinose, on the opposite flank of the tumor, to induce ZsGreen expression. At 72 hours mice were sacrificed and blood, tumor, liver, and spleens were harvested for analysis.

The mice from the large tumor group showed significantly higher plasma ZsGreen concentration compared to the control mice, with an average tumor weight of 0.557 ± 0.104 g and a plasma ZsGreen concentration of 1.1 ± 0.34 ng/ml (Figure 11A, $P<0.05$). The small tumor group was not significantly different than the control or the large tumor group. Plasma ZsGreen concentration increased with tumor weight with slope of 0.81 ± 0.32 $ng \cdot ml^{-1} \cdot g^{-1}$ (Figure 11B; slope>0; $P<0.05$).

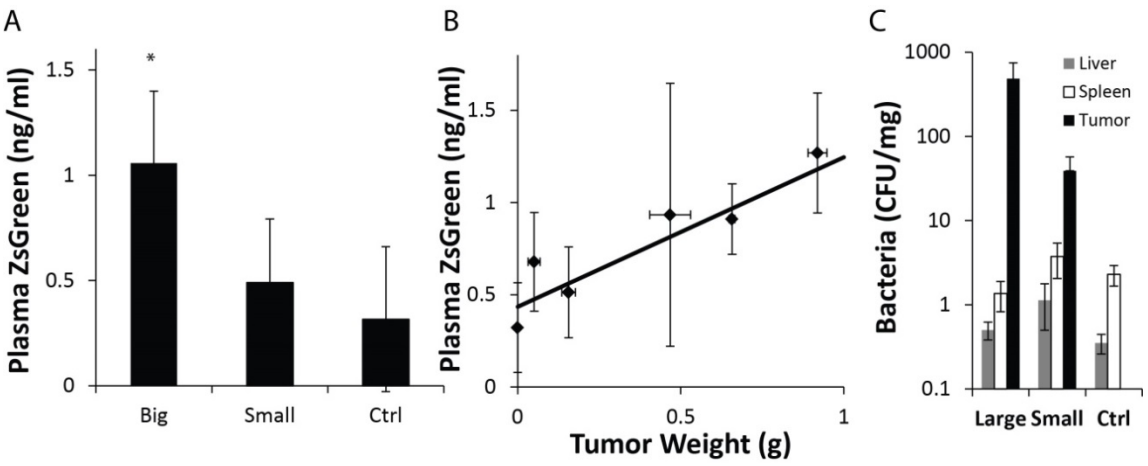

Figure 11. Tumor-targeting bacteria detect tumors by release of recombinant ZsGreen
A) The **l**arge tumor group showed significantly higher amount of plasma ZsGreen than the control (**slope>0;** $P<0.05$). **B)** Plasma ZsGreen concentration increased with tumor size with a statistically significant, positive slope ($P<0.05$). **C)** Colony counting showed tumors with the highest bacterial density after 72 hours with large tumors having an average bacterial density of 500 CFU/mg. Livers and spleens showed little to know bacterial density with averages around 1 CFU/mg.

The y-intercept, in Figure 11B, indicates ZsGreen production from healthy organs of approximately 0.44 ± 0.16 ng/ml, 24 hours after inducing with L-arabinose. Colony plating showed that the large tumor group contained the highest number of bacteria with an average bacterial density of 485 CFU/mg. Healthy tissues contained little bacteria with an average density of 1.6 CFU/mg (Figure 11C).

3.3.3 ZsGreen expression was higher in viable tissue than necrotic regions

ZsGreen expression was higher in viable tissue but the majority of bacteria and ZsGreen were observed in necrotic regions of the tumor. Necrosis (N) was identified by DAPI staining. Necrotic regions were identified by pyknosis, regions with small and sparse nuclei caused by the irreversible compacting of the chromatin in the nucleus associated with necrotic and apoptotic tissue (Elmore, 2007; Kroemer et al., 2009). Viable tissue (V) was identified by large, evenly

distributed, and dense nuclei. Boundaries between viable and necrotic tissue were drawn for tumors with necrotic regions (n=5; yellow line; Figure 12A). Immunofluorescent staining identified bacteria, red, and ZsGreen, green. The small tumor group and tumors without necrosis in the large tumor group had little to no bacteria or ZsGreen (n=13, Figure 12 B, top). Over 80% of bacteria and ZsGreen were found in necrotic regions of large tumors (Figure 12B, bottom, C). Intratumoral ZsGreen correlated well with the weight of necrotic tissue (Figure 12D). Multiplying the bacteria and ZsGreen pixels by the Euclidian distance map of the transition boundary enabled measurement of pixel area as a function of distance from the boundary. The majority of bacteria and ZsGreen were found within 500 μm of the transition boundary, the interface between viable and necrotic tissue (Figure 12E,F). As distance away from this transition boundary increased the magnitude of detected bacteria and ZsGreen dropped, with higher levels of both found in necrosis, compared to viable regions (Figure 12E,F). The absolute pixel area difference between ZsGreen and bacteria as a function of distance was positive in viable regions and negative in necrotic regions of the tumor, indicating less ZsGreen produced per bacteria in necrotic regions (Figure 12G). The relative ratio of ZsGreen to bacteria, as a function of distance, shows a higher level of ZsGreen production per bacteria in viable regions, at -500 μm on the x-axis, with an exponential drop with distance across the transition boundary into necrosis (Figure 12H). The relative production rate of ZsGreen per bacteria was higher in viable regions of the tumors compared to necrotic regions (Figure 12I).

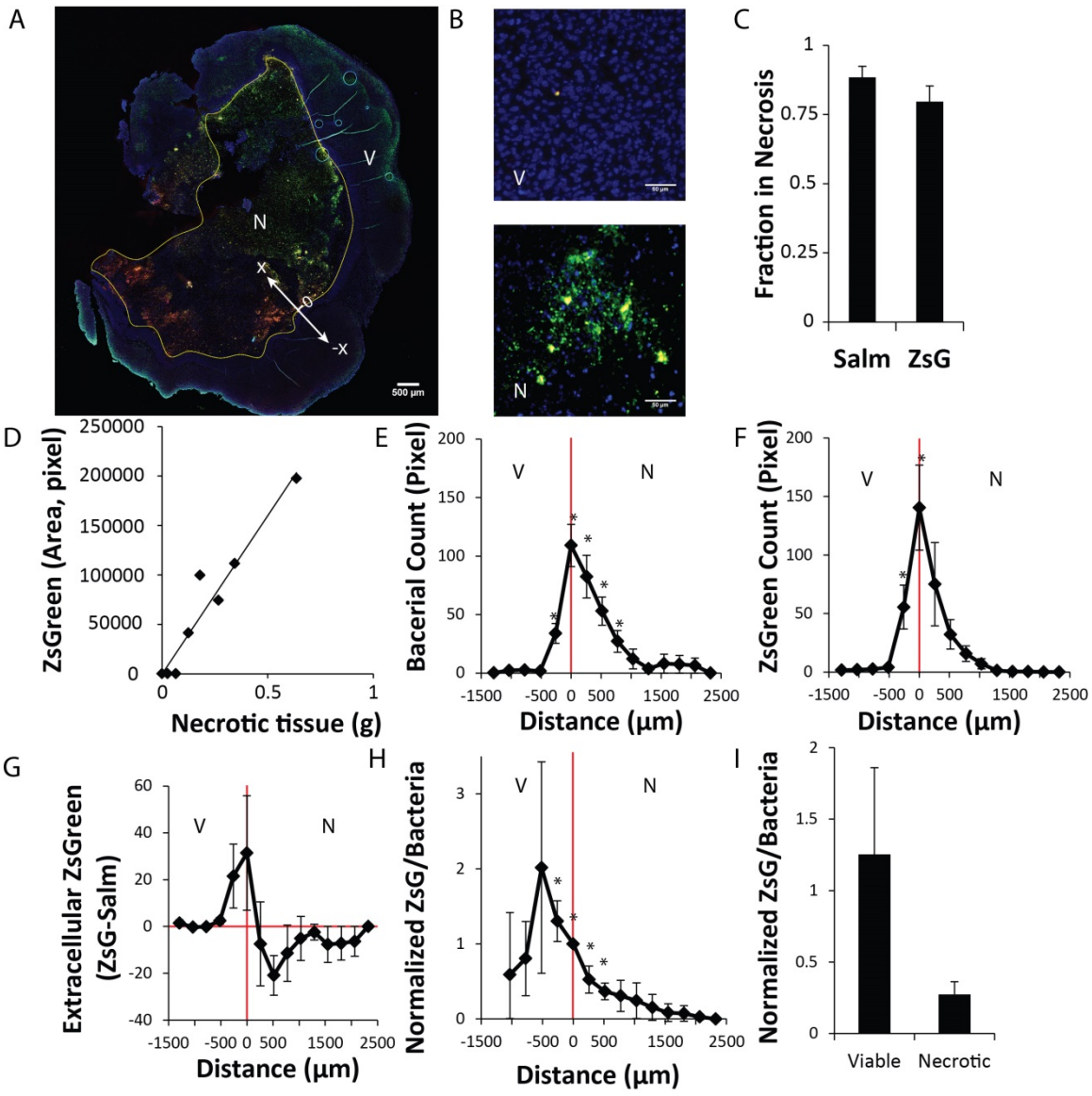

Figure 12. ZsGreen expression was higher in viable tumor tissue

A) Tumors were immune-stained with DAPI, anti-*Salmonella* antibody, red, and anti-ZsGreen antibody, green. The transition boundary (yellow line) between viable (V) and necrotic (N) tumor tissue was identified by size and density of nuclei from the DAPI stain. **B)** Necrotic regions of the tumor (bottom) contained most of the bacteria and observed ZsGreen release, whereas viable regions (top) did not. **C)** The majority of both Salmonella and ZsGreen were found in necrotic regions in the tumors (n=5, tumors with necrosis). **D)** The intratumoral concentration of ZsGreen scaled linearly with the weight of necrotic tissue. Five tumors from the large tumor group were identified with high levels of necrosis. **E,F)** The transition boundary between viable and necrotic tissue had the highest density of bacteria and concentration of ZsGreen, which decreased with distance away from this boundary (reported as average pixel area; *, $P<0.05$). **G)** The difference between ZsGreen and bacterial staining area was positive in the viable region of tumors and negative in the necrotic region away from the transition boundary. **H,I)** The normalized ratio of ZsGreen produce per bacteria showed higher production of ZsGreen in viable tissue compared to necrotic regions(*, $P<0.05$). Negative distance on the x-axis indicates viable tissue and positive x-values indicate necrotic tissue (panels E,F,G, and H).

3.3.4 ZsGreen diffuses through solid tumor tissue

Bacterial colonies were measured for ZsGreen expression, size, and extent of local ZsGreen release. Approximately 10,000 colonies across five tumors were analyzed for ZsGreen release. From the overlay of DAPI, Salmonella antibody, and ZsGreen antibody, the size and location colonies and ZsGreen were measured (Figure 13A). Colony size was measured by computing the pixel area and converting to radius in microns, assuming the area was of a perfect circle (red dotted circle about the yellow bacteria colony; Figure 13B). To determine the ZsGreen concentration as a function of distance, area of ZsGreen was divided by the theoretical maximum area of the shell at distance r_i from the colony radius. The theoretical area was calculated as the difference in the area of a circle with outer radius, r_i+r_{colony}, and the inner radius, $r_{i-1}+r_{colony}$ (Figure 13B). Colony size distribution showed the majority of colonies were small with an average colony radius of 0.66 µm (Figure 13C**)**. On average, 57% of the bacterial colonies produced ZsGreen across all tumors (See Appendix A1). Secretion was independent of colony size with an average distance of 6.6 ±1.0 µm from the colony edge (Figure 13D). Relative ZsGreen concentration decreased with radial distance from the colony (Figure 13E). ZsGreen concentration can be modeled as a point source production rate with a constant rate of ZsGreen release of m (Red line, Figure 13 E). This is dependent upon the diffusion coefficient for ZsGreen in tissue and the production rate from the colony. It was assume that at 24 hours after ZsGreen expression that the system has reached a pseudo-steady-state. The colony level production rate of ZsGreen, $\dot{m}$, was found to be 1.14×10^{-5} ng/CFU/ml with a minimum detectable concentration of, C_0= 0.1 µmole/L for indirect immunofluorescence (Davis et al., 2003), and a diffusion coefficient within tumor interstitium of, $D= 1.95 \times 10^{-06} cm^2/s$ (Pluen et al., 2001).

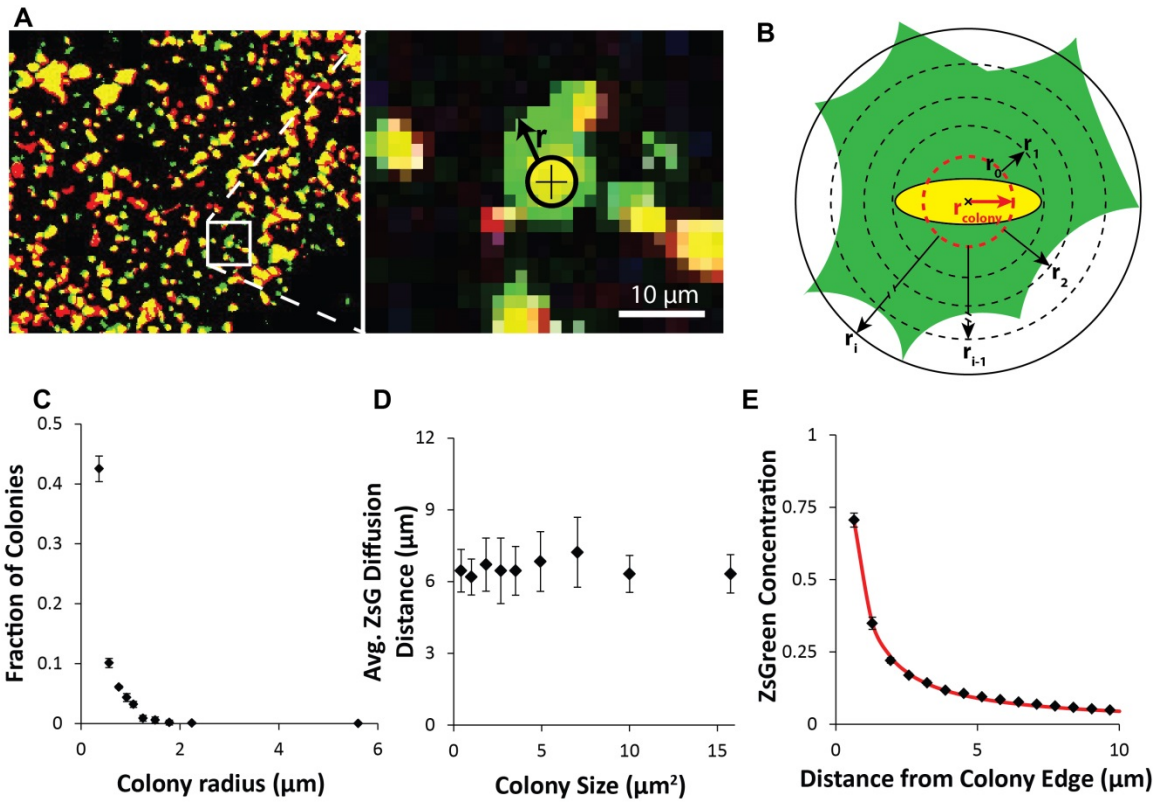

Figure 13. ZsGreen diffuses from colonies independent of colony size
A) Salmonella, red, and ZsGreen, green, were identified in tumor tissue by immunofluorescent staining. Colonies expressing ZsGreen were identified extracellular ZsGreen were identified. **B)** A schematic of how colony radius, r_o, was radius of a circle with equal volume as colony pixels measured. Concentration was calculated as the ratio of area of ZsGreen pixels in a given shell over the theoretical area of the shell $\pi [(r_i+r_o)^2-(r_{i-1}+r_o)^2]$. **C)** The average colony radius was 0.66 µm, across all tumors. **D)** ZsGreen diffusion distance was independent of colony size with an average ZsGreen diffusion distance of 6.6 ±1.0 µm. **E)** ZsGreen concentration dropped as radial distance from a colony increased. ZsGreen production and diffusion was modeled as a continuous point source production from the edge of the colony, red line.

3.3.5 Re-evaluation of two-compartment mathematical model

Incorporation of the measured half-life, bacterial density, and measured ZsGreen detection limit, into a two compartment mathematical model (equation (3)) enabled prediction of tumor detection in mice and in humans. Mouse blood volume was assumed to be 2 ml (Vp), half-life was found to be 2.7 hours ($t_{1/2}$) (Figure 10), bacterial density was measured as 485 CFU/mg ($C_{b,max}$) (Figure 11C), and the detection limit for ZsGreen was 1 ng/ml (See Appendix A3).

At the ZsGreen production rate from colony level analysis, $\dot{m}$=1.14 x 10^{-5} ng/ CFU/ h, the ZsGreen concentration vs. tumor size relationship is greater than the observed ZsGreen production rate from tumor study measurements (Figure 14 A). The actual production rate was determined by solving equation (3) for K_p with the measured ZsGreen concentration and tumor sizes from Figure 11B. The actual K_p was found to be 1.52 x10^{-6} ng/ CFU/ h, ten-fold smaller than the observed colony level production rate. This indicates there is a discontinuity between the amount of ZsGreen produced in the tumor and the amount reaching the blood stream.

At the measured bacterial density, C_B= 485 CFU/mg and K_p, the minimum detectable tumor size was found to be greater than 1 kg for tumor detection in humans (Figure 14B). Increasing the bacterial density to 100,000 CFU/mg, densities previously seen in murine tumor models with the same *Salmonella* (Forbes et al., 2003), enables detection of tumor mass less than 10g (Figure 14B,C). At this tumor weight the diameter of a single lesion with the same mass is estimated to be 25 mm across (Figure 14D). To enable detection of microscopic tumors in humans, at the tomographic detection limit, previously stated as 6-8 mm in diameter, the bacterial production rate of ZsGreen, K_p, would need to be improved 100-fold (Figure 14D).

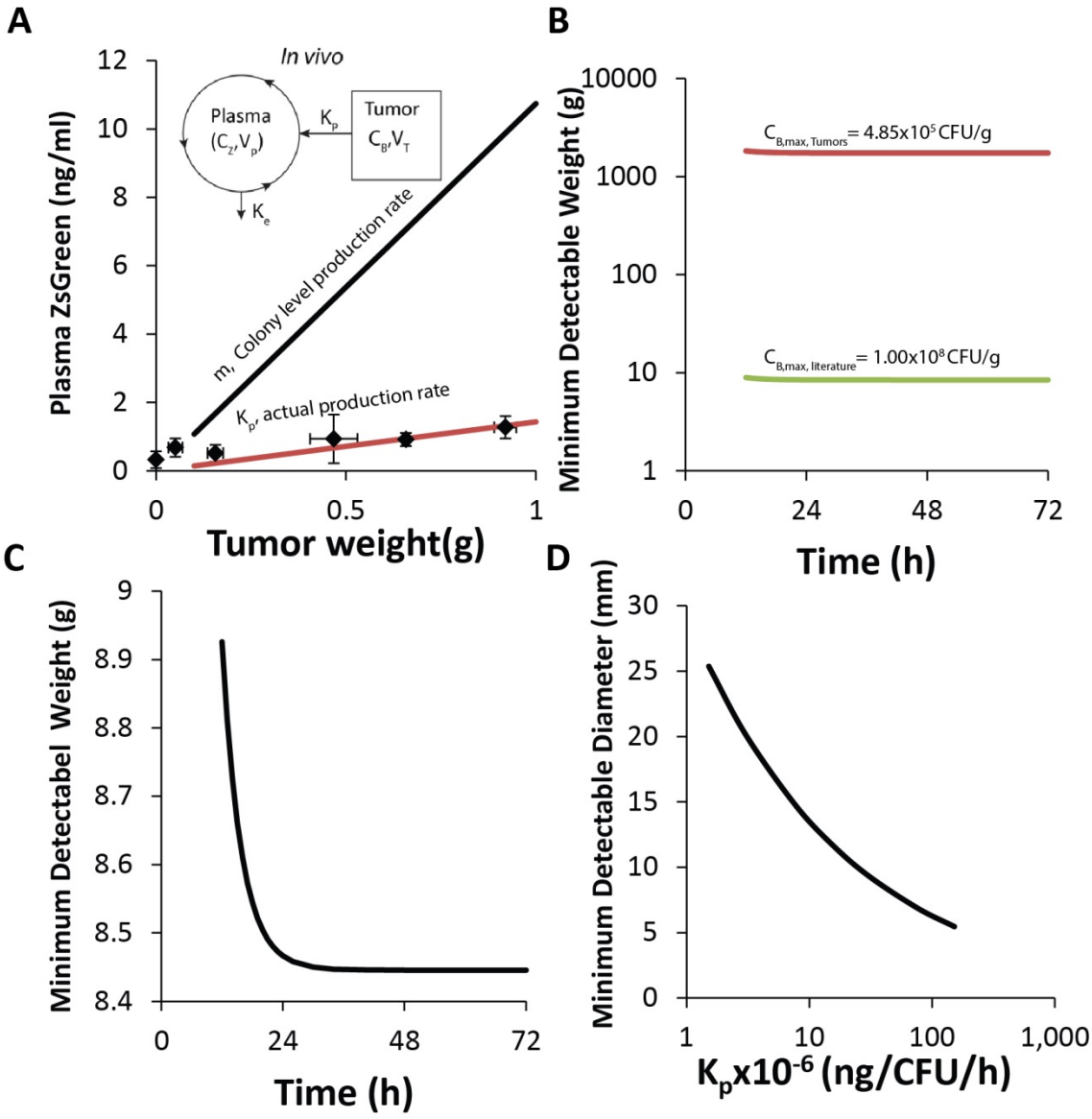

Figure 14. Mathematical analysis of efficacy in mice

A) Model predictions for tumor detection in mice taking into account the bacterial density 485 CFU/ml, the half-life, 2.7 hours, the plasma volume, 2ml, and the minimum detectable concentration of blood on single layer antibody dots ~1ng/ml and the colony level production rate $\dot{m} = 1.14 \times 10^{-5}$ ng/CFU/ml (black line) compared to the actual $K_p = 1.52 \times 10^{-6}$ ng/ CFU/ h (red line). **B,C)** Model predictions for detection in humans based on bacterial density in this tumor study compared to previously reported bacterial densities. Detection of tumors >1kg with current production rate and bacterial density of 485 CFU/ml, red line. Increased bacterial density to 100,000 CFU/mg would improve detection 200-fold to less than 10 g. **D)** Increasing production rate, K_p, 100-fold would then put bacterial detection of tumors in the range of the current limits of tomographic detection techniques (6-8mm in diameter).

3.4 Discussion

Bacteria administered to tumor models were able to detect tumors by release of ZsGreen from within the tumor site (Figure 11). ZsGreen concentration in plasma samples increased with tumor size (Figure 11B) confirming predictions from the mathematical model (Figure 9E). Statistical difference was seen between the large tumor group and the control, indicating that bacteria were able to produce enough ZsGreen from the tumors to detect large tumor masses. The average concentration of ZsGreen detected in control mice was not statistically greater than background blood measurements (Figure 10), but the average is not zero, indicating bacteria colonizing healthy organs contribute to the observed ZsGreen production.

Mathematical analysis determined the efficacy for tumor detection given the half-life, bacterial density, and ZsGreen concentration relationship to tumor size (Figure 14). At the bacterial production rate in mice (Figure 11B, 14A) 0.695 g tumors were detected above the detection limit of 1 ng/ml. In humans, this is much larger, approximately 1kg (Figure 14B). Bacterial tumor detection is dependent the bacterial density, which in this study is far less than other reported bacterial tumor studies, and the production rate which is 10,000-fold less than seen in previous microfluidic studies (Panteli et al., 2015). Other literature reports bacterial densities in tumors of 100,000 CFU/mg of tissue (Forbes et al., 2003). The observed low bacterial density is likely due to high dosing of ampicillin in this study, exceeding the toxic level for bacteria and plasmid retention. This would explain the limited colonization in small and large tumors with viable tissue and explains why bacteria and ZsGreen were mainly observed in necrotic regions.

This also indicates that ampicillin has difficult time diffusing through tissue because necrotic regions still had bacteria present (Figure 12). Ampicillin might not be needed for short studies as the plasmid stability suggests the bacteria are stable at low densities (Figure 7; Panteli

et al., 2015). Another alternative would be to incorporate the ZsGreen expression into the genome to create a stable strain. Insertion of multiple copies of ZsGreen operons into the genome would likely be equivalent to plasmid expression and eliminate the need for antibiotic burden. Alternatively a balanced-lethal system could also be employed like ASD dependence in and ASD deficient strain (Galán et al., 1990). This may encounter its own problems in that the number of ASD copies required for plasmid retention may be much lower than the number of ZsGreen copies needed to have adequate secretion.

Pharmacokinetic measurement of ZsGreen shows a half-life of 2.7 hours in circulation. This is small compared to albumin which has a half-life of 19 days (Hassan et al., 1997). Model predictions indicate that increasing protein half-life would facilitate detection of smaller tumors (Figure 9). Several strategies could be employed to increase stability. Incorporation of a albumin binding site into the termini of ZsGreen could provide longer circulation time (Dennis et al., 2002). The albumin binding site of a phage, DICLPRWGCLW, has been identified and fused to a recombinant protein with a normal half-life in rabbits of 0.8h and increased half-life to 32 h, a 40-fold increase in protein retention. A 40-fold increase in ZsGreen half-life would yield a half-life of about 4.5 days. Another option is to fuse ZsGreen directly to albumin, which could improve protein half-life 10-fold (Huang et al., 2008). New ZsGreen fusions to full length albumin or small peptides would have to be re-evaluated for secretion from the bacteria. Small peptide fusions to ZsGreen are likely to be more successful and have already been shown to maintain secretion in VNP20009 *Salmonella* (See Appendix A2).

L-arabinose injection was sufficient to activate gene expression within the tumor but expression varied with distance into necrosis. In LS174T tumors, ZsGreen was observed in the plasma (Figure 11) and by immunofluorescent labeling (Figure 12) indicating L-arabinose

induction enable production of ZsGreen and significant amounts of ZsGreen transported out of tumors into circulation. The amount of ZsGreen produced within the tumor sites varied with distance from the transition boundary (Figure 12E,F). The relative ratio of the ZsGreen to bacteria shows a decreasing level of ZsGreen expression starting just beyond the transition boundary (-500μm) deep into tumor necrosis (+ x direction). This indicates that L-arabinose has difficulty diffusing deep into tumor sites. The amount of extracellular ZsGreen also decreased with distance (Figure 12 G), indicating that ZsGreen must build up in colonies before it is released into the surroundings.

3.5 Conclusions

The efficacy of a tumor detecting bacterial strategy was evaluated in murine tumor models. Genetically modified tumor-targeting bacteria were engineered to release a reporter protein for detection. The circulation half-life of the reporter protein, ZsGreen, was found to be 2.7 hours. Production of ZsGreen from tumor-targeting *Salmonella* detected tumors larger than 0.2g in mice. In murine tumor models, ZsGreen release into the blood was seen to have a statistically positive correlation with tumor size. At the newly determined parameters, mathematical analysis of these results predicts detection of tumor masses as small 0.695 g in mice, comparable to the observed experimental results. These results show proof of concept for tumor detection in humans but production rate and bacterial density limit the efficacy of this technique. A 100-fold increase in ZsGreen production in a stably expressing strain could improve detection of smaller tumors and improve overall performance down to the current limits of tomographic techniques.

CHAPTER IV

GENETICALLY ENGINEERED BACTERIA TO SENSE SUGAR GRADIENTS IN TUMOR MICROENVIRONMENT

4.1 Introduction

Cancer tissue is difficult to treat owing to its heterogeneous microenvironment. To reach all viable cells in the tumor, anticancer drugs must be delivered efficiently through the tumor vasculature, cross the vessel wall, and diffuse the tumor tissue (Trédan et al., 2007). Small molecules are able to reach highly proliferating cells closest to vasculature but transport limitations in the tumor microenvironment and metabolic differences in tumor growth regions hinder effective drug exposure throughout the tumor (Jain, 1994; Jain, 2001; Trédan et al., 2007). Enabling effective targeting of all viable cancer tissue could improve treatment efficacy.

Targeting cancer's food source may be a way to identify viable regions in the tumor. Glucose and glutamine are the primary carbon sources in proliferating cells (Wellen et al., 2010). Many cancers thrive on glucose uptake with over 70% of all human cancers overexpressing glycolysis-related genes (Hirschhaeuser et al., 2011) and glucose transporters (Bos et al., 2002; Burt et al., 2001). Mean glucose concentration of normal and tumor tissues are 1,220 ± 150 (mean ± SE) and 123 ± 43 nmol/g, respectively, in colon and 1,290 ± 168 and 424 ± 131 nmol/g, respectively, in stomach (Hirayama et al., 2009). Equipping bacteria to recognize areas of high and low glucose concentration could enable more effective treatment of viable regions of tumors and overcome the limitations that conventional small molecules.

Bacteria have membrane receptors, called chemotaxis receptors, which allow them to sense sugar in their environment. Chemotaxis is the ability of bacteria to sense their environment

and actively swim towards a chemo-attractants or away from repellants. There are five basic chemoreceptors in *E. coli* and *S. typhimurium*: Tsr (serine), Trg (ribose, glucose, galactose), Tar, (aspartate), Aer (redox), and Tap (dipeptide) (DeFranco et al., 1979). Chemotaxis has been shown to affect localization and colonization within the tumor microenvironment (Kasinskas and Forbes, 2007). In particular, the Trg chemotaxis receptor enables bacteria to detect glucose and ribose via their respective periplasmic binding proteins, ribose binding protein (RBP) or the glucose/galactose binding protein (GBP)(Scholle et al., 1987). Utilizing the glucose sensing of the Trg receptor could enable bacterial recognition of nutrient gradients within the tumor microenvironment and enable recombinant protein production throughout viable tumor tissue.

A fusion protein that couples the ribose/glucose sensing of Trg to genetic output has previously been created (Baumgartner et al., 1994). Baumgartner et al. show the sensitivity of their fusion protein, Trz1, which combines the periplasmic domain of chemotactic transducer, Trg, to the cytoplasmic domain of osmoporin sensor, EnvZ, to induce lacZ expression (β-galactosidase activity). Normally, the EnvZ osmoporin transduces solute concentrations across the cell membrane and regulates formation of pores through activation or inactivation of promoter, P_{OmpC} (Waukau and Forst, 1992). The sensing pathways for native EnvZ and Trg are shown in Figure 15. Changes in solute concentration cause conformational change in the histidine kinase tail of EnvZ. This causes phosphorylation of OmpR, a cytoplasmic phosphotransferase, which then activates transcription of ompC. When ribose or glucose ligand binds their respective binding protein, the protein complex interacts with the Trg periplasmic receptor domain inducing a conformational change in the cytoplasmic tail. This allows phosphotransfer to chemotaxis protein CheW activating chemotaxis (Figure 15).

To create a bacterial-based sensor of the tumor microenvironment for use in microscopic analysis, *E. coli* were equipped with fusion protein Trz1 regulating expression of green fluorescent protein, GFP. We hypothesized that sugar gradients in the tumor environment could be used to identify regions with high cell viability in tissue. To test this hypothesis *E. coli* were administered to a tumor-mimic microfluidic device designed to mimic nutrient and oxygen gradients of the cancer microenvironment. Sugar response in the microfluidic device was compared to apoptosis activity from previously published work (Kasinskas and Forbes, 2007). Mathematical analysis was used to determine the efficacy of a sugar sensing bacterial treatment compared to small molecule treatment. Developing a sugar-sensing bacterial-based treatment of cancer has potential to improve specificity to cancer and prevent off-target effects.

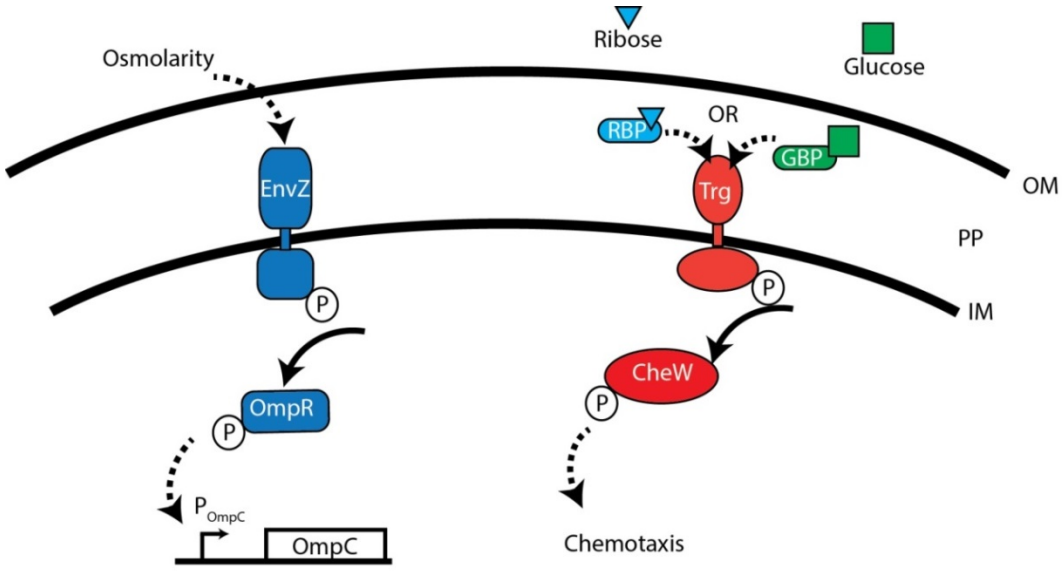

Figure 15. EnvZ osmosensor and the Trg Chemoreceptor
Osmolarity is detected by solute ions flowing freely through the outer membrane (OM) interacting with the periplasmic (PP) domain of the EnvZ osmosensor causes conformational change in the cytoplasmic domain across the inner membrane (IM). This conformational change enables phosphotransferase to cytoplasmic Osmoporin regulator OmpR. Phosphorylated OmpR then activates gene transcription of the osmoporin promoter P_{OmpC} controlling formation of membrane pores. The Trg chemoreceptor responds to ribose, glucose, and galactose concentrations to cause flagella rotation. Sugar molecules freely diffuse across the outer membrane and interact with their respective binding protein, RBP for ribose and GBP for glucose and galactose. In the ligand bound form the binding protein complex then interacts with the periplasmic domain of Trg and causes conformational change leading to phosphorylation of a chemotaxis regulator CheW.

4.2 Materials and Methods

4.2.1 Plasmid construction and strains

Plasmid OmpC-GFP was generated by polymerase chain reaction (PCR) insertion of P_{OmpC} from pMY150 into plasmid pFVP25 containing green fluorescent protein, GFP mut3 (pOmpC-GFP). Plasmid pMY150 was a gift from the Inouye lab(Mizuno et al., 1983). *Trz1* was cloned from pRB020 plasmid and PCR inserted into pOmpC-GFP under control of P_{lac} promoter downstream of the first operon with a t1 terminator separating the two operons (pTrz1a). HB3519 is a background strain containing plasmid pRB020 producing the Trz1 protein. HB3521 is a derivative of *E. coli* MH225 with plasmid pAI12, containing the RBP which has been knockout of the genome, and a genomic deletion of $\Delta EnvZ::Km^r$. *Envz* is the osmoporin sensor that activates transcription of the P_{OmpC} promoter. Knock down of EnvZ salt sensing capabilities is required to prevent activation of the OmpC promoter from salt concentrations. Both of these strains, HB3519 and HB3521, were generous gifts from the Hazelbauer and Park labs(Baumgartner et al., 1994; Park and Hazelbauer, 1986). To generate pTrz1 the P_{lac} promoter of pTrz1a was replaced with the P_{BAD} promoter. Plasmid pTrz1-red was created by adding a third operon downstream of the first two consisting of DsRed-Express2 fluorescent reporter under control of the P_{lac} promoter. See Table 1 for complete list of plasmids and strains.

Sensitivity studies were performed by transforming the desired plasmid (pOmpC-GFP, pTrz1a, pTrz1, or pTrz1-red) into strain HB3521 containing the RBP plasmid (PAI12), except in the case of evaluating Trz1 receptor abundance. Isopropyl beta-D-thiogalactoside (IPTG) inducibility was used to evaluate Trz1 abundance to transduce signal via salt (NaCl) sensing. Plasmid pTrz1a was transformed into a in Top-ten F` strain of *E. coli (*Life Technologies)

containing the *lacIq* repressor and functional EnvZ to evaluate signal transduction while varying receptor (Trz1) expression. All bacteria were grown in LB broth or M9 minimal media, to control for glucose concentrations, at 37˚C and 225rpm, supplemented with 100 ng/µl Ampicillin and/or Chloramphenicol, as required.

Table 1. Plasmids and Strains

Plasmids and strains used in this study:		
Plasmid	**Description**	**Source or Reference**
pMY150	contained OmpC promoter POmpC	gift from Inouye Lab (Mizuno et al, 1983)
pFVP25	GFP expression plasmid	Addgene.org/20667, Raphael Valdiva, 1995
pRB020	Contains Trz1 fusion protein under Tac promoter	Gift form Hazelbauer lab, (Baumgartner et al., 1994)
PAI12	Expresses Ribose Binding Protein	Gift form Hazelbauer lab, (Baumgartner et al., 1994)
pOmpC-GFP	pFVP25 with GFP under control of OmpC promoter	This work
spTrz1a	pOmpC-GFP with downstream P_{Tac}-Trz1 operon separated by t1-terminator	This work
pTrz1	P_{Tac} replaced by P_{BAD} promoter in pTrz1a	This work
DsRed Express2	Contains DsRed, red fluorescent protein	Clontech
pTrz1-red	pTrz1 with downstream P_{lac}-DsRed Operon	This work
Strain		
HB3521	MH225 K-12 E.coli (ΔEnvZ) with pAI12 plasmid	Gift form Hazelbauer lab, (Baumgartner et al., 1994)
HB3519	Source of pRB020 plasmid containing Trz1 sequence	Gift form Hazelbauer lab, (Baumgartner et al., 1994)
DH5α	E.coli cloning strain used for all plasmid construction	New England BioLabs Inc.
One Shot-Top-Ten F'	Contains F´ episome which carries the *lacI*^{q} repressor for inducible expression from *trc*, *tac*, and *lac* promoters using IPTG.	LifeTechnologies

4.2.2 *In vitro* sensing in aqueous solutions

Plasmid pOmpC-GFP was grown with 0.17 M Nacl and 0.27 M nacl in DH5a to test functionality of the promoter, P_{OmpC}. Knockout EnvZ strain HB3521 was used as a negative control as was a vector free DH5α E. coli. All GFP expression levels were measured in a microtiter plate reader (SpectraMax M5, Molecular Devices, Sunnyvale, CA), with excitation 495 nm and emission 511 nm.

To test Trz1 abundance on signal transduction growth medium was supplemented with 0,8,80 and 800 µM concentrations of IPTG, an inhibitor of the *lac* repressor, and GFP expression was measured from pTrz1a-Top-Ten in LB broth. This led to changing promoter strength from P_{lac} to P_{BAD} and creation of pTrz1. pTrz1 was transformed into HB3521 *E. coli* and grown up in LB broth supplemented with 0, 10,100, and 1000 µM concentrations of ribose in 3 ml overnight cultures to determine if the P_{BAD} promoter effectively produced Trz1 protein at levels that allowed signal transduction.

Sensitivity of both ribose and glucose sensing in pTrz1-HB3521was measured in M9 minimal media supplemented with glucose and ribose concentrations ranging from 0 to 10,000 µM of each ligand and quantified by GFP fluorescence after overnight culture at 37˚C at 225rpm.

4.2.3 Sensing study in 3D tumor-mimic microfluidic device

To test for bacterial ability to sense sugar gradients in 3D tumor tissue, pTrz1-red-HB3521 were administered to the flow channel to mimic an IV injection into the body. Tumor spheroids were administered to the device in phosphate buffered saline (PBS) solution to prevent glucose accumulation in the back of tumors and create the gradient in nutrients from the flow channel. Bacteria were administered at a density of $2x10^6$ CFU/ml in PBS solution to prevent

premature activation of the sensing machinery from growth media. After bacterial administration, DMEM (without phenol red, to avoid autofluorescence for DsRed) +10% FBS, 25mM HEPES with 100µg/ml ampicillin and 100µg/ml Chloramphenicol, for plasmid retention was added as growth media at 3ul/min. Fluorescent microscopy was used to acquire position of bacteria, red fluorescence, and the extent of sugar concentration, green fluorescence. Absolute values of RFP intensity to bacterial density were determined in the device by flowing known densities of cultures of Trz1-red *E.coli*, constitutively expressing DsRed, through the device chambers and acquiring image intensities at identical camera settings to the tumor cell mass experiments, there was no autofluorescence from LS174T tissues prior to addition of bacteria, indicating the RFP intensity to be solely from bacterial colonization.

4.2.4 Calculated glucose and bacterial counts in 3D-tumors

GFP and RFP intensities were normalized to their respective maximum intensity in tissue to generate relative intensity vs. distance plots. At each time, t, the ratio of normalized GFP to RFP was determined. The relative ratio of GFP to RFP was assumed to be directly proportional to the ratio of GFP produced per bacteria at a given time and shown to be time independent. The concentration of glucose in DMEM is 5500 µM. It was assumed that the ratio of GFP to RFP scaled linearly with glucose concentration to generate the profile seen in Figure 15 B.

4.2.5 Mathematical modeling of sugar-sensing bacterial treatment of solid tumors

For free drug, the mathematical model was comprised of equations (6) and (7). The concentration (A) at the front edge (x = 0) was modeled as exponential decay, $C_{x=0} = e^{-kt}$, mimicking a bolus dose of therapeutic molecule and clearance systemically. A symmetry

boundary condition was used at the rear end (x = 600 μm). The two equations were solved using the pdepe function in MATLAB (The Mathworks Inc., Natick, MA). See Appendix B. For bacteria, the mathematical model was comprised of equations (7)-(9). This is similar to free drug, but includes a generation term as a function of distance in the tumor, which was determined from the rate GFP expression observed in devices and fit to a hyperbolic tangent function, equation (9). The initial condition for cell viability in both models was estimated from caspase-3 activity measured in tumor-on-a-chip microfluidic devices (Kasinskas and Forbes, 2007). Caspase-3 activity is an indicator of apoptosis and cell death. These data are fit to a hyperbolic tangent function and input as the initial conditions in the pdepe solver.

4.3 Results

4.3.1 Construction of Trz1 switch for ribose and glucose sensing

To create a sugar sensing bacteria using the fusion protein, Trz1, green fluorescent protein (GFP) was cloned under control of the osmoporin promoter, P_{OmpC} (Figure 16). Native EnvZ-P_{OmpC} signal transduction was tested by the addition of salt and measuring the expression of GFP (Figure 17). Increasing salt concentration increased GFP intensity per bacteria in liquid culture. To eliminate interference of salt activation of the P_{OmpC}, a ΔEnvZ strain of bacteria was employed for subsequent sugar sensing experiments. Knockout of the osmosensor, *EnvZ*, eliminated salt sensitivity of plasmid pOmpC-GFP and no GFP expression was observed; this was equivalent to a vector free control (Figure 17A).

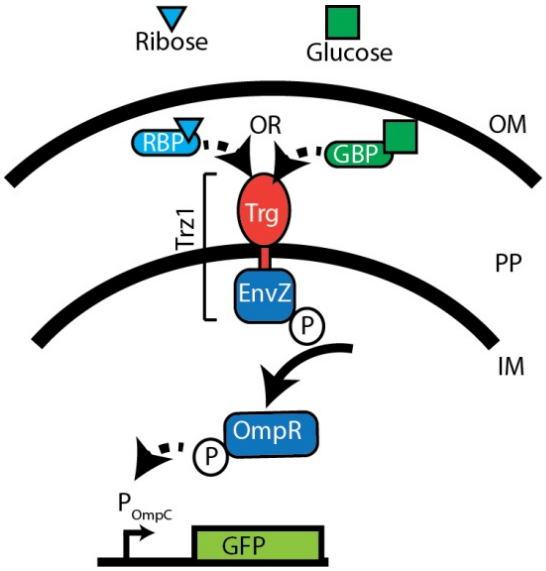

Figure 16. Fusion TrZ1 protein enables ribose and glucose sensing
A fusion of receptor proteins Trg and EnvZ enables signal transduction of sugars into genetic output. Ribose or glucose ligands freely diffuse across the outer membrane (OM) of the bacteria and binds their respective periplasmic (PP) binding protein (RBP or GBP). The bound complex then interacts with the periplasmic domain of Trg causing conformational change in the cytoplasmic domain of osmoporin EnvZ. This conformational change leads to autophosphorylation of osmoporin regulator, OmpR. The phosphorylated state of OmpR then activates the osmoporin promoter, P_{OmpC} activating gene expression (GFP in this study) (Baumgartner et al., 1994).

To enable sensing of ribose and glucose, the Trz1 fusion protein was cloned into the OmpC-GFP plasmid on a separate operon under control of the P_{Tac} promoter, forming plasmid pTrz1a (Figure A5). P_{Tac} is a derivative of the *lac* promoter. The *lac* operon functions with a repressor *lacIq*, which inhibits expression of genes under control of the P_{lac} promoter. The repressor binds DNA inhibiting expression when lactose is not available. In the presence of lactose, bacteria metabolize the sugar to allolactose, which inhibits the *lac* repressor's DNA binding ability and activates transcription by the promoter P_{lac}. K-12 *E.coli*, containing the *lac* repressor, were transformed with pTrz1a and grown with increasing concentrations of IPTG (Figure 17B). Addition of IPTG should increase the expression of the Trz1 fusion protein. GFP intensity of the cultures decreased with increasing IPTG concentration. Only under the highly repressed state, with no added IPTG, did the system produce GFP (Figure 17B). This meant that low abundance of Trz1 receptor protein was more favorable to induce GFP expression. As a

result of this study, the promoter regulating Trz1 gene expression was changed to allow low level constitutive production under the repressed state of the P_{BAD} promoter, creating plasmid pTrz1 (Figure 17D). Addition of ribose to LB cultures of pTrz1 in *E. coli* increase GFP intensity (Figure 17C).

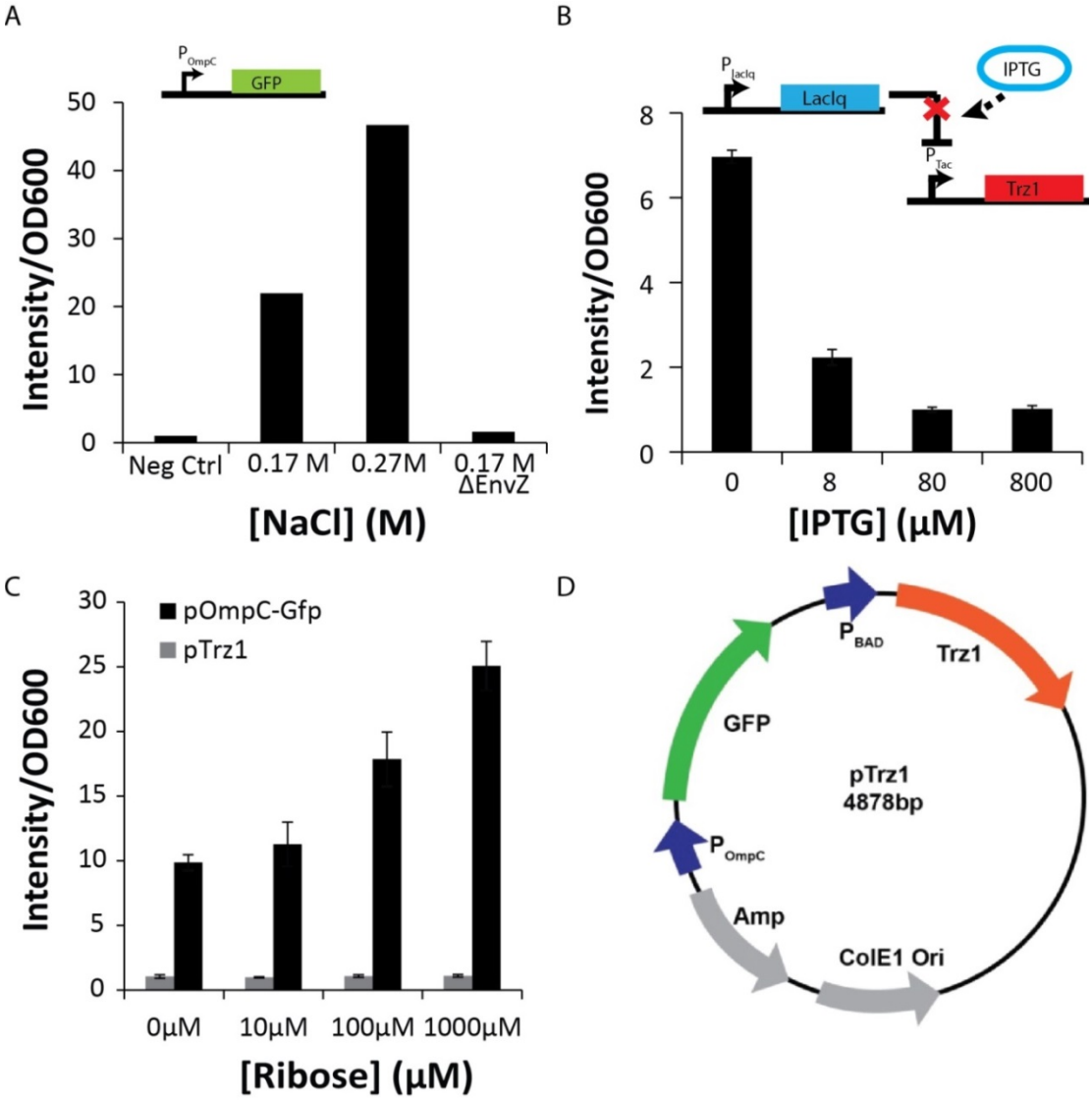

Figure 17. Construction of pTrz1 sugar sensing switch
A) Salt normally activates the OmpC promoter. GFP expression increases with increasing salt concentration, in the presence of functional EnvZ osmoporin. Knockout of EnvZ eliminates salt sensitivity. **B)** Increasing the number of Trz1 receptors inhibited signal transduction leading to lower GFP expression. **C)** Sugar sensing achieved with **D)** pTrz1 plasmid construct in ΔEnvZ *E. coli* HB3521.

4.3.2 Bacteria sense ribose and glucose sugar gradients and express GFP

Increasing ribose or glucose concentration in liquid cultures increased GFP intensity of pTrz1-Δ*EnvZ -E. coli* (Figure 18). GFP expression increased with ribose concentrations from 1 µM to 1 mM and with glucose concentrations from 10 µM to 10 mM concentrations. Plasmid pTrz1- Δ*EnvZ -E. coli* shows a higher sensitivity to ribose than glucose, with GFP expression at 10-fold less ligand concentration (Figure 18A; $P<0.05$). Ribose and glucose together had an additive effect on GFP expression (Figure 18B).

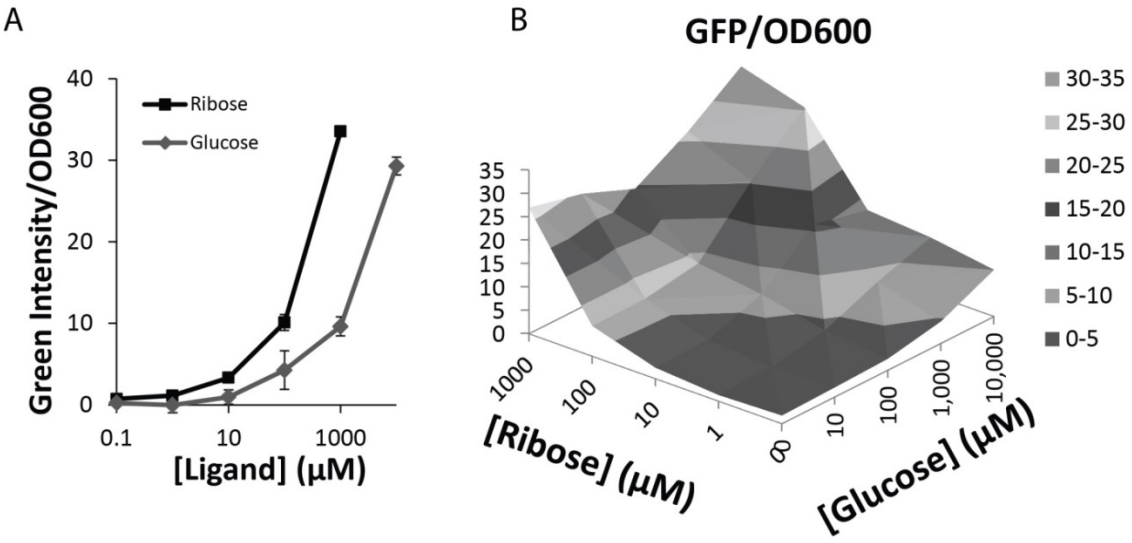

Figure 18. **Ribose and glucose sensitivity of pTrz1- Δ*EnvZ -E. coli***
A) Trz1 switch is more sensitive to ribose and glucose. **B)** Both sugars act cooperatively and induce signal transduction of Trz1 simultaneously in liquid culture.

4.3.3 Sugar gradients were detected in small *in vitro* tumor cell masses

Tumor-on-a-chip microfluidic devices have previously shown gradients in pH, cell viability and apoptosis, but gradients in sugar have yet to be observed (Walsh et al., 2009). *E. coli*

bearing pTrz1-red-Δ*EnvZ* were administered to a tumor-on-a-chip microfluidic device to test the ability to sense sugar gradients within tissue (Figure 19). Bacteria were administered for 1hour in glucose-free media and flushed to mimic an intravenous injection and clearance *in vivo*. Over the following 44 hours, time-lapse fluorescent microscopy recorded the location and number of bacteria via constitutive expression of the RFP and the amount of sugar sensed by the bacteria with GFP expression (Figure 19A).

GFP and RFP fluorescence of the tumor-on-a-chip tissues increased over time (Figure 19B,C). GFP intensity was higher closer to the flow channel and dropped with distance from the flow channel. At distances greater than 400 µm, GFP intensity was small (Figure 19B). RFP intensity was observed throughout tissue more than 600µm deep. RFP Intensity was converted to bacterial density, based on control measurements of bacterial densities in the device, and showed bacterial growth throughout the tissues (Figure 19C). Bacteria were shown to colonize throughout the tumor cell masses independent of distance from the flow channel.

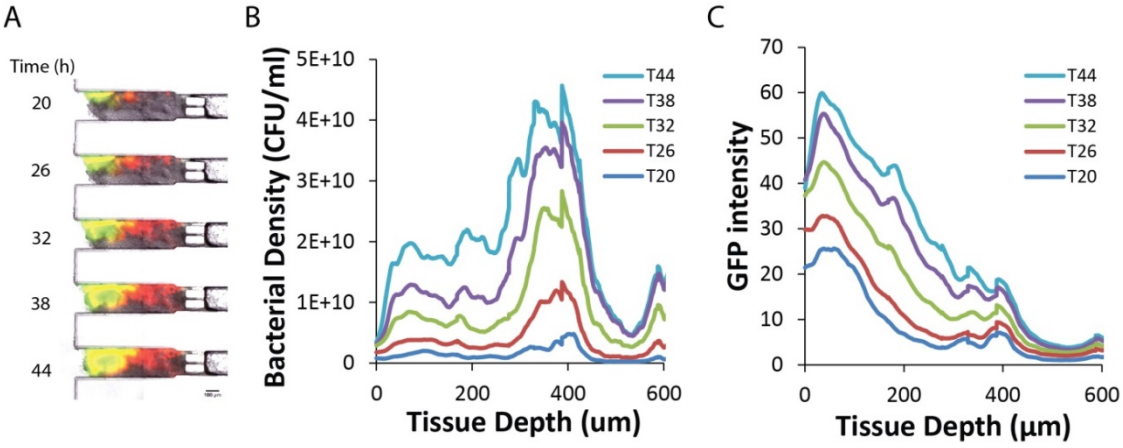

Figure 19. pTrz1-Red-ΔEnvZ *E. coli* identify sugar gradient in tumor-on-a-chip devices
A) LS174T tumor tissue administered with pTrz1-Red ΔEnvZ HB3521 shows initial colonization, red fluorescence, and sugar sensing, green fluorescence over time in microfluidic devices. **B)** Bacterial growth increases over time with a peak at 300-400 µm away from flow channel. **C)** GFP expression increases over time with an exponential decay and with tissue depth to minimal fluorescence past 400 µm.

The ratio of GFP to RFP intensity enabled calculation of the GFP expression per bacteria (Figure 20). Over time, GFP per bacteria ratios drop with depth in tissue but remain constant in time (Figure 20A). The time average GFP per bacteria ratio was used to estimate the sugar concentration within the tissue of the device (Figure 20B). The growth medium glucose concentration was 5500 µM. Assuming the GFP intensity scales linearly with glucose concentration near the edge of tissue, the glucose concentration drops to less than 10 µM glucose at distances farther than 400 µm away from the flow channel (Figure 20B).

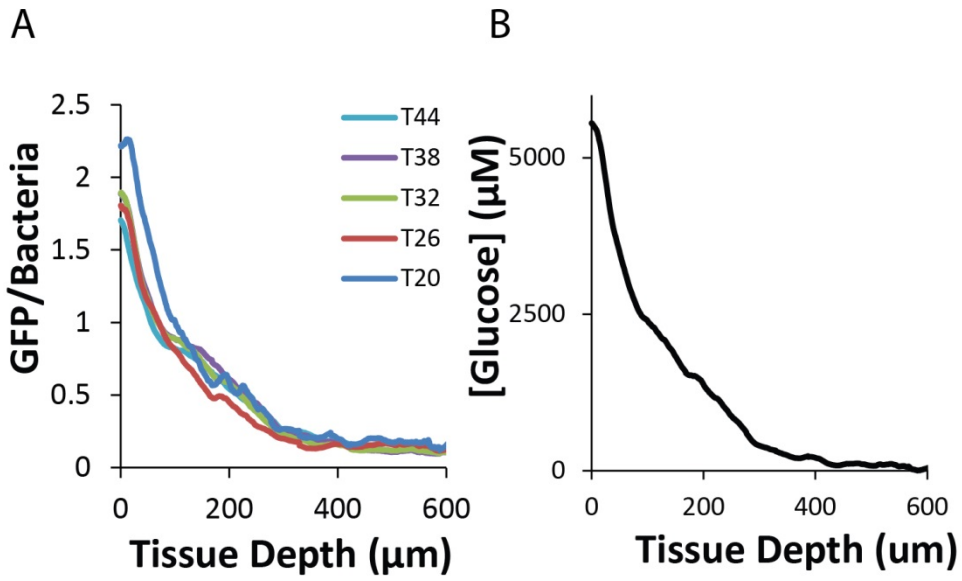

Figure 20. Estimation of glucose concentration in device tissues
A) GFP to RFP (GFP/bacteria) indicates that the sugar gradient is at steady state in microfluidic device at 20 hours. **B)** Estimation of glucose concentration based on GFP/Bacterial average value. At the flow channel glucose concentration will be equal to the DMEM media concentration, 5500 µM. Increasing depth in tissue shows less GFP expression and thus a drop in sugar concentration.

4.3.4 Mathematical prediction of tumor treatment with sugar sensing bacteria.

Most chemotherapeutics lack the ability to target different regions of the tumor tissue and typically target cells with up-regulated cell division, effectively treating only cells closest to vasculature. Utilizing a bacterial therapy, engineered to recognize the health of the target tissue,

enables spatial dose control by producing more therapeutic proteins in the regions are most aggressive (Figure 21). This means that proliferating tissue, tissue that has the highest nutrient availability, will get the strongest dose while quiescent tissue will get a nominal dose based on local nutrient availability.

Tumor tissue has gradients in sugar and cell viability and with distance from vasculature (Figure 5B and 6A, respectively). In previous studies, caspase-3 activity, a measure of cell apoptosis, was determined as a function of depth in tumor spheroids (Kasinskas et al., 2014). This correlates to cell viability decrease as a function of distance from vasculature (Figure 21A,B). A large gradient in tissue viability exists in tumor spheroids with over 95% cell death at 400 μm from edge of the tissue (Figure 21A). This drop in cell viability coincides with the bacterial measurement of sugar concentration in tumor spheroids in the microfluidic device (Figure 21B).

Conventional chemotherapeutic drugs are limited by systemic clearance and diffusion into the tumor site. Drug concentration (C), pharmacokinetic stability ($t_{1/2}$), transport properties, diffusivity (D), and toxicity (μ_{max} and K_m), determine how well the drug will penetrate tissue and kill the target cells.

Drug concentration can be described as a diffusion model, 1-D in x, with boundary conditions that satisfy systemic clearance: $C_{x=0} = e^{-kt}$, where half-life in circulation is $t_{1/2} = \ln(2)/k$:

$$\frac{\partial C}{\partial t} = D\frac{\partial^2 C}{\partial x^2} \quad (6)$$

And tumor tissue cell viability, *l*, (the live cell fraction), can be modeled as a saturation kinetic model with a maximum death rate, μ_{max}, and saturation constant, K_m.

$$\frac{\partial l}{\partial t} = \left(\frac{-\mu_{max} C}{K_m + C}\right) l \quad (7)$$

Initial cell viability for the model system was set to the measured profile based on caspase-3 activity (Figure 21A; adapted from (Kasinskas and Forbes, 2007)).

A systemically administered drug diffuses into tissue but rapidly clears from the tumor site as it is eliminated in circulation (Figure 6C). Initial drug concentration is high closest to vasculature but, due to diffusion limitations and rapid clearance, drug concentration decreases with distance in tissue and in time.

Drug production by sugar sensing bacteria can be modeled by diffusion and production (Figure 21B,D).

$$\frac{\partial C}{\partial t} = D\frac{\partial^2 C}{\partial x^2} + f(x) \quad (8)$$

Where *f(x)*, is the rate of production of GFP as a function of tissue depth, modeled as a sigmoidal tangential function, fit to the GFP expression from tumor spheroid microfluidic studies (Figure 21B).

$$f(x) = \frac{\alpha}{2}\left(1 - \tanh\left(\frac{x-p}{2w}\right)\right) \quad (9)$$

Where $\alpha = 1.3533$, $p = 0.6712$ and $w = 0.1567$ (Figure 21B).

Drug expression by sugar sensing bacteria increases with time and decreases with distance in tissue (Figure 21D). Drug production is highest near the edge of the tissue where nutrient availability is the highest and decreases to nominal levels 400 μm in depth.

For a systemically administered drug, tumor cell viability decreases in regions with the highest drug concentration but transport limitations hinder drug penetration and not all tissue sees

an effective dose to eliminate the tumor (Figure 21E). Tumor tissue closest to vasculature is exposed to the largest drug concentration and is effectively treated, but as depth in tissue increases, less cells are killed due to poor drug penetration, resulting in an area of surviving tumor cells of approximately 25% of starting cell population.

The same bacterial administered drug is produced continuously from the microbes in a sugar dependent dose profile and is able to eliminate the hard to treat region of the tumor due to effective drug delivery (Figure 21F). Closest to vasculature sugar concentration is highest leading to increased drug production. As sugar concentration drops with distance from

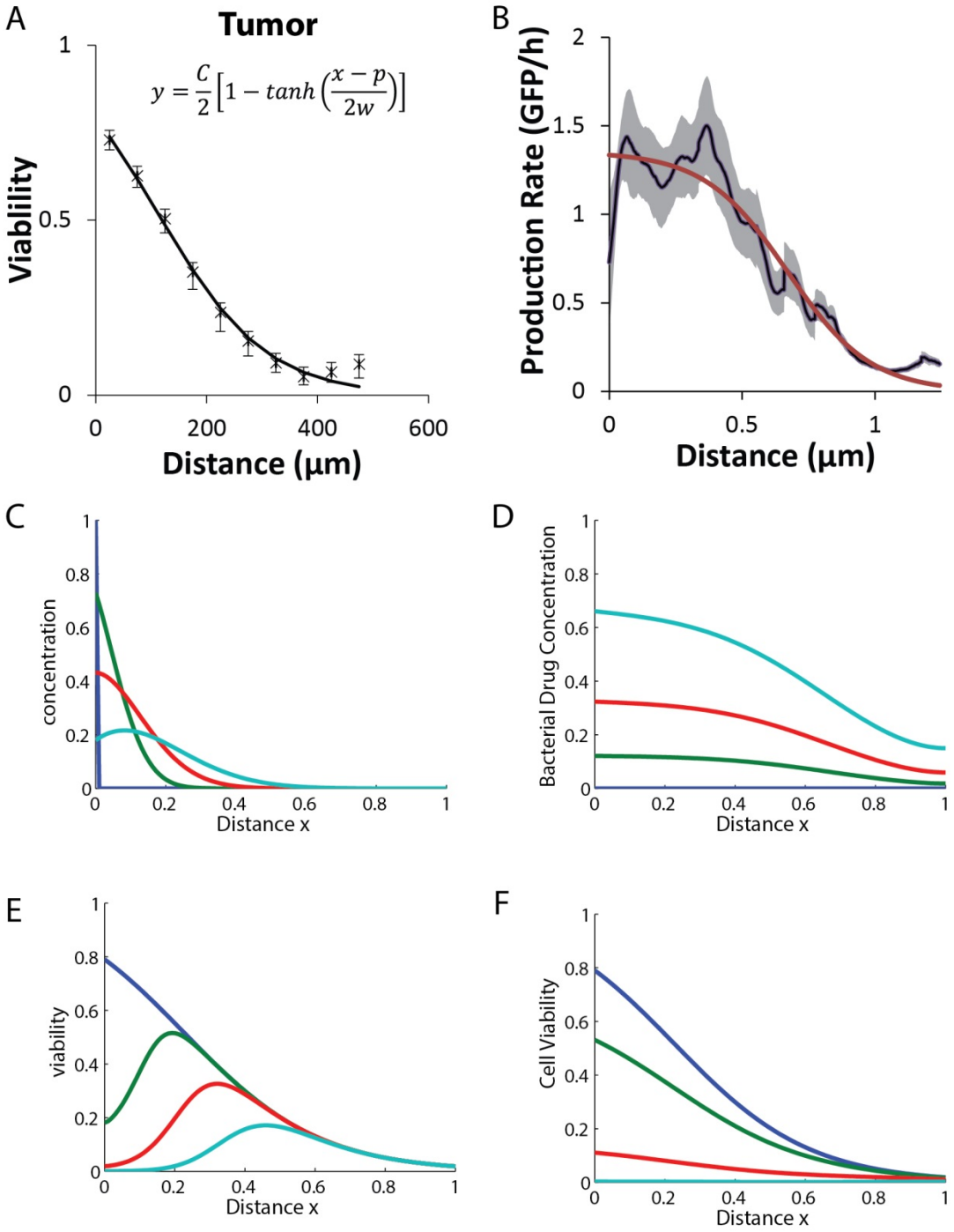

Figure 21. Sugar sensing bacteria could enable treatment of quiescent regions of a tumor
A) Tumor tissue viability as a function of tissue depth as measured by caspase-3 activity. **B)** GFP production rate as a function in tissue depth in tumor spheroids on a tumor-on-a-chip microfluidic device. **C)** Free drug molecule administered to tumor will diffuse into tissue and washout quickly. **D)** The same drug produced by sugar-sensing, tumor-targeting bacteria, persists and increases in magnitude with time. **E)** Free drug washes in and out of tumor tissue

but is unable to eliminate all viable cells. **F)** Bacterial delivered drug persists in tumor site and eliminates all viable tissue within the same time frame.

vasculature, so does the rate at which drug is produced, however; the drug is produced at low levels allowing accumulation and continued drug exposure to these hard to treat regions of the tumor. This enables almost complete eradication (7% remaining) of viable tumor tissue over time.

4.4 Discussion

Glucose and ribose sensing triggered GFP expression. Utilizing the bacteria's native chemotaxis machinery and rewiring the signal transduction of two proteins enabled signal transduction, which normally triggers protein-protein interactions, activation of a promoter controlling expression of GFP. This enabled the bacteria to sense environmental ribose and glucose concentrations when grown in liquid culture and express GFP relative to that concentration. This switch enabled visualization of sugar gradients within the tumor-on-a-chip microfluidic device that have previously only been hypothesized. These bacteria have the potential to aid in diagnosis by determining the rate of glycolysis which has been shown to be correlated with more aggressive tumors. Glycolysis rates might be reflected in the shallowness or sharpness of the glucose concentration and could be reflected by the bacterial expression of GFP using this switch.

GFP expression was higher closer to the flow channel than in the back of the tissue, indicating that a gradient in sugars exists in tumor-on-a-chip devices (Figure 19, 20). In the microfluidic device, flow of media is passed by the tissues at a constant rate (3µl/min) supplying tissue with the needed oxygen and nutrients. The increased intensity of GFP produced in the front

of the tissue indicates that the glucose in that media is reaching the bacteria 400 μm deep but not beyond this depth. Little to no detectable GFP expression is seen beyond 400 μm, indicating that glucose levels are below the detectable limit of 10 μM (Figure 21B, 19A). The glucose is limited by diffusion and consumption by bacteria and tumor tissue in the chambers. The drop in GFP may be increased as a result of nutrient deprivation by bacterial colonization (Low et al., 1999; Weibel et al., 2008). The level of glycolysis in the tumor tissue should also determine how drastic the drop in GFP with tissue depth. The bacteria are able to measure extracellular glucose levels and if the glycolysis rate of cells is high, the available glucose for detection would be less. More aggressive tumors should cause a more drastic drop in GFP levels than slower growing ones.

A peak in RFP intensity at the 300-400 μm away from vasculature indicates an optimal growth region at this depth in tissue (Figure 19B). RFP intensity directly reflects the number of bacteria within the tissue in that area. RFP expression enabled tracking of the bacteria within tumor-on-a-chip microfluidic device. The peak in bacterial density indicates that regardless of the glucose concentration (Figure 20B) the bacteria are still attracted to the transition between viable and necrotic tissue (Figure 21A); likely due to attraction to a metabolite from necrotic tissue.

Identifying other key characteristics of the necrotic tissue which attract bacteria could make a safer switch for genetic expression. The bacteria used in this study are a K-12 strain of *E.coli*, MH225. This strain was able to colonize throughout tissue where other K-12 *E. coli* strains have shown difficulty (Toley and Forbes, 2012). This strain could potentially provide a more effective treatment for use *in vivo* studies than other *E. coli* strains owing to better penetration ability.

Increasing the number of Trz1 receptors decreased GFP expression (Fig 17B). Bacterial cells maintain optimal numbers of chemoreceptors for signaling. The native Trg chemoreceptor is

present in low quantities in bacteria compared to other chemoreceptors (Barnakov et al., 1998). Sensitivity could not be increased by increasing the expression of Trz1. Amplifying the number of receptors, in an effort to improve signal transduction, was seen to hamper GFP expression. By reducing expression of Trz1, sugar sensing capability was restored and higher GFP expression was observed (Figure 17C). Controlling the number of receptors could improve the dynamic range of sugar sensing and allow for more sensitive sugar measurements.

Drug delivery systemically was shown to clear rapidly and have limited ability to kill the tumor (Figure 21C,F) but sugar sensing bacterial delivered therapy overcomes transport barriers and enabled production based on detection of nutrient rich regions in the tumor site (Figure 21D,E). Continued production by bacterial production increased the dose exposure to the cells regions that are harder to treat improving the killing efficiency of an identical drug compound than when delivered systemically. Sugar sensing bacteria would enable killing in tumors with glucose concentrations greater than 10 μM. Sugar sensitivity between 1μM and 10 mM is well within the dynamic range for Trz1. Normal blood glucose levels range from 5.5 mM to 8 mM concentration. Preventing normal blood glucose from activating gene expression prior to reaching the tumor site would improve this system for specific gene activation in tumor environments. This could be achieved by specific recognition of tumor site receptors.

4.5 Conclusions

In this study bacteria are engineered to sense ribose and glucose concentration and trigger GFP expression. These bacteria were used to visualize gradients in glucose in a tumor-on-a-chip microfluidic device that have previously only been speculated to exist. The gradient in estimated glucose concentration in the device coincides spatially with previously detected caspase-3

activity, an indicator of apoptosis. A mathematical model was used to predict cancer cell treatment with sugar sensing bacteria compared to bolus small molecule drug administration. The results of this model shows sugar sensing bacteria are able to activate recombinant therapeutic expression in distal regions of tumors where small molecules have difficulty reaching. These bacteria have potential to treat cancer with dosing schemes that scale with activity of the cells they are targeting with higher doses of recombinant drug expression at the sites of higher nutrient availability.

CHAPTER V

IDENTIFICATION OF ANTI-CANCER PROTEIN TOXINS FOR BACTERIAL TREATMENT OF CANCER

5.1 Introduction

Current cancer therapies are limited by transport barriers, drug resistance, and their ability to target the quiescent cancer cells. Tumor targeting bacteria producing toxic protein should be able to specifically eliminate tumor cells and lead to tumor regression by direct delivery of therapeutic deep within tissue.

For over 150 years bacteria have been seen to eradicate tumors after severe infection. The attenuated *Salmonella,* VNP2009, has been shown to reduce tumor growth and prolong survival of tumor bearing mice (Clairmont et al., 2000; Low et al., 1999; Luo et al., 2001). In addition to varying bacterial strains several different strategies and therapeutic payloads have been employed to treat cancer. Delivery of anti-cancer proteins like TRAIL (Ganai et al., 2009) to induce apoptosis have shown some efficacy, but this scheme is limited by host cell mutations in the apoptosis pathway drug resistance. Other bacterial therapies have expressed enzymes that activate pro-drugs at the site of tumors (Cheng et al., 2008; Green et al., 2013; Lehouritis et al., 2013). More recent work has used bacteria as gene delivery vectors reprogramming cancer cells to commit suicide (Baban et al., 2010; Chen et al., 2012; Lemmon et al., 1997). These strategies have worked well in some cases but the rate of infection is low as is the rate of gene transduction (Wybranietz et al., 2001). Discovering new protein therapeutics may enable bacteria to combat this disease more effectively via targeted delivery.

In this work, a screen for toxic proteins was conducted (Swofford et al., 2014). The goal was to identify new and plausible anti-cancer proteins for bacterial therapy that are released from bacteria, able to diffuse through tissue and effectively kill cancer cells. If a toxin protein is not release from bacteria, it has little chance to reach the cancer cell. Over 130 toxins were considered from literature. Toxins were classified by their mechanism of action and ease of genetic expression. In this study seven families of toxins were examined: pore-forming, ADP-ribosylating, glycosylating and deamidating toxins, oxidoreductases, cytolethal distending toxins, neurotoxins, and superantigenic toxins.

Five favorable candidates were identified with different mechanisms of action and screened for their therapeutic potential. Once identified, toxins were transformed into a cloning vector and tested for their ability to release from bacteria under control of an inducible promoter. The intracellular and extracellular protein fractions were then tested for their ability to kill tumor cells in monolayer. This was a collaborative study with Dr. Charles Swofford and Dr. Adam St. Jean. I was involved in the protein screening and selection process, cloning of protein toxins, testing protein release and efficacy in against cancer cells, and an animal study to determine if lower dosage of *E.coli* bearing the toxin, SAH, *Staphylococcus aureus* α-hemolysin, reduced systemic toxicity in mice. In this study SAH delivered by *E. coli* was shown to cause tumor regression and necrosis in murine tumors.

5.2 Materials and Methods

5.2.1 Plasmids and strains

Genomic DNA was isolated for the various strains of gram negative and positive bacteria using Wizard Genomic DNA purification kit (PROMEGA, Madison, WI, USA). Toxins were

amplified from their genomes and cloned into pBAD-myc/his/A (LifeTechnologies). This plasmid served as a delivery vector and contains an inducible genetic switch under control of the P_{BAD} promoter and also has the low to moderate copy number (57±4 copies) origin of replication pBR322, to obtain stability (Lupski et al., 1986; Sutcliffe, 1979). To obtain stability in animal models, pBAD-myc/his/A was incorporated with ASD. Plasmid pBAD-SAHa was constructed by cloning SAH into the pBAD-ZsGreen, which contains the pUC origin of replication (500-700 copies), in place of the fluorescent reporter.

These plasmids also contained the gene encoding for aspartate-semialdehyde dehydrogenase (*asd*) that allows for plasmid retention in the nonpathogenic msbB$^-$, purI$^-$, xyl$^-$, asd$^-$ *Salmonella* strain, VNP200010. All murine models used VNP200010, an ASD deficient derivative of, VNP20009.

5.2.2 Western blotting and protein release

Protein release was quantified by Western blotting. Bacteria were grown at 37˚C at 225 rpm supplemented with 100 ng/µl Ampicillin in LB broth and induced with 0.2% w/v L-arabinose in mid-log phase (OD600≈0.5), an inhibitor of the P_{BAD} repressor AraC. Cell fractions were isolated from culture by initial centrifugation at >12,000 rpm, sterile filtration of supernatant fraction through a 0.22 µm filter and mechanical lysis of the cell pellet using glass beads. Western Blotting was performed on the cell fractions, lysate (L) and supernatant (S), with anti-toxin antibodies(Swofford et al., 2014). Primary antibody was applied overnight after SDS page electrophoresis. Blocking was done in 5 % milk in PBS-Tween. Secondary antibody conjugated with horseradish peroxidase (HRP).

5.2.3 MTS cytotoxicity assay of 4T1 and LS174T monolayers

Monolayer cultures of 4T1 mammary carcinomas and LS174T colon carcinoma cells were seeded at 7,500 cells/well and grown for 24 hours. Growth media was aspirated and replaced with supernatant fractions of toxin producing bacteria in a 1:10 dilution with growth medium. After 4 hours cell viability was measured using a 1 hour treatment with MTS. An MTS (3-(4, 5-dimethylthiazol-2-yl)-5-(3-carboxymethoxyphenyl)-2-(4-sulfophenyl)-2H-tetrazolium) assay (Promega, Madison, WI), is a viability assay that measures the ability of the mitochondrial enzymes to reduce the substrate and is measurable by colorimetric change of the solution at 490nm. Relative viability was determined by normalization to PBS controls. Transmitted microscopy captured cellular lysis after treatment.

5.2.4 Bacterial delivered SAH in tumor-on-a-chip devices

To test SAH toxicity in 3D tumor tissue pBAD-SAHa-VNP9 were administered to tumor-on-a-chip microfluidic device tumors stained with cytotoxic stain to measure extent of cell death. $2.77x10^{7}$CFU/ml of pBAD-SAHa-VNP9 was administered to tumors for 1hour and then flushed with DMEM+10%FBS, 25mM HEPES and ethidium homodimer (1:500 v/v). Bacteria were allowed to grow for 12 hours before inducing SAH with media supplemented with 0.2% L-arabinose. Fluorescent and transmitted microscopy show tumor size and intensity of the ethidium homodimer stain in test SAH bearing salmonella and control, untreated tumors.

5.2.5 Murine tumor models

SAH producing *E.coli* was administered to 4T1 murine mammary carcinoma tumors in BALB/c mice to test efficacy of the bacterial produced toxin. Plasmid pBAD-SAH and pBAD-

ZsGreen control were transformed into *E. coli* strain χ 6212 (EC-SAH), a Δ*asd* derivative of DH5α. At 8 weeks, female BALB/c mice received a subcutaneous injection of 50,000 4T1 cells in saline on their right flank. Tumor volumes were measured using calipers and calculated by (length*width*height) π/6. When tumors reached a volume of 400mm^3 the mice received 2x10^6 of either EC-SAH or EC-ZsG (control) via tail vein injection. After 2 days mice received another tail vein injection of 40mg arabinose in 100µl saline. Mice were sacrificed when morbid or when tumor volumes exceeded 1000mm^3. Tumor and healthy organs were harvested and fixed. Hematoxylin and eosin (H&E) staining showed the extent of necrosis in harvested tissues. Tumors were sectioned and stained via anti-salmonella and anti-SAH antibodies. Immunofluorescence revealed the location of bacteria and toxin.

5.3 Results

5.3.1 Literature review of toxins

Over 130 Toxic proteins were classified based on their mechanism of action, the organism they originated from, the number of paper counts, whether or not they were considered for cancer therapy, the number of subunits they contained, the number of rare codons they contained, the length of aa/ rare codons, and their overall length. Of these, 5 were identified as potential candidates (Swofford et al., 2014).

Table 2. List of selected toxins

Toxin	Class	Organism	Paper Count	Previously Considered for Cancer Therapy	Subunits[1]	Number of Rare Codons[1]	Length/Rare Codons (aa/#)[1]	Size (aa)[1]
Phospholipase C (PLCs)	Pore-forming	*P. aeruginosa* (Gram-)	348	(Wang et al., 2012)	1	15	48.7	730
α-hemolysin	Pore-forming	*S. aureus* (Gram+)	906	(Johansson et al., 2008)	1	14	22.8	319
Pseudomonas exotoxin A	ADP-Ribosylating	*P. aeruginosa* (Gram-)	2228	(Wolf and Elsässer-Beile, 2009)	1	13	49.2	639
Dermonecrotic Toxin (DNT)	Glycosylating and Deamidating	*B. pertussis* (Gram-)	65	No	1	29	50.4	1461
Azurin	Oxidoreductase	*P. aeruginosa* (Gram-)	793	(Bernardes et al., 2013)	1	0	N/A	149

[1]Data collected from the NCBI Protein Database http://www.ncbi.nlm.nih.gov/protein

5.3.2 Toxins transformed into inducible expression vector

The five candidate toxins: *Pseudomonas* exotoxin (PEA), *Staphylococcus aureus* α-hemolysin (SAH), *Pseudomonas* phospholipase C, *B. pertussis* dermonecrotic toxin (DNT), and *Pseudomonas* azurin toxin (Table I). Genomic DNA was isolated from the respective hosts of the toxin genes, amplified by PCR, and cloned into the delivery vector the under control of the P_{BAD} promoter and the low to moderate copy number (57±4) origin of replication pBR322 (Figure 22) (Lupski et al., 1986; Sutcliffe, 1979).

5.3.3 Bacteria release expressed toxin SAH

To test whether bacteria released each toxin, a K-12 derivative *E. coli* cloning strain, DH5α, and an attenuated *S. Typhimurium* VNP20009, were transformed with the toxin producing plasmids, pBAD-PEA, pBAD-SAH, pBAD-PLC, pBAD-DNT, pBAD-Azurin (Figure 22) and intracellular lysates and extracellular supernatant fractions were measured for toxin content. These results showed that PEA and SAH were found in both the lysates and supernatants(Swofford et al., 2014).

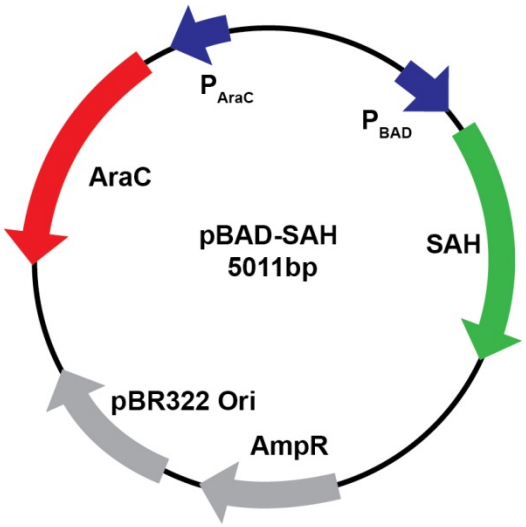

Figure 22. Plasmid pBAD-SAH
Toxin SAH was cloned into the pBAD-myc/hisA vector to test inducible expression under control of the L-arabinose inducible system. This system contains the pBR322 origin of replication known to achieve ~57 copies per cell.

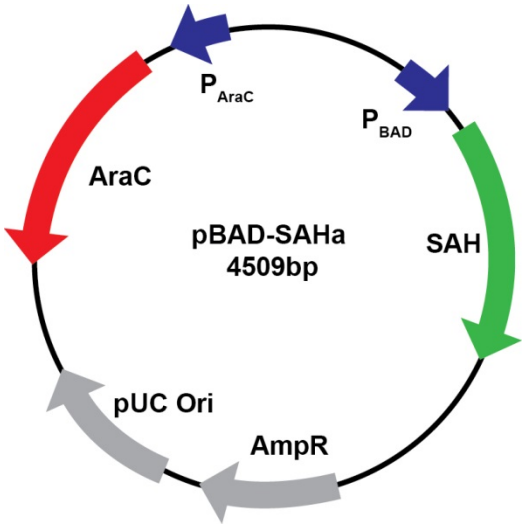

Figure 23. Plasmid pBAD-SAHa
Toxin SAH was cloned into the pBAD-ZsGreen vector to produce toxin under expression of the pUC origin of replication known to produce 500-700 copies per cell.

Initial studies with SAH on the pBAD-SAH plasmid showed secretion from *E.coli* but not from *Salmonella*. A second plasmid vector with higher copy number, pUC19 origin of replication (500-700)(Lin-Chao et al., 1992) was used in an effort to increase the amount of SAH

produced, plasmid pBAD-SAHa (Figure 23). Attenuated S. typhimurium VNP20009 were transformed with pBAD-SAHa (pBAD-SAHa-VNP9) and grown in the same culture conditions as the initial study. Western blot analysis shows lysate and supernatant fractions of induced culture, with 0.2%L-arabinose compared to uninduced culture, and a positive control, pBAD-SAH-*E.coli* (pBAD-SAH-DH5α) (Figure 24).SAH appears at the ~34kDa band in agreement with the positive control in both the lysate and supernatant fractions of the induced culture. Uninduced culture fractions showed faint presence of the protein in the lysate and none in the supernatant.

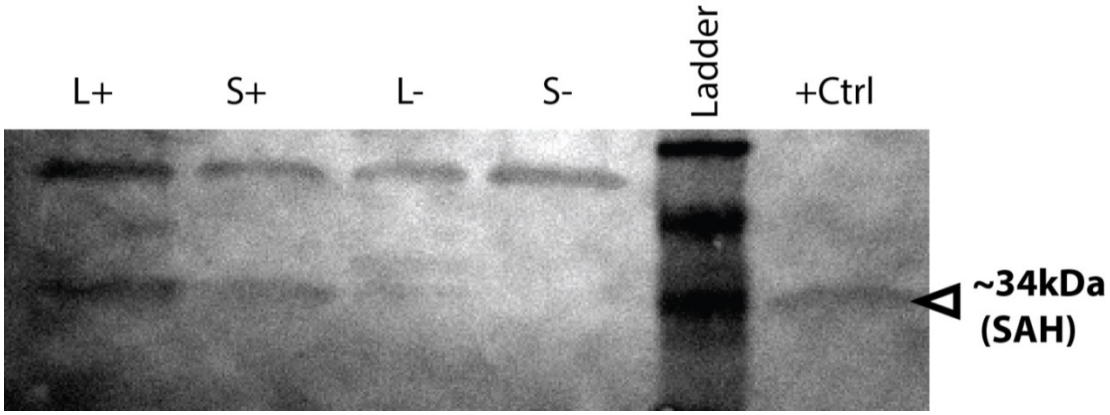

Figure 24.Western blot of SAH lysates and supernatant fractions
pBAD-SAH -DH5α and pBAD-SAHa VNP20009 bacteria were grown in overnight liquid culture. Induced (+) and uninduced (-) cell lysate (L) and supernatant (S) fractions were isolated from *S. typhimurium* and compared to the supernatant fraction from the *E. coli* (+Ctrl). Lysate and supernatant fractions of the *S. typhimurium* show SAH production in induced culture in both and very little in the lysate of the uninduced culture. Bands agree with the positive control.

5.3.4 Assay for recombinant toxin efficacy

To test efficacy of recombinant protein toxins against cancer cells, MTS Assays were run on multiple cancer cell types for toxin lysates and supernatants. This study revealed SAH and PEA as potential anti-cancer toxins as they were the only two proteins to reduce cell survival in monolayer(Swofford et al., 2014).

For the pBAD-SAHa-VNP9, MTS assays showed equivalent cell death to the published data, the E. coli positive control pBAD-SAH-DH5α (Figure 25A,B). Supernatant fractions of pBAD-SAHa-VNP9, pBAD-SAH-DH5a, and negative control, vector in bacteria, were applied to two cell lines, MCF7 mammary carcinoma and LS174T, human colon carcinoma. After 4 hours incubation, both supernatant fractions with SAH reduced cell survival to 20% and 60% on MCF7 and LS174T cells, respectively ($P<0.05$) (Figure 25 A,B). Transmitted microscopy confirmed death with SAH in both cell lines (Figure 25C,D).

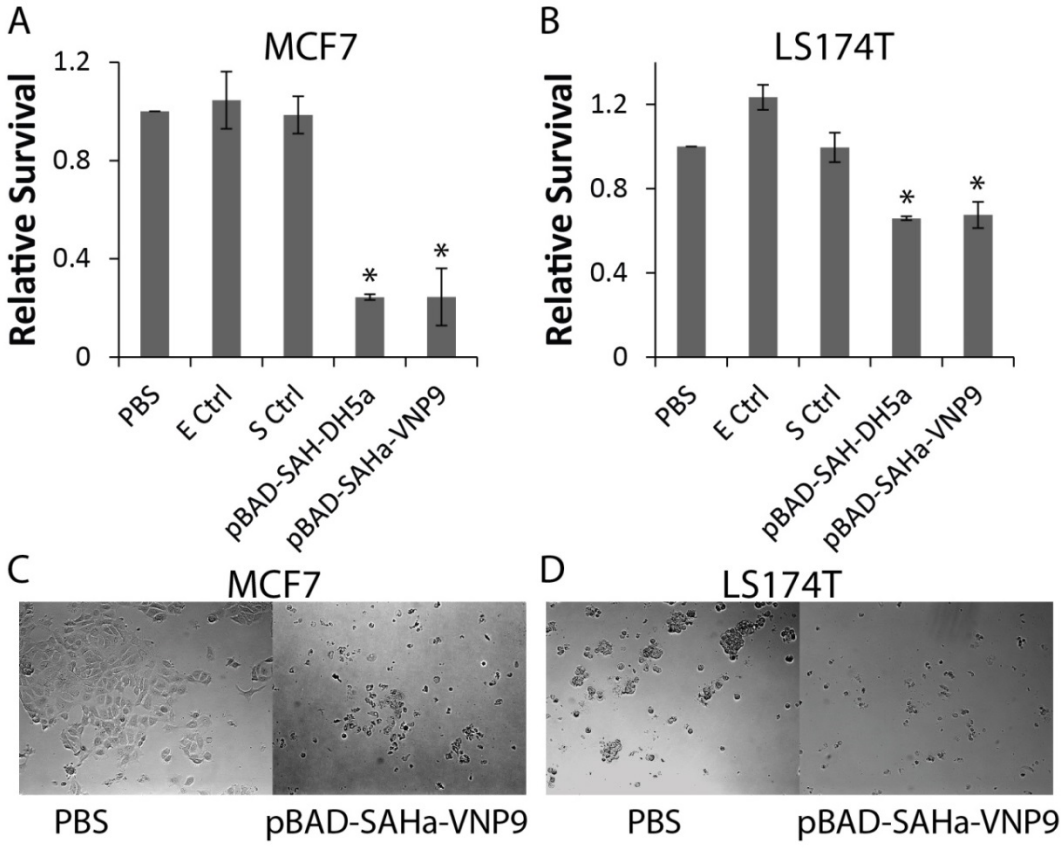

Figure 25. Cytotoxicity Assay of SAH from *S. typhimurium* and *E. coli* show both are lethal
A,B) MTS assays of negative control lane 1) PBS, negative control vectors for 2) *E. coli* and 3) *S. typh.* 4) Induced SAH from *E. coli* and 5) induced SAH from *S. typh.* of culture supernatants on both MCF7 and LS174T monolayers. **C,D)** Transmitted light images of SAH killing from supernatants of *S. typhimurium* VNP20009.

5.3.5 SAH bearing bacteria cause tumor regression and cell death in *in vitro* tumors

A tumor-on-a-chip microfluidic device was used to test efficacy in 3D tissue, prior to animal studies. This device enabled us to study if gene induction of bacteria in 3D tumor tissue could activate SAH expression and cause tumor regression. pBAD-SAHa-VNP9 were administered to the tumor-on-a-chip microfluidic device for 1hr , followed by a 12 dose of media alone to allow bacterial clearance to mimic clearance from healthy tissue in the body. After the 12 hour growth period SAH expression was induced with the addition of L-arabinose. Growth media in the device was supplemented with ethidium homodimer I which to monitor relative viability of the tissue. Fluorescence microscopy showed an increase in cell death overtime with tumor regression within 4 hours of induction compared to the untreated control (Figure 26A). SAH treated tumor volume decreased to 80% of the starting volume with twice as much cell death than the untreated tumors (Figure 26B,C).

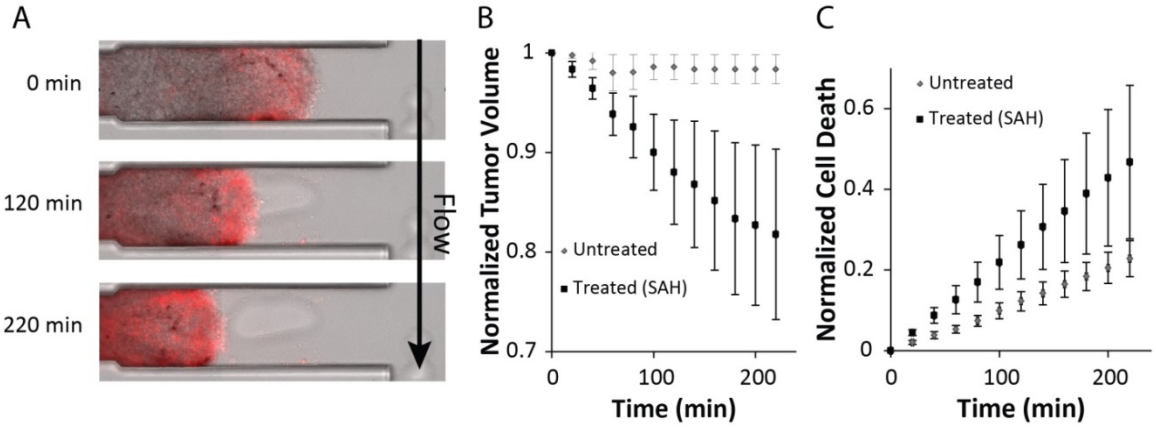

Figure 26. SAH induced death in Tumor-on-a-Chip Devices from pBAD-SAHa VNP20009
A) Time lapse transmitted and fluorescent imaging of LS174T tumors administered with pBAD-SAHa-VNP9 show tumor size regression and increase in uptake of dead stain. **B)** Quantified tumor size regression show an average size reduction of almost 20% 220 minutes after induction with L-arabinose. **C)** Increased ethidium homodimer I uptake shows increase in normalize cell death between treated and untreated control.

5.3.6 SAH *E. coli* cause tumor regression and necrosis in murine tumor models

SAH producing *E. coli* were administered to tumor bearing mice. SAH was found to cause significant tumor reduction and necrosis in tumors compared to control (Figure 27). Three days after bacterial injection, tumors treated with SAH bearing E.coli showed significant drop in tumor volume from their starting volume and the compared to the ZsGreen expressing *E. coli* control (Figure27 A, $P<0.05$). Within 3 days the average drop of tumor size was approximately 66% of the initial tumor volume. H&E staining of tumors show very little viable tissue remaining in SAH treated tumors compared to the control.

Survival curves showed that the strain of *E.coli*, **χ**6212, was toxic to mice as both EC-SAH and the control bacteria EC-ZsG caused severe sepsis. There was no significant difference in mouse survival between the SAH and control groups (Figure 28A). A second experiment with 10-fold fewer bacteria injected showed prolonged survival time compared to the higher dose experiment ($P<0.05$), but no significant difference between SAH and control tumors (Figure 28B). Liver damage in both SAH and control group indicate that the strain of *E. coli*, **χ6212**, is toxic. H&E of livers from both groups of mice showed significant amounts of necrosis with no statistical difference between SAH and control (Figure 29)(St Jean et al., 2014).

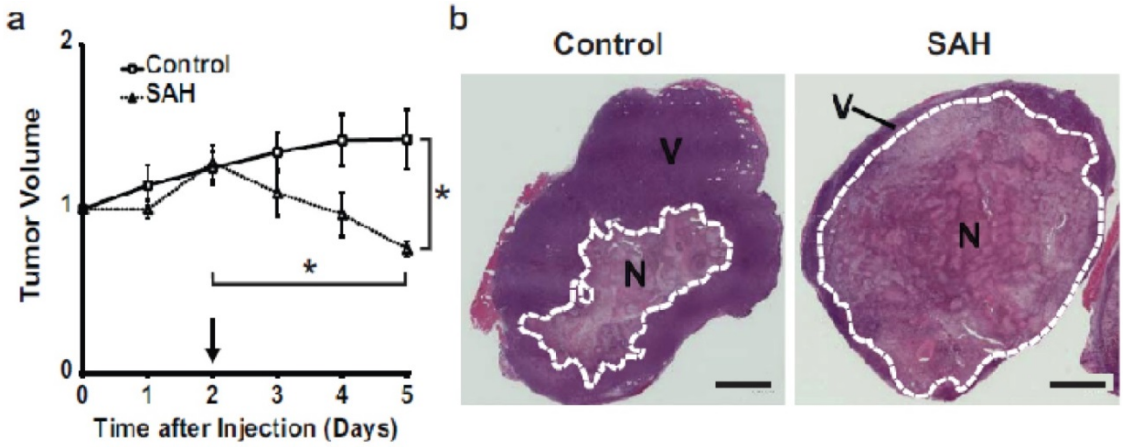

Figure 27. SAH bearing *E. coli* cause regression and necrosis in 4T1 mammary carcinomas
A) Tumor volume for pBAD-SAH-X6212 show tumor size reduction after L-arabinose tail vein injection after 2 days of bacterial infection. **B,C)** Tumor necrosis for control bacteria and SAH bearing bacteria show significantly more necrotic tumor tissue in SAH treated mice (St Jean et al., 2014).

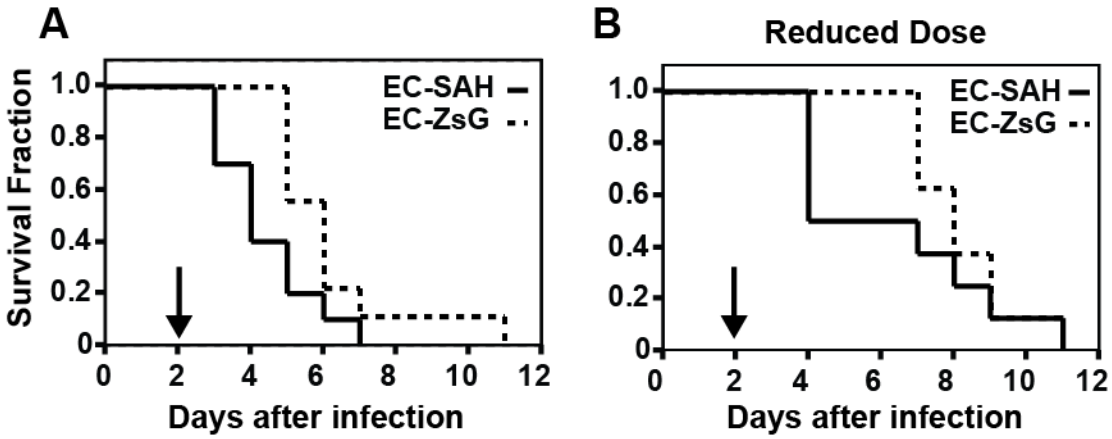

Figure 28. Survival curves for SAH bearing E. coli X6212
A) No significant difference was observed between the survival of mice treated with 100,000 CFU/g of EC-SAH or EC-ZsG (both χ6212). L-arabinose was injected into all mice at 48 hours (arrow). **B)** Reducing the dose tenfold to 10,000 CFU/g, increased survival ($P<0.05$). No statistical difference was seen between EC-SAH and EC-ZsG at this dose (St Jean et al., 2014).

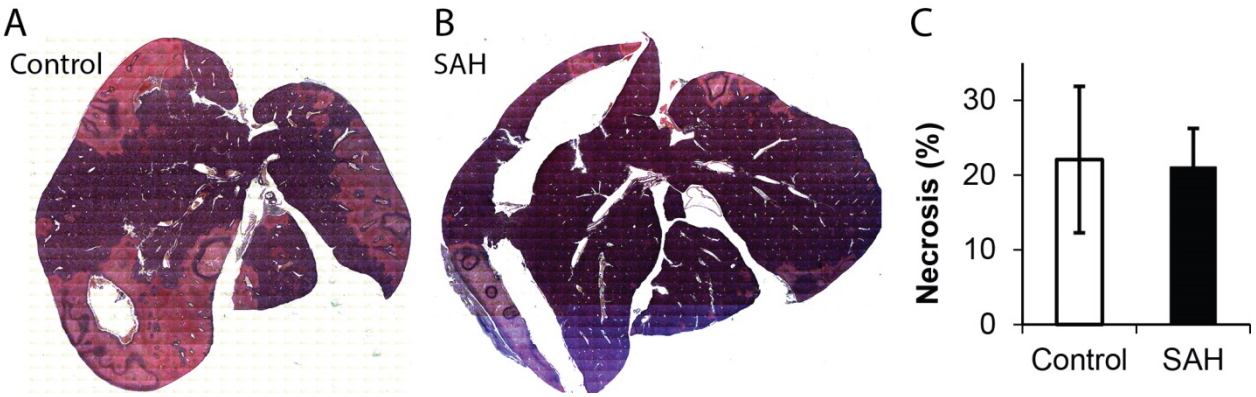

Figure 29. Liver Damage in Mice Injected with E. coli χ6212
A,B) H&E stained liver sections from mice injected with (*A*) EC-ZsG (control) or (*B*) EC-SAH (both χ6212). Areas of necrosis appear in pink where healthy tissue is a dark purple. **C)** Areas of necrosis for mice injected with EC-ZsG (control) or EC-SAH (SAH). There is no significant difference between the two groups, n=3 (St Jean et al., 2014).

5.4 Discussion

Bacterial supernatants of pBAD-SAH-DH5α and pBAD-SAHa-VNP9 administered to tumor cells in monolayer showed significant and equivalent cell death (Figure 25). This shows that SAH is exported from both *Salmonella* and *E. coli* in functional form (Figure 24). It also showed that extraceullar administration is sufficient for cell death. This suggests that these two gram negative bacteria share a secretion mechanism for export of SAH. The first 26 residues on the N-terminus of SAH contains a signal sequence that is cleaved upon secretion (Dinges et al., 2000). After cleavage, monomer subunits integrate into the eukaryotic host cell membrane and form a heptomeric ring that causes lysis due to an inability to regulate osmolarity (Thompson et al., 2011). Because SAH gets cleaved, both of these bacteria must also contain a protein to cleave the immature form of the protein. Identifying the particular secretion mechanism could enable engineering of a more efficient release of the protein as significant amounts of SAH still remains in the cell lysate (Figure 24).

MTS cytotoxicity assays showed 20 % cell survival in MCF7 mammary carcinoma cells and 65 % survival in LS174T colon carcinoma cells, with equivalent cell numbers (Figure 25).

This implies that some cancer cells are more susceptible to the treatment than others, which could be due to membrane structure. MCF7 cells are much larger and more dendritic-like in monolayer culture whereas LS174T cells are much smaller and form stronger cell-cell adhesions. Determining the sensitivity of different cell types to SAH could identify tumors better suited to treatment using this toxin.

SAH bacteria were found to kill 3D tumor cells in a microfluidic device and in murine tumor models (Figures 26,27). The rapid drop in tumor volume and uptake of ethidium homodimer I in the device indicates cell death and effective delivery of SAH toxin. These results were confirmed in murine models, where tumor growth was suppressed in concurrence with necrosis; however survival curves showed rapid rates of mouse death even in the GFP expressing control (Figure 28). Cross-sections of H&E stained liver tissue show large amounts of necrosis in both the EC-SAH and control EC-ZsG (Figure 29). This indicates that the bacterial vector χ6212 was toxic to the mice and likely caused the related cell death. Using another safer bacterial vector, like VNP20009, might enable better results in mouse survival.

5.5 Conclusions

Several bacterial toxins were screened for their ability to kill cancer cells and be recombinantly expressed and secreted from *E. coli* and *Salmonella*. SAH, Staphylococcus aureus α-hemolysin, was found to be a promising candidate. Secretion from both *Salmonella* and *E. coli* make it a robust therapeutic agent, with extremely lethal killing time of 6 minutes on monolayer. In a tumor-mimic-microfluidic device, SAH -*Salmonella* showed tumor regression within hours. In murine tumor models, SAH –*E.coli* caused significant amounts of tumor regression, but suffered from toxicity of the strain.

CONCLUSIONS

This thesis describes several strategies to genetically engineer bacteria for diagnostic and therapeutic approaches for cancer. Current therapy and diagnostic tools suffer from poor specificity to cancer causing systemic toxicity in the case of treatment or misdiagnosis in the case of detection. Gram negative bacteria have been shown to overcome the transport limitations hindering effective treatments and detection methods and colonize tumors with 2,000-10,000-fold higher specificity than healthy tissues. In this dissertation, I have describe several strategies to utilize the tumor targeting nature of the bacteria and engineer microbes to perform multiple tasks once they reach the tumor site, from triggered release of a biomarker protein for detecting the presence of cancer, to engineering the bacteria to recognize sugar gradients autonomously for visualization of viable regions of tumors, to delivery and production of toxic proteins directly at the tumor site. These strategies were all tested *in vitro* environments and *in vivo* models that have similar gradients and transport limitations that therapies and diagnostic tools have to overcome in the patients. Mathematical analysis was used to evaluate the efficacy of these strategies in the clinic. The engineered bacterial detection and treatment strategies tested here in vitro and in vivo have direct applications to the clinic and could have a broad impact on the current methods for cancer treatment and detection.

Cancer detection is a broad field of study with many imaging techniques and biochemical assays used in conventional screening in the clinic. These methods are currently limited in their specificity to cancer and eliminate false positives. In this dissertation, I present a novel method that combines the sensitivity of biomarker assays with the specificity of tumor-targeting bacteria. Bacteria were engineered to release a recombinant fluorescent reporter protein, ZsGreen, to serve as an exogenous biomarker that would not be confused with any native proteins in the body. To

the best of my knowledge this strategy for tumor detection has not been attempted before. The bacteria were tested *in vitro* and *in vivo* murine tumor models for recombinant expression and release of the biomarker protein from cancer tissue. The results show successful identification of microscopic tumor masses in microfluidic devices that mimic tumor tissue adjacent to blood vessels as well as detection of tumors less than 1 g in weight in murine tumor models. These results demonstrate the feasibility for bacterial tumor detection in the clinic with the elimination of background signal by production of an exogenous biomarker from the cancer site.

Engineering autonomous bacterial sensing could improve specificity to cancer and enable measurement of the tumor microenvironment. In this dissertation I present a novel bacterium that is able to sense sugar gradients in its surroundings. Applied to cancer, these microbes have the ability to enable visualization of the glucose gradient that exists in a tumor mimic microfluidic device. The gradient in sugar is shown to correlate with the level of apoptosis activity of the tumor cells. Bacteria to sense the tumor microenvironment have the potential to improve therapeutic and diagnostics of cancer. Combined with the specificity of the bacteria to the tumor site, identifying gradients within the tumor microenvironment may enable more specific targeting for treatment. This bacterium can serve as a platform system for sensing other metabolites in tumors, as the binding pocket for the ligand site has previously been modified for sensing of other ligands than glucose or ribose. L-lactate is a promising target for metastatic disease and future work could enable bacterial detection of metastatic sites through lactate sensing.

Cancer therapy has several limitations from transport phenomena to cancer acquired drug resistance through mutation. In this dissertation I present a strategy that overcomes the transport limitations that hinder small molecule therapeutics and acquired drug resistance by specific bacterial delivery of a cytotoxic protein staphylococcus aureus alpha-hemolysin, SAH. Functional

recombinant protein expression and release was evaluated in vitro in monolayer and in 3D tumor microfluidic devices. SAH producing bacteria were then tested in murine tumor models for specificity and tumor treatment. These results show SAH is extremely toxic to several cancer cell lines and is functionally expressed and released in liquid culture and from within tumor tissue. In murine tumors, delivery of SAH was shown to cause significant tumor reduction and necrosis within tumors, however; the strain of bacteria used in this study proved toxic to the mice. Reduction in bacterial dose showed minimal improvement in survival. Future studies aim to use less toxic bacteria for the anti-cancer vector. These results demonstrate the effectiveness of targeted delivery of an extremely cytotoxic molecule for treatment of tumors.

APPENDIX A

ADDITIONAL FIGURES

A1 Individual tumors show varying levels of ZsGreen expression

Detection of tumors in mice shows varying bacterial ZsGreen expression. Individual Tumors show different levels of bacterial activation, indicating transport limitations are different in different tumors. Some were activated well, with almost 75% of the bacteria in the tumor of mouse #2 activating ZsGreen, but others, like mouse #10, only had 25% of the bacteria producing ZsGreen. This indicates that L-arabinose diffusion into the tumors may affect success of this detection method, although the majority of these bacteria were found in necrotic regions, which may not contribute to the overall ZsGreen release as suggested by Figure 12.

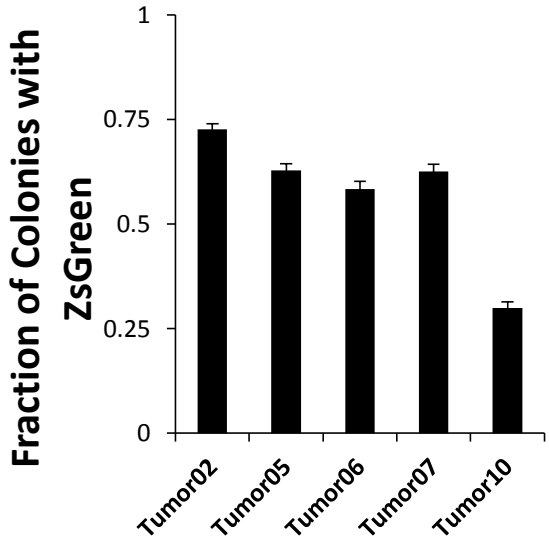

Figure A1. Individual tumors show varying levels of ZsGreen expression. On average, 57% of the bacterial colonies produced ZsGreen (n=5).

A2 N-terminus fusions to ZsGreen maintained secretion in VNP20009 Salmonella

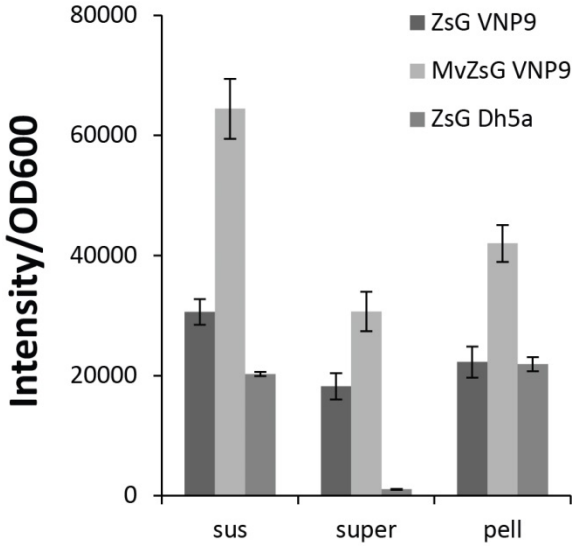

Figure A2. ZsGreen fusions to the n-terminus of MVSSSSIS maintained secretion of the protein from Salmonella VNP20009. DH5alpha control shows E. coli do not secrete ZsGreen, even with fusion of MVSSSSIS, not shown.

A3 Single-layer antibody dots calibration of intensity to ng/ml ZsGreen

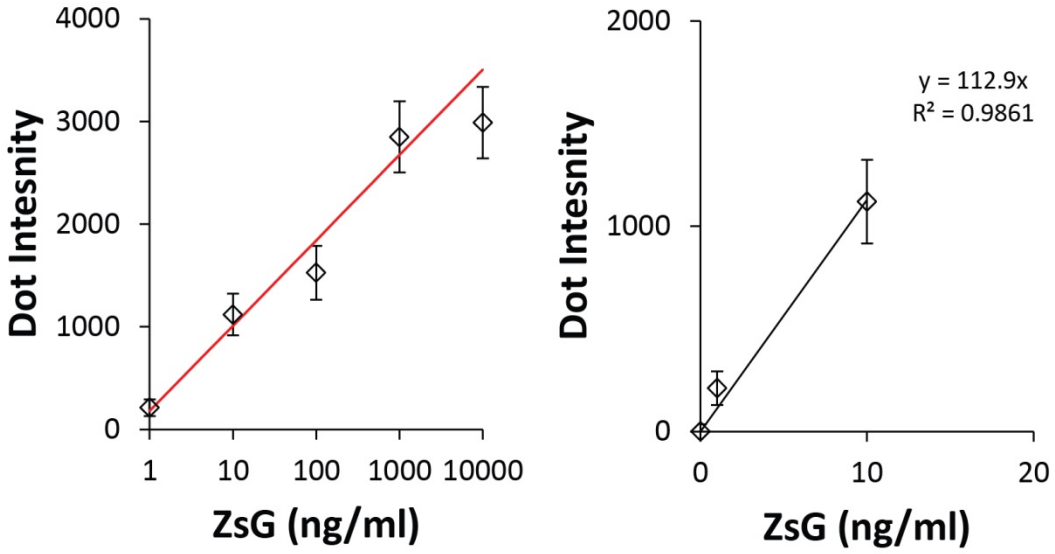

Figure A3 Single-layer antibody dots in Bovine plasma. Fluorescence intensity from single-layer-antibody dots was converted to concentration of ZsGreen in plasma with sensitivity in the ng/ml range. Purified ZsGreen concentration was first determined by Bradford assay. Intensity at 400ms exposure (I) is related to the concentration (C, ng/ml), I, by the following equation: (line, log plot) I= A ln(C)+B. This logarithmic relationship on the left plot is due to the saturation of binding sites on the dot surface. The linear range between 0 and 10 ng/ml was used to convert small the fluorescence intensities, which was in the range of the observed the plasma from the half-life and tumor studies.

A4 Sensitivity of ZsGreen detection ELISA

Large error in tumor blood measurements using single-layer antibody dots, suggests poor sensitivity of the technique at the ng/ml level. A sandwich ELISA was developed, which had excellent capabilities in saline but did not work well in plasma and 1:10 plasma: PBS samples (Figure A4). Improving ZsGreen detection sensitivity would decrease the minimum detectable tumor size (Figure 14). Decreasing the detection limit of ZsGreen would enable identification of smaller tumor masses. Single layer-antibody dots show ng/ml sensitivity of ZsGreen in blood and PBS (Figure A3, 6) compared to ELISA which was only sensitive to ZsGreen in PBS (Figure A4). Measurement of small concentrations of proteins in blood is difficult and requires extensive assay optimization. The single-layer-antibody dots appear to be more robust than a sandwich ELISA but they still show a significant amount of error (Figure A3).

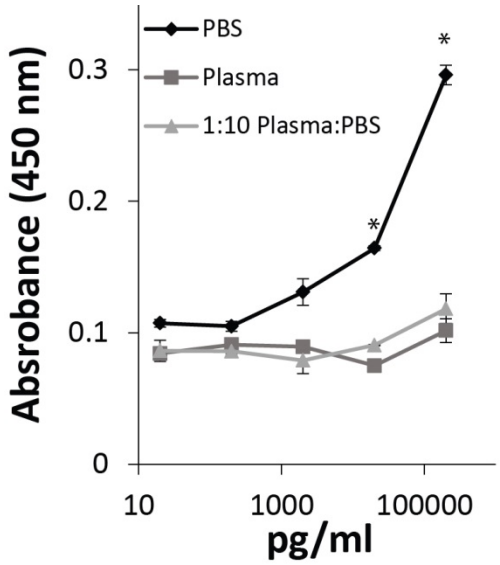

Figure A4 ELISA of ZsGreen. The procedure is as follows: **1)** 100 µl Anti-ZsGreen antibody, Anti-ZsGreen monoclonal antibody (Clontech) was adhered to microtiter plate in PBS at 1:500 overnight at room temp. **2)** Wash 3x 200 µl with TBS-T (TBS-Tween 0.05%). **3)** Block with 10 mg/ml BSA in TBS at room temp for 1 hour. **4)** Wash 3x. **5)** 100 µl of ZsGreen samples in PBS, bovine plasma, or 1:10 bovine plasma in PBS were applied to wells for 2 hours. **6)** Wash 3x. **7)** 100µl Rabbit-Anti-RCFP polyclonal antibody (Clontech) was incubated at 1:500 in TBS-T +1mg/ml BSA for 1 hour at room temp. **8)** Wash 3x. **9)** Apply 100 µl of 1:1000 anti-rabbit-HRP in TBS-T +1mg/ml BSA was applied for 1 hour. **10)** Wash 3x.11). **11)** Use trimethylbenzidine (TMB, Sigma) substrate kit and measure at absorbance 450nm.

A5 Plasmid constructs to create sugar sensing Trz1 construct

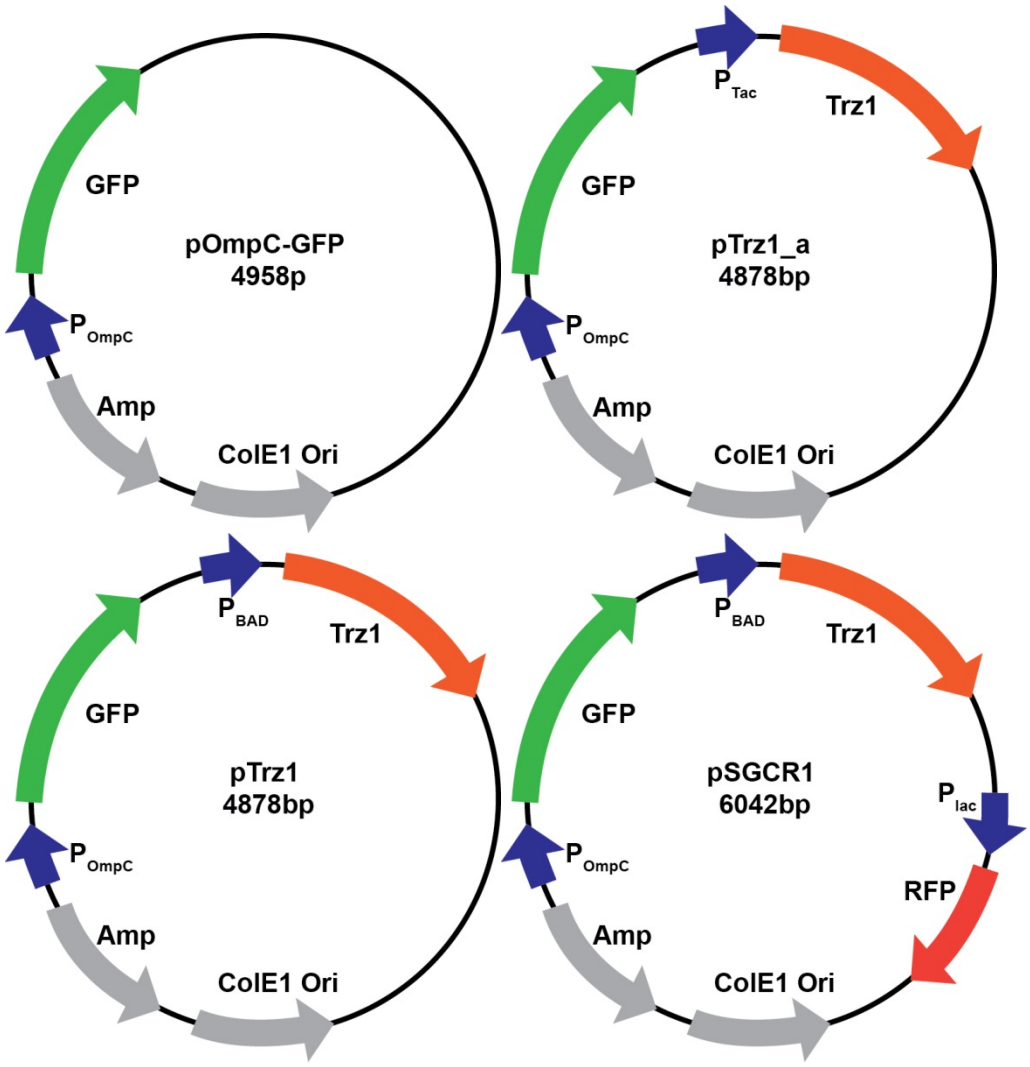

Figure A5 Plasmid constructs to make SGCR1.

APPENDIX B.

MATLAB CODE FOR SOLVING SYSTEM OF PDES

Matlab code to solve drug diffusion vs. sugar sensing bacteria drug delivery
Main function:

```
function Diffusion3viability
% this is the main function. within this function the meshes are defined,
%PDEPE is called and the results are plotted.
clear; close all;

%% prameters:
P(1)=.05; %diffusion coefficient D m^2/s

P(2)=1; %c0 uM drug

P(3)=20; %death rate mu (1/h)


P(4)=.2;%km saturation concentration uM

P(5)=.2; %t-half drug (1/h)


P(6)=0.1; %glucose diffusion coefficient
P(7)=2; %uptake rate (first order due to saturation concentration >> than c
%P(8)=
%everything is dimensionless in this solution
L=1; %length of the domain (m)
maxt=1; %max. simulation time (h)
t=linspace(0,maxt,100); %tspan
x=linspace(0,L,100);%xmesh


%%
%Call of PDEPE. It needs the following arguments
%m: see above
%DiffusionPDEfun: function containing the PDEs
%DiffusionICfun: Function containing the ICs for t=0 at all x
%DiffusionBCfun: Function containing the BCs for x=0 and x=L
%x: xmesh and t: tspan
%PDEPE returns the solution as multidemensional array of size
%xmesh x tspan x (# of variables)
m=0;% 0 for rectangular coordinates, 1 for cylindrical, 2 for spherical
sol= pdepe(m,@DiffusionPDEfun3,@DiffusionICfun3,@DiffusionBCfun3,x,t,[],P);
%%plotting
%3-D surface plot
u1 = sol(:,:,1);
u2 = sol(:,:,2);
u3 = sol(:,:,3);
u4 = sol(:,:,4);
figure(1)

surf(x,t,u1);
 xlabel('Distance x','fontsize',20,'fontweight','b','fontname','arial')
 ylabel('Time t','fontsize',20,'fontweight','b','fontname','arial')
```

```
 zlabel('Species u','fontsize',20,'fontweight','b','fontname','arial')

 figure(2)
surf(x,t,u2);
 xlabel('Distance x','fontsize',20,'fontweight','b','fontname','arial')
 ylabel('Time t','fontsize',20,'fontweight','b','fontname','arial')
 zlabel('viabilty','fontsize',20,'fontweight','b','fontname','arial')


% figure(1)
% surf(x,t,u(1),'edgecolor','none');
% xlabel('Distance x','fontsize',20,'fontweight','b','fontname','arial')
% ylabel('Time t','fontsize',20,'fontweight','b','fontname','arial')
% zlabel('Species u','fontsize',20,'fontweight','b','fontname','arial')
% axis ([0 L 0 maxt 0 P(2)])
% set(gcf(), 'Renderer', 'painters')
% set(gca, 'FontSize', 18, 'fontweight', 'b', 'fontname', 'arial')
%
%2-D line plot
figure(3)
hold all
for n=[1 10 25 50 100]
   plot(x,sol(n,:,1), 'LineWidth',2)
end
xlabel('Distance x','fontsize',20,'fontweight','b','fontname','arial')
ylabel('concentration','fontsize',20,'fontweight','b','fontname','arial')
axis([0 L 0 P(2)])
set(gca, 'FontSize', 18, 'fontweight', 'b', 'fontname', 'arial')
Hold off

figure(4)
hold all
for n=[1 10 25 50 100]
   plot(x,sol(n,:,2), 'LineWidth',2)

end

xlabel('Distance x','fontsize',20,'fontweight','b','fontname','arial')
ylabel('viability','fontsize',20,'fontweight','b','fontname','arial')
axis([0 L 0 P(2)])
set(gca, 'FontSize', 18, 'fontweight', 'b', 'fontname', 'arial')
% ylim([0.8 1])
Hold off

figure(5)
hold all
for n=[1 10 25 50 100]
   plot(t,sol(:,n,2), 'LineWidth',2)

end
xlabel('Time t','fontsize',20,'fontweight','b','fontname','arial')
ylabel('viability','fontsize',20,'fontweight','b','fontname','arial')
axis([0 L 0 P(2)])
set(gca, 'FontSize', 18, 'fontweight', 'b', 'fontname', 'arial')

figure(6)

hold all
for n=[1 10 25 50 100]
```

```
   plot(t,sol(:,n,1), 'LineWidth',2)

end


xlabel('Time t','fontsize',20,'fontweight','b','fontname','arial')
ylabel('concentration','fontsize',20,'fontweight','b','fontname','arial')
axis([0 L 0 P(2)])
set(gca, 'FontSize', 18, 'fontweight', 'b', 'fontname', 'arial')
% ylim([0.8 1])
Hold off

figure (7)
C=1.0364;
z=0.2257;
w=0.1936;
%x=linspace(0,L,100);
v=(C/2)*(1-tanh((x-z)/(2*w)));
plot(x,v)
xlabel('Distance x','fontsize',20,'fontweight','b','fontname','arial')
ylabel('Viability','fontsize',20,'fontweight','b','fontname','arial')
axis([0 L 0 P(2)])
set(gca, 'FontSize', 18, 'fontweight', 'b', 'fontname', 'arial')

figure(8)
surf(x,t,u3);
 xlabel('Distance x','fontsize',20,'fontweight','b','fontname','arial')
 ylabel('Time t','fontsize',20,'fontweight','b','fontname','arial')
 zlabel('[GFP]','fontsize',20,'fontweight','b','fontname','arial')

 figure(9)
surf(x,t,u4);
 xlabel('Distance x','fontsize',20,'fontweight','b','fontname','arial')
 ylabel('Time t','fontsize',20,'fontweight','b','fontname','arial')
 zlabel('Viability (GFP)','fontsize',20,'fontweight','b','fontname','arial')

%for the drug concentration produced by bacteria:
%we get the following:
% dl/dt =(-mumax*CD/(km-Co))*l
%and
%CD=k(x)*t
%wher k(x) was found from excel fitting to the rate of GFP produced as a
%function of x
C2=1.3533;
z2=0.6712;
w2=0.1567;
Cnot=1;
%CDgfp= Cnot*(C2/2)*(1-tanh((x-z2)/(2*w2)))*t;
kgfp=Cnot*(C2/2)*(1-tanh((x-z2)/(2*w2)));
%solving the equation:
%dl/dt=(-mumax*(Cnot*(C2/2)*(1-tanh((x-z2)/(2*w2)))*t)/(km-Co))*l
%gives:
%ln(l)- constant of int(viability initial(given as a
%sigmoidal))=((-mumax*kgfp) /(Km-Co))*(1/2)*t^2

figure(10)
hold all
for n=[1 10 25 50 100]
   plot(x,sol(n,:,3), 'LineWidth',2)
```

```
end
xlabel('Distance x','fontsize',20,'fontweight','b','fontname','arial')
ylabel('GFP','fontsize',20,'fontweight','b','fontname','arial')
axis([0 L 0 P(2)])
set(gca, 'FontSize', 18, 'fontweight', 'b', 'fontname', 'arial')
Hold off

figure(11)
hold all
for n=[1 10 25 50 100]
   plot(x,sol(n,:,4), 'LineWidth',2)
end
xlabel('Distance x','fontsize',20,'fontweight','b','fontname','arial')
ylabel('viability','fontsize',20,'fontweight','b','fontname','arial')
axis([0 L 0 P(2)])
set(gca, 'FontSize', 18, 'fontweight', 'b', 'fontname', 'arial')
Hold off
mean(sol(1,:,4))
mean(sol(1,:,2))
mean(sol(100,:,4))
mean(sol(100,:,2))
end
```

PDEs defined:

```
function [c,f,s]=DiffusionPDEfun3(x,t,u,dudx,P)
%Function defining the PDE

%Extract parameters from main function
D=P(1);
mumax=P(3);
km=P(4);
Dg=P(6);
kuptake=P(7);
%pde  c dxdt= f dudx+ s
% in this case for simple diffusion
%our equation is:
%dxdt= d(D.*dudx)dx +0
%c=1;
%f=D.*dudx;
%s=0;

C2=1.3533;
P2=0.6712;
W2=0.1567;
kgfp=(C2/2)*(1-tanh((x-P2)/(2*W2)));
cnot=1;

c=[1;1;1;1];
f=[D;0;D;0].*dudx;
s=[0;-(mumax*u(1))*u(2)/(km+u(1));cnot*kgfp;-(mumax*u(3))*u(4)/(km+u(3))];
```

Boundary Conditions:

```
function [pl,ql,pr,qr]= DiffusionBCfun3(xl,ul,xr,ur,t,P)
%Boundary conditions for x=0 and x=L;

%extract parameters
c0=P(2); %defined at 1 on main function Diffusion3viability.m
mumax=P(3);
km=P(4);
```

```
%BCs: No flux boundary at the right boundary and constant concentration %on the left boundary
%define time points and data points for bc
T0=10000;
thalf=P(5); %dimensionless halflife
k=0.693/thalf;
%c = exp(-k*t)

%parameters for fit to tanh function for viabiltiy data from kasinskas 2014
C=1.0364;
z=0.2257;
w=0.1936;
%x=linspace(0,1,100);
%v=(C/2)*(1-tanh((x-p)/(2*w))); initial condition needed to solve constant
%of integration
vnew=(C/2)*(1-tanh((-z)/(2*w))); %evaluated at x=0, t=0

bnew=(mumax/k)*(log((km+1)))-log(vnew);% constant of integration at b.c. and i.c.

C2=1.3533;
P2=0.6712;
W2=0.1567;
kgfpl=(C2/2)*(1-tanh((xl-P2)/(2*W2)));
kgfpr=(C2/2)*(1-tanh((xr-P2)/(2*W2)));
cnot=1;

 pl=[ul(1)-exp(-k*t);(ul(2)-(exp((mumax/k)*(log((km+exp(-k*t))))-(bnew))));ul(3)-kgfpl*t;ul(4)-exp((-(kgfpl*t-
km*log(km+kgfpl*t))/kgfpl*mumax)+log(vnew)-(km*log(km)/kgfpl*mumax))];
    %(exp((mumax/k)*(log((km+exp(-k*t))))-(bnew))))];
%solution for boundary condition of cell viability, is found by calculating
%the constant of integration for dl0dt=(-mu*C/km+C) *l by separating
%integrating and solving at x=0 and the initial condition l(0,0)=1
%(assuming all cells near the vessel are alive at (x=0,t=0)).
ql=[0;0;0;0];
pr=[0;0;0;0];
qr=[1;1;1;1];
%ur(3)-cnot*kgfpr*t
```

Initial Conditions:

```
function u0= DiffusionICfun3(x,P,L)
%initial conditions for t=0; can be a function of x
%u0=[0;1]; %assuming all cells are living at all x values at t=0

%tumor tissue will have necrotic tissue prior to administration of %drug, to account for this we will incorporate a gradient in tissue %viability according to measured values of ethidium homodimer uptake %from Bhushan Toley's studies:

%v=(C/2)*(1-tanh((x-p)/(2*w)))
%from least squares regression in excel: Figure6_data %analysis_viability_jan adjusted for fit(1).xlsx

C=1.0364;
z=0.2257;
w=0.1936;
%x=linspace(0,1,100);
v=(C/2)*(1-tanh((x-z)/(2*w)));
u0=[0;v;0;v];
```

APPENDIX C.

IMAGEJ/FIJI MACROS FOR IMAGE ANALYSIS

C1 Imagej/Fiji Macro for binary image alignment

```
macro "align 2 color images in a stack and do colony size analysis with secretion"

//Set measurements in fiji only to 'integrated density' option and 'display label' mark, this will enable appropriate output in the log file and save time in the calculations.
{
//define image names
//print("\\Clear");
run("Clear Results");
//selectWindow("Log");
print("\\Clear");
inputFolder = "C:\\Users\\jans laptop\\Documents\\research\\Experiments2\\IHC-IF zsgreen tumor study\\11_4_2014_tumor staining big group 1_10 aStyph\\Tumor07\\";
//getDirectory("align 2 color using bUnwarpJ - Choose the input folder!"); //don't use bunwarpJ it skews pixels which is wrong to do for data
//open input directory
outputFolder= "C:\\Users\\jans laptop\\Documents\\research\\Experiments2\\IHC-IF zsgreen tumor study\\11_4_2014_tumor staining big group 1_10 aStyph\\Tumor07\\Aligned_folder_6\\";
//getDirectory("choose the output folder!");
 v=newArray(70,71,72,73,74,75,76,77,78,79);//tumor07 distance analysis

 //v=newArray(41,75,90,118,122,149);//tumor02
//v=newArray(19,27,40,45,50,61);// tumor05
//v=newArray(53,68,97,112,117,122,141);//tumor03
//v=newArray(29,38,51,82,118,139);//tumor04
//v=newArray(36,82,95,118,136,149);//tumor06
//v=newArray(34,45,52,76,106,112);//tumor07
//v=newArray(19,20,25,26,32,37,38);//tumor09
//v=newArray(18,19,21,28,33,35,36,43);//tumor10
for (i=0; i <v.length; i++) {//select the images you want to align  (adjust for each folder of images 1 more than the number of the last image
                num_img=IJ.pad(v[i],3);//IJ.pad pads number value with zeros in the front 3 digits and returns the string
run("Clear Results");
open(inputFolder+"Salm_"+num_img+".ipl");
run("Subtract Background...", "rolling=25");
//tumor02,05,03,04,10 used salm at 550
//tumor06: set to 250
//tumor07: 238
//tumor09:275
//tumor10: 238
setThreshold(238, 66000); //threshold bacteria after background subtract to
run("Convert to Mask");
saveAs("Tiff", outputFolder+"Salm_bin_"+num_img);
//makes binary of salmonella stained pics

open(inputFolder+"ZsGreen_"+num_img+".ipl");
run("Subtract Background...", "rolling=25");
```

```
setThreshold(645, 66000);
//tumor02,05,03,04,10 used salm at 700
//tumor06, set to 250
//tumor07: 645
//tumor09:700
//tumor
run("Convert to Mask");
saveAs("Tiff", outputFolder+"ZsGreen_bin_"+num_img);
//background subtracts with 50pix and then binary
print("image #",num_img);
//starting image agreement
		imageCalculator("Multiply create", "ZsGreen_bin_"+num_img+".tif","Salm_bin_"+num_img+".tif");
run("Measure");
selectWindow("Result of ZsGreen_bin_"+num_img+".tif");
close();
selectWindow("ZsGreen_bin_"+num_img+".tif");
close();

//calcuate initial match agreement
var a=getResult("RawIntDen",0);//results table starts with row index of zero
m=0;//x start
n=0;//y start
//try to do 2 single arrays for x and y shift:
k=1;//counter for results table
//translates into 49 different positions
for(o=-4; o<5; o++){
for(j=-4; j<5; j++){
		open(outputFolder+"ZsGreen_bin_"+num_img+".tif");
		selectWindow("ZsGreen_bin_"+num_img+".tif");
		run("Translate...", "x=o y=j interpolation=None");
		//translates orignal image
		imageCalculator("Multiply create", "ZsGreen_bin_"+num_img+".tif","Salm_bin_"+num_img+".tif");
run("Measure");
selectWindow("Result of ZsGreen_bin_"+num_img+".tif");
close();
selectWindow("ZsGreen_bin_"+num_img+".tif");
close();
max_agree=getResult("RawIntDen",k);//gets max rawIntDensity from results table
print(k,max_agree,a);
if (max_agree>a) {
a=max_agree;
m=o;
n=j;
}//if statement to determine max agreement between
k=k+1;

}
}//end translation loop

print(num_img,m,n); //the translational posistion for the optimized colocalization
open(outputFolder+"ZsGreen_bin_"+num_img+".tif");
run("Translate...", "x=m y=n interpolation=None");
saveAs("Tiff", outputFolder+"ZsGreen_bin_align_"+num_img);//saves the aligned binary image

		//translates orignal image
//print("Image"+num_img);
selectWindow("Salm_bin_"+num_img+".tif");
close();
selectWindow("ZsGreen_bin_align_"+num_img+".tif");
```

```
close();
print(num_img,m,n);
}
```

C2 Imaej/Fiji Macro for measuring colony size distribution and ZsGreen diffusion

```
macro "align 2 color images in a stack and do colony size analysis with secretion"

//Set measurements in fiji only to 'integrated density' option and 'display label' mark, this will enable appropriate output in the log file and save time in the calculations.
//Note. Input and output must exist in specified locations, Imagej will not create them if they don't exist.
{
//define image names
//print("\\Clear");
run("Clear Results");

//selectWindow("Log");
print("\\Clear");
//inputFolder = "C:\\Users\\jans laptop\\Documents\\research\\Experiments2\\IHC-IF zsgreen tumor study\\11_4_2014_tumor staining big group 1_10 aStyph\\Tumor02\\";
//getDirectory("align 2 color using bUnwarpJ - Choose the input folder!"); //don't use bunwarpJ it skews pixels which is wrong to do for data
//open input directory
outputFolder= "C:\\Users\\jans laptop\\Documents\\research\\Experiments2\\IHC-IF zsgreen tumor study\\11_4_2014_tumor staining big group 1_10 aStyph\\Tumor07\\Aligned_folder_6\\";
//getDirectory("choose the output folder!");
v=newArray(78,79);//70,71,72,73,74,75,76,77,,79
//v=newArray(41,75,90,118,122,149);//tumor02
//v=newArray(19,27,40,45,50,61)// tumor05
//v=newArray(53,68,97,112,117,122,141);//tumor03
//v=newArray(29,38,51,82,118,139);//tumor04
//v=newArray(36,82,95,118,136,149);//tumor06
//v=newArray(34,45,52,76,106,112);//tumor07
//v=newArray(19,20,25,26,32,37,38);//tumor09
//v=newArray(18,19,21,28,33,35,36,43);//tumor10
//for (ij=0; ij <v.length; ij++)
for (ij=0; ij <v.length; ij++) {//select the images you want to align  (adjust for each folder of images 1 more than the number of the last image
        num_img=IJ.pad(v[ij],3);
        //num_img=IJ.pad(v,3);//IJ.pad pads number value with zeros in the front 3 digits and returns the string
//for (i=81; i <82; i++) {//select the images you want to align  (adjust for each folder of images 1 more than the number of the last image
//        num_img=IJ.pad(i,3);//IJ.pad pads number value with zeros in the front 3 digits and returns the string
//---------------------------------------------------------------------------------------------------------------

//loop partical analyzer for different sizes of salmonella colonies to determine if there is a relationship between colony size and secretion

//isolates colonies of a certain size (defined as pixel area via the imagej particle analysis plugin)
inc=1; //increment by 'inc' pixel^2 bins
p=newArray(0, 2, 4, 6, 8, 10, 15, 20, 30, 50, 10000);//size array
 for (i=1; i<p.length; i++) {
//for (z=1; z<50;z++){// size loop every inc pixels in area to test (set bounds for size
        //start at 2 because the particle analyzer doesn't register anything between 0-1 r^2=1.6 for 1 pixel
open(outputFolder+"Salm_bin_"+num_img+".tif");
```

```
//open(outputFolder+"ZsGreen_bin_align_"+num_img+".tif");
selectWindow("Salm_bin_"+num_img+".tif");
            run("Analyze Particles...", "size="+(p[i-1])+"-"+(p[i]-0.0001)+" include summarize add in_situ");
            // increment pixel area by 5 (i.e. first is from 0-5)
            //not sure how accurate the pixel size is? how many decimal places is appropriate to
            //include lower bound and exclude upper to avoid repeated points?

            print("particle_size="+p[i-1]+"-"+p[i]+".",((p[i-1])),p[i]);
              selectWindow("Summary");
  lines = split(getInfo(), "\n");
  headings = split(lines[0], "\t");
  values = split(lines[lengthOf(lines)-1], "\t");
  for (ni=0; ni<headings.length; ni++){
 print(headings[ni]+": ",values[ni]);
  }
     selectWindow("Summary");
     run("Close");
           count=roiManager("count");
array=newArray(count);
for(s=0; s<count;s++) {
      array[s] = s;

}
selectWindow("Salm_bin_"+num_img+".tif");
run("Select All");
setBackgroundColor(1, 1, 1);//clears image completely
run("Clear", "slice");// with line above clears image completely
//roiManager("Select", array);
selectWindow("ROI Manager");
run("Select All");//selects all ROIs from particle analysis in size z1^2-z2^2
roiManager("Fill");//fills in selected rois in white(255 value)
setThreshold(82, 255);
setOption("BlackBackground", true);
run("Convert to Mask");
saveAs("Tiff", outputFolder+"Salm_bin_colonysize_"+i+"");//saves colony picture of size

roiManager("Deselect");
roiManager("Reset");//close ROI manager to clear for next size

//}// move to end once this is working ok


//-------------------------------------------------union/dialate series
//start unionizing
open(outputFolder+"ZsGreen_bin_align_"+num_img+".tif");
selectWindow("Salm_bin_colonysize_"+i+".tif");//grabs image of size z particles

imageCalculator("Multiply create", "ZsGreen_bin_align_"+num_img+".tif","Salm_bin_colonysize_"+i+".tif");
//multiplies the aligned salmonella and zsgreen images
saveAs("Tiff", outputFolder+"ZsGreen_bin_align_U0");// save initial colocalized pixels salm and zsg
//close();
run("Measure");
//jj=getResult("RawIntDen",k);
print(num_img,0,getResult("RawIntDen",0));

run("Clear Results");
for (b=1; b<50;b++){
//now perform the dialtion and union to generate the histogram of the zsgreen as a function of distance from salmonella
//b is the number of dialations/unions
```

```
selectWindow("ZsGreen_bin_align_U"+b-1+".tif");
//run("Dilate");//dialate the colocaliziation

//this runs the edm dilate function which better represents increasing radius
run("Options...", "iterations=1 count=1 black edm=8-bit do=Nothing");
run("Invert");
run("Distance Map");
setThreshold(0, 1);
setOption("BlackBackground", true);
run("Convert to Mask");

saveAs("Tiff", outputFolder+"ZsGreen_bin_align_D"+b);//save dialation
selectWindow("ZsGreen_bin_align_U"+b-1+".tif");
close();
imageCalculator("Multiply create", "ZsGreen_bin_align_D"+b+".tif","ZsGreen_bin_align_"+num_img+".tif");
//multiplies the dialited image back on top of the aligned zsgreen
saveAs("Tiff", outputFolder+"ZsGreen_bin_align_U"+b);// save initial colocalized pixels salm and zsg
run("Measure");
print(num_img,b,getResult("RawIntDen",0));
run("Clear Results");
selectWindow("ZsGreen_bin_align_D"+b+".tif");
close();
//open(outputFolder+"ZsGreen_bin_align_U"+b-1+".tif");

//selectWindow("ZsGreen_bin_align_U"+b+".tif");

}//end dialation loop
selectWindow("ZsGreen_bin_align_U"+b-1+".tif");
close();
selectWindow("ZsGreen_bin_align_"+num_img+".tif");
close();
//selectWindow("Salm_bin_"+num_img+".tif");
close();
run("Clear Results");
selectWindow("ROI Manager");
run("Close");
}//end size loop
//
}//end image loop
selectWindow("Log");
saveAs("Results",outputFolder+"Results2.csv");
}//end macro
```

BIBLIOGRAPHY

Agrawal V, Maharjan S, Kim K, Kim N-J, Son J, Lee K, Choi H-J, Rho S-S, Ahn S, Won M-H, Ha S-J, Koh GY, Kim Y-M, Suh Y-G, Kwon Y-G. 2014. Direct endothelial junction restoration results in significant tumor vascular normalization and metastasis inhibition in mice. *Oncotarget* 5:2761–77.

Alberts B, Johnson A, Lewis J, Raff M, Roberts K, Walter P. 2002a. Extracellular Control of Cell Division, Cell Growth, and Apoptosis. Garland Science.

Alberts B, Johnson A, Lewis J, Raff M, Roberts K, Walter P. 2002b. Molecular Biology of the Cell. Garland Science.

Altenberg B, Greulich KO. 2004. Genes of glycolysis are ubiquitously overexpressed in 24 cancer classes. *Genomics* 84:1014–20.

Apostolou P, Tsantsaridou A, Papasotiriou I, Toloudi M, Chatziioannou M, Giamouzis G. 2011. Bacterial and fungal microflora in surgically removed lung cancer samples. *J Cardiothorac Surg* 6:137.

Baban CK, Cronin M, O'Hanlon D, O'Sullivan GC, Tangney M. 2010. Bacteria as vectors for gene therapy of cancer. *Bioeng Bugs* 1:385–94.

Bakker-Woudenberg IA, de Bos P, van Leeuwen WB, Michel MF. 1981. Efficacy of ampicillin therapy in experimental listeriosis in mice with impaired T-cell-mediated immune response. *Antimicrob Agents Chemother* 19:76–81.

Barnakov AN, Barnakova LA, Hazelbauer GL. 1998. Comparison In Vitro of a High- and a Low-Abundance Chemoreceptor of Escherichia coli: Similar Kinase Activation but Different Methyl-Accepting Activities. *J Bacteriol* 180:6713–6718.

Barrett T, Kobayashi H, Brechbiel M, Choyke PL. 2006. Macromolecular MRI contrast agents for imaging tumor angiogenesis. *Eur J Radiol* 60:353–66.

Baumgartner JW, Kim C, Brissette RE, Inouye M, Park C, Hazelbauer GL. 1994. Transmembrane signalling by a hybrid protein: communication from the domain of chemoreceptor Trg that recognizes sugar-binding proteins to the kinase/phosphatase domain of osmosensor EnvZ. *J Bacteriol* 176:1157–63.

Behjatnia B, Sim J, Bassett LW, Moatamed N a, Apple SK. 2010. Does size matter? Comparison study between MRI, gross, and microscopic tumor sizes in breast cancer in lumpectomy specimens. *Int J Clin Exp Pathol* 3:303–9.

Belião S, Ferreira A, Vierasu I, Blocklet D, Goldman S, Metens T, Matos C. 2012. MR imaging versus PET/CT for evaluation of pancreatic lesions. *Eur J Radiol* 81:2527–32.

Bolhassani A, Zahedifard F. 2012. Therapeutic live vaccines as a potential anticancer strategy. *Int J Cancer* 131:1733–43.

Bos R, van Der Hoeven JJM, van Der Wall E, van Der Groep P, van Diest PJ, Comans EFI, Joshi U, Semenza GL, Hoekstra OS, Lammertsma AA, Molthoff CFM. 2002. Biologic correlates of (18)fluorodeoxyglucose uptake in human breast cancer measured by positron emission tomography. *J Clin Oncol* 20:379–87.

Brader P, Stritzker J, Riedl CC, Zanzonico P, Cai S, Burnazi EM, Ghani ER, Hricak H, Szalay A a, Fong Y, Blasberg R. 2008. *Escherichia coli* Nissle 1917 facilitates tumor detection by positron emission tomography and optical imaging. *Clin Cancer Res* 14:2295–302.

Brismar TB, Kartalis N, Kylander C, Albiin N. 2012. MRI of colorectal cancer liver metastases: comparison of orally administered manganese with intravenously administered gadobenate dimeglumine. *Eur Radiol* 22:633–41.

Brooks JD. 2012. Translational genomics: the challenge of developing cancer biomarkers. *Genome Res* 22:183–7.

Burt BM, Humm JL, Kooby DA, Squire OD, Mastorides S, Larson SM, Fong Y. 2001. Using positron emission tomography with [(18)F]FDG to predict tumor behavior in experimental colorectal cancer. *Neoplasia* 3:189–95.

C. Lee L-MZXLCK. 2000. Comparative Evaluation of the Acute Toxic Effects in Monkeys, Pigs and Mice of a Genetically Engineered Salmonella Strain (VNP20009) Being Developed as an Antitumor Agent. *Int J Toxicol* 19:19–25.

Carmeliet P, Jain RK. 2000. Angiogenesis in cancer and other diseases. *Nature* 407:249–57.

Chary SR, Jain RK. 1989. Direct measurement of interstitial convection and diffusion of albumin in normal and neoplastic tissues by fluorescence photobleaching. *Proc Natl Acad Sci U S A* 86:5385–9.

Chatterjee SK, Zetter BR. 2005. Cancer biomarkers: knowing the present and predicting the future. *Future Oncol* 1:37–50.

Chen J, Yang B, Cheng X, Qiao Y, Tang B, Chen G, Wei J, Liu X, Cheng W, Du P, Huang X, Jiang W, Hu Q, Hu Y, Li J, Hua Z-C. 2012. *Salmonella*-mediated tumor-targeting TRAIL gene therapy significantly suppresses melanoma growth in mouse model. *Cancer Sci* 103:325–33.

Cheng C-M, Lu Y-L, Chuang K-H, Hung W-C, Shiea J, Su Y-C, Kao C-H, Chen B-M, Roffler S, Cheng T-L. 2008. Tumor-targeting prodrug-activating bacteria for cancer therapy. *Cancer Gene Ther* 15:393–401.

Choi J, Shin D, Ryu S. 2007. Implication of quorum sensing in *Salmonella enterica serovar typhimurium* virulence: the luxS gene is necessary for expression of genes in pathogenicity island 1. *Infect Immun* 75:4885–90.

Clairmont C, Lee KC, Pike J, Ittensohn M, Low KB, Pawelek J, Bermudes D, Brecher SM, Margitich D, Turnier J, Li Z, Luo X, King I, Zheng LM. 2000. Biodistribution and genetic stability of the novel antitumor agent VNP20009, a genetically modified strain of *Salmonella typhimurium*. *J Infect Dis* 181:1996–2002.

Contag CH, Contag PR, Mullins JI, Spilman SD, Stevenson DK, Benaron DA. 1995. Photonic detection of bacterial pathogens in living hosts. *Mol Microbiol* 18:593–603.

Cook GJ, Houston S, Rubens R, Maisey MN, Fogelman I. 1998. Detection of bone metastases in breast cancer by 18FDG PET: differing metabolic activity in osteoblastic and osteolytic lesions. *J Clin Oncol* 16 :3375–3379.

Corpet DE, Lumeau S, Corpet F. 1989. Minimum antibiotic levels for selecting a resistance plasmid in a gnotobiotic animal model. *Antimicrob Agents Chemother* 33:535–40.

Cronin M, Akin AR, Collins S a, Meganck J, Kim J-B, Baban CK, Joyce S a, van Dam GM, Zhang N, van Sinderen D, O'Sullivan GC, Kasahara N, Gahan CG, Francis KP, Tangney M. 2012. High resolution in vivo bioluminescent imaging for the study of bacterial tumour targeting. *PLoS One* 7:e30940.

Czernin J, Phelps ME. 2002. Positron emission tomography scanning: current and future applications. *Annu Rev Med* 53:89–112.

Dai Y, Toley BJ, Swofford CA, Forbes NS. 2013. Construction of an inducible cell-communication system that amplifies Salmonella gene expression in tumor tissue. *Biotechnol Bioeng* 110:1769–81.

Dang LH, Bettegowda C, Huso DL, Kinzler KW, Vogelstein B. 2001. Combination bacteriolytic therapy for the treatment of experimental tumors. *Proc Natl Acad Sci U S A* 98:15155–60.

Davis MDP, Plager DA, George TJ, Weiss EA, Gleich GJ, Leiferman KM. 2003. Interactions of eosinophil granule proteins with skin: limits of detection, persistence, and vasopermeabilization. *J Allergy Clin Immunol* 112:988–94.

DeFranco AL, Parkinson JS, Koshland DE. 1979. Functional homology of chemotaxis genes in Escherichia coli and Salmonella typhimurium. *J Bacteriol* 139:107–14.

Dennis MS, Zhang M, Meng YG, Kadkhodayan M, Kirchhofer D, Combs D, Damico L a. 2002. Albumin binding as a general strategy for improving the pharmacokinetics of proteins. *J Biol Chem* 277:35035–43.

Dinges MM, Orwin PM, Schlievert PM. 2000. Exotoxins of Staphylococcus aureus Exotoxins of Staphylococcus aureus 13.

Dittmer ULF, Race B, Hasenkrug KIMJ. 1999. Kinetics of the Development of Protective Immunity in Mice Vaccinated with a Live Attenuated Retrovirus. *J Viorl* 73:8435–8440.

Egesten A, Frick I-M, Mörgelin M, Olin AI, Björck L. 2011. Binding of albumin promotes bacterial survival at the epithelial surface. *J Biol Chem* 286:2469–76.

Elmore S. 2007. Apoptosis: a review of programmed cell death. *Toxicol Pathol* 35:495–516.

Ernst MF, Roukema J a. 2002. Diagnosis of non-palpable breast cancer: a review. *Breast* 11:13–22.

Filloux A. 2004. The underlying mechanisms of type II protein secretion. *Biochim Biophys Acta* 1694:163–79.

Fogelman I, Cook G, Israel O, Van der Wall H. 2005. Positron emission tomography and bone metastases. *Semin Nucl Med* 35:135–42.

Folkman J, Watson K, Ingber D, Hanahan D. 1989. Induction of angiogenesis during the transition from hyperplasia to neoplasia. *Nature* 339:58–61.

Forbes NS. 2010. Engineering the perfect (bacterial) cancer therapy. *Nat Rev Cancer* 10:785–794.

Forbes NS, Munn LL, Fukumura D, Jain RK. 2003. Sparse Initial Entrapment of Systemically Injected Salmonella typhimurium Leads to Heterogeneous Accumulation within Tumors. *Cancer Res* 63:5188–5193.

Francetic O, Belin D, Badaut C, Pugsley a P. 2000. Expression of the endogenous type II secretion pathway in *Escherichia coli* leads to chitinase secretion. *EMBO J* 19:6697–703.

Franci C, Zhou J, Jiang Z, Modrusan Z, Good Z, Jackson E, Kouros-Mehr H. 2013. Biomarkers of Residual Disease, Disseminated Tumor Cells, and Metastases in the MMTV-PyMT Breast Cancer Model. *PLoS One* 8:e58183.

Friebel M, Do K, Hahn A, Mu G, Berlin D-, Medizin- L-, Universita F. 1999. Optical properties of circulating human blood in the wavelength range 400-2500 nm. *J Biomedial Opt* 4:36–46.

Fukumura D, Jain RK. 2008. Imaging angiogenesis and the microenvironment. *APMIS* 116:695–715.

Galán JE, Nakayama K, Curtiss R. 1990. Cloning and characterization of the asd gene of Salmonella typhimurium: use in stable maintenance of recombinant plasmids in Salmonella vaccine strains. *Gene* 94:29–35.

Ganai S, Arenas RB, Forbes NS. 2009. Tumour-targeted delivery of TRAIL using *Salmonella typhimurium* enhances breast cancer survival in mice. *Br J Cancer* 101:1683–91.

Ganai S, Arenas RB, Sauer JP, Bentley B, Forbes NS. 2011. In tumors *Salmonella* migrate away from vasculature toward the transition zone and induce apoptosis. *Cancer Gene Ther* 18:457–66.

Gillet J-P, Gottesman MM. 2010. Mechanisms of multidrug resistance in cancer. *Methods Mol Biol* 596:47–76.

Gillies RJ, Schornack PA, Secomb TW, Raghunand N. 1999. Causes and effects of heterogeneous perfusion in tumors. *Neoplasia* 1:197–207.

Gillies RJ, Robey I, Gatenby RA. 2008. Causes and consequences of increased glucose metabolism of cancers. *J Nucl Med* 49 Suppl 2:24S–42S.

Goldsmith SJ. 2004. PET-CT Fusion Imaging in Differenti- ating Physiologic from Pathologic FDG Uptake 1 OBJECTIVES:1411–1431.

Green LK, Syddall SP, Carlin KM, Bell GD, Guise CP, Mowday AM, Hay MP, Smaill JB, Patterson A V, Ackerley DF. 2013. Pseudomonas aeruginosa NfsB and nitro-CBI-DEI--a promising enzyme/prodrug combination for gene directed enzyme prodrug therapy. *Mol Cancer* 12:58.

Griffeth LK. 2005. Use of PET/CT scanning in cancer patients: technical and practical considerations. *Proc (Bayl Univ Med Cent)* 18:321–30.

Hanahan D, Weinberg RA. 2000. The Hallmarks of Cancer. *Cell* 100:57–70.

Hanahan D, Weinberg R a. 2011. Hallmarks of cancer: the next generation. *Cell* 144:646–74.

Hasegawa M, Sone S, Takashima S, Li F, Yang ZG, Maruyama Y, Watanabe T. 2000. Growth rate of small lung cancers detected on mass CT screening. *Br J Radiol* 73:1252–9.

Hassan M, Azzazy E, Christenson RH. 1997. All About Albumin: Biochemistry, Genetics, and Medical Applications. Theodore Peters, Jr. San Diego, CA: Academic Press, 1996, 432 pp, $85.00. ISBN 0-12-552110-3. *Clin Chem* 43:2014a–2015.

Hill PJ, Stritzker J, Scadeng M, Geissinger U, Haddad D, Basse-Lüsebrink TC, Gbureck U, Jakob P, Szalay A a. 2011. Magnetic resonance imaging of tumors colonized with bacterial ferritin-expressing *Escherichia coli*. *PLoS One* 6:e25409.

Hirayama A, Kami K, Sugimoto M, Sugawara M, Toki N, Onozuka H, Kinoshita T, Saito N, Ochiai A, Tomita M, Esumi H, Soga T. 2009. Quantitative metabolome profiling of colon and stomach cancer microenvironment by capillary electrophoresis time-of-flight mass spectrometry. *Cancer Res* 69:4918–25.

Hirschhaeuser F, Sattler UGA, Mueller-Klieser W. 2011. Lactate: a metabolic key player in cancer. *Cancer Res* 71:6921–5.

Hoption Cann SA, van Netten JP, van Netten C. 2003. Dr William Coley and tumour regression: a place in history or in the future. *Postgrad Med J* 79:672–680.

Horwitz SB. 1994. Taxol (paclitaxel): mechanisms of action. *Ann Oncol* 5 Suppl 6:S3–6.

Huang Y-J, Lundy PM, Lazaris A, Huang Y, Baldassarre H, Wang B, Turcotte C, Côté M, Bellemare A, Bilodeau AS, Brouillard S, Touati M, Herskovits P, Bégin I, Neveu N, Brochu E, Pierson J, Hockley DK, Cerasoli DM, Lenz DE, Wilgus H, Karatzas CN, Langermann S. 2008. Substantially improved pharmacokinetics of recombinant human butyrylcholinesterase by fusion to human serum albumin. *BMC Biotechnol* 8:50.

Jain RK. 1994. Barriers to drug delivery in solid tumors. *Sci Am* 271:58–65.

Jain RK. 1999. Transport of molecules, particles, and cells in solid tumors. *Annu Rev Biomed Eng* 1:241–63.

Jain RK. 2001. Delivery of molecular and cellular medicine to solid tumors. *Adv Drug Deliv Rev* 46:149–68.

Kanehisa M. 2000. KEGG: Kyoto Encyclopedia of Genes and Genomes. *Nucleic Acids Res* 28:27–30.

Kasinskas RW, Forbes NS. 2006. *Salmonella typhimurium* specifically chemotax and proliferate in heterogeneous tumor tissue *in vitro*. *Cell.*

Kasinskas RW, Forbes NS. 2007. *Salmonella typhimurium* lacking ribose chemoreceptors localize in tumor quiescence and induce apoptosis. *Cancer Res* 67:3201–9.

Kasinskas RW, Venkatasubramanian R, Forbes NS. 2014. Rapid uptake of glucose and lactate, and not hypoxia, induces apoptosis in three-dimensional tumor tissue culture. *Integr Biol (Camb)* 6:399–410.

Kerr JR. 2000. Gram-negative Bacterial Protein Secretion. *J Infect:*121–126.

Koscielny S, Tubiana M, Lê MG, Valleron AJ, Mouriesse H, Contesso G, Sarrazin D. 1984. Breast cancer: relationship between the size of the primary tumour and the probability of metastatic dissemination. *Br J Cancer* 49:709–15.

Kroemer G, Galluzzi L, Vandenabeele P, Abrams J, Alnemri ES, Baehrecke EH, Blagosklonny M V, El-Deiry WS, Golstein P, Green DR, Hengartner M, Knight RA, Kumar S, Lipton SA, Malorni W, Nuñez G, Peter ME, Tschopp J, Yuan J, Piacentini M, Zhivotovsky B, Melino G. 2009. Classification of cell death: recommendations of the Nomenclature Committee on Cell Death 2009. *Cell Death Differ* 16:3–11.

Kulemann B, Pitman MB, Liss AS, Valsangkar N, Fernández-Del Castillo C, Lillemoe KD, Hoeppner J, Mino-Kenudson M, Warshaw AL, Thayer SP. 2015. Circulating Tumor Cells Found in Patients With Localized and Advanced Pancreatic Cancer. *Pancreas.*

Lehouritis P, Springer C, Tangney M. 2013. Bacterial-directed enzyme prodrug therapy. *J Control Release* 170:120–31.

Lemmon MJ, van Zijl P, Fox ME, Mauchline ML, Giaccia a J, Minton NP, Brown JM. 1997. Anaerobic bacteria as a gene delivery system that is controlled by the tumor microenvironment. *Gene Ther* 4:791–6.

Li J, Attila C, Wang L, Wood TK, Valdes JJ, Bentley WE. 2007. Quorum sensing in *Escherichia coli* is signaled by AI-2/LsrR: effects on small RNA and biofilm architecture. *J Bacteriol* 189:6011–20.

Lim HS, Yoon W, Chung TW, Kim K, Park JG, Kang HK, Bom S, Yoon JH. 2007. FDG PET / CT for the Detection and Evalua- tion of Breast Diseases : Usefulness and Limita- OBJECTIVES:197–214.

Lin-Chao S, Chen WT, Wong TT. 1992. High copy number of the pUC plasmid results from a Rom/Rop-suppressible point mutation in RNA II. *Mol Microbiol* 6:3385–93.

Low KB, Ittensohn M, Le T, Platt J, Sodi S, Amoss M, Ash O, Carmichael E, Chakraborty A, Fischer J, Lin SL, Luo X, Miller SI, Zheng L, King I, Pawelek JM, Bermudes D. 1999. Lipid A mutant *Salmonella* with suppressed virulence and TNFalpha induction retain tumor-targeting *in vivo*. *Nat Biotechnol* 17:37–41.

Ludwig J a, Weinstein JN. 2005. Biomarkers in cancer staging, prognosis and treatment selection. *Nat Rev Cancer* 5:845–56.

Luo X, Li Z, Lin S, Le T, Ittensohn M, Bermudes D, Runyab JD, Shen SY, Chen J, King IC, Zheng LM. 2001. Antitumor effect of VNP20009, an attenuated *Salmonella*, in murine tumor models. *Oncol Res* 12:501–8.

Lupski JR, Projan SJ, Ozaki LS, Godson GN. 1986. A temperature-dependent pBR322 copy number mutant resulting from a Tn5 position effect. *Proc Natl Acad Sci U S A* 83:7381–5.

Lutz AM, Willmann JK, Cochran F V, Ray P, Gambhir SS. 2008. Cancer screening: a mathematical model relating secreted blood biomarker levels to tumor sizes. *PLoS Med* 5:e170.

Milosevic M, Warde P, Ménard C, Chung P, Toi A, Ishkanian A, McLean M, Pintilie M, Sykes J, Gospodarowicz M, Catton C, Hill RP, Bristow R. 2012. Tumor hypoxia predicts biochemical failure following radiotherapy for clinically localized prostate cancer. *Clin Cancer Res* 18:2108–14.

Min J-J, Kim H-J, Park JH, Moon S, Jeong JH, Hong Y-J, Cho K-O, Nam JH, Kim N, Park Y-K, Bom H-S, Rhee JH, Choy HE. 2008a. Noninvasive real-time imaging of tumors and metastases using tumor-targeting light-emitting *Escherichia coli*. *Mol Imaging Biol* 10:54–61.

Min J-J, Nguyen VH, Kim H-J, Hong Y, Choy HE. 2008b. Quantitative bioluminescence imaging of tumor-targeting bacteria in living animals. *Nat Protoc* 3:629–36.

Minchinton AI, Tannock IF. 2006. Drug penetration in solid tumours. *Nat Rev Cancer* 6:583–92.

Mizejewski GJ. 2002. Biological role of alpha-fetoprotein in cancer: prospects for anticancer therapy. *Expert Rev Anticancer Ther* 2:709–35.

Mizuno T, Chou MY, Inouye M. 1983. A comparative study on the genes for three porins of the Escherichia coli outer membrane. DNA sequence of the osmoregulated ompC gene. *J Biol Chem* 258:6932–40.

Mok TSK, Wu Y-L, Soo Lee J, Yu C-J, Sriuranpong V, Sandoval-Tan J, Ladrera G, Thongprasert S, Srimuninnimit V, Liao M, Zhu Y, Zhou C, Fuerte F, Margono B, Wen W, Tsai J, Truman M, Klughammer B, Shames DS, Wu L. 2015. Detection and Dynamic Changes of EGFR Mutations from Circulating Tumor DNA as a Predictor of Survival Outcomes in NSCLC Patients Treated with First-line Intercalated Erlotinib and Chemotherapy. *Clin Cancer Res.*

Narang P, Bhushan K, Bose S, Jayaram B. 2005. A computational pathway for bracketing native-like structures fo small alpha helical globular proteins. *Phys Chem Chem Phys* 7:2364–75.

Natale P, Brüser T, Driessen AJM. 2008. Sec- and Tat-mediated protein secretion across the bacterial cytoplasmic membrane--distinct translocases and mechanisms. *Biochim Biophys Acta* 1778:1735–56.

Nemunaitis J, Cunningham C, Senzer N, Kuhn J, Cramm J, Litz C, Cavagnolo R, Cahill A, Clairmont C, Sznol M. 2003. Pilot trial of genetically modified, attenuated *Salmonella* expressing the *E. coli* cytosine deaminase gene in refractory cancer patients. *Cancer Gene Ther* 10:737–44.

Nguyen DX, Massagué J. 2007. Genetic determinants of cancer metastasis. *Nat Rev Genet* 8:341–352.

Orr GA, Verdier-Pinard P, McDaid H, Horwitz SB. 2003. Mechanisms of Taxol resistance related to microtubules. *Oncogene* 22:7280–95.

Panteli JT, Forkus BA, Van Dessel N, Forbes NS. 2015. Genetically modified bacteria as a tool to detect microscopic solid tumor masses with triggered release of a recombinant biomarker. *Integr Biol (Camb).*

Park C, Hazelbauer GL. 1986. Mutations specifically affecting ligand interaction of the Trg chemosensory transducer. *J Bacteriol* 167:101–9.

Pawelek JM, Low KB, Bermudes D. 1997. Tumor-targeted *Salmonella* as a Novel Anticancer Vector:4537–4544.

Pawelek JM, Low KB, Bermudes D. 2003. Bacteria as tumour-targeting vectors. *Lancet* 4:548–556.

Platt J, Sodi S, Kelley M, Rockwell S, Bermudes D, Low KB, Pawelek J. 2000. Antitumour effects of genetically engineered *Salmonella* in combination with radiation. *Statistics (Ber)* 36:2397–2402.

Pluen A, Boucher Y, Ramanujan S, McKee TD, Gohongi T, di Tomaso E, Brown EB, Izumi Y, Campbell RB, Berk DA, Jain RK. 2001. Role of tumor-host interactions in interstitial diffusion of macromolecules: cranial vs. subcutaneous tumors. *Proc Natl Acad Sci U S A* 98:4628–33.

Rak J, Yu JL, Klement G, Kerbel RS. 2000. Oncogenes and Angiogenesis: Signaling Three-Dimensional Tumor Growth. *J Investig Dermatology Symp Proc* 5:24–33.

Rakheja R, DeMello L, Chandarana H, Glielmi C, Geppert C, Faul D, Friedman KP. 2013. Comparison of the accuracy of PET/CT and PET/MRI spatial registration of multiple metastatic lesions. *AJR Am J Roentgenol* 201:1120–3.

Rusling JF, Kumar C V, Gutkind JS, Patel V. 2010. Measurement of biomarker proteins for point-of-care early detection and monitoring of cancer. *Analyst* 135:2496–511.

Schima W. 2005. Liver metastases of colorectal cancer: US, CT or MR? *Cancer Imaging* 5:S149–S156.

Schindelin J, Arganda-Carreras I, Frise E, Kaynig V, Longair M, Pietzsch T, Preibisch S, Rueden C, Saalfeld S, Schmid B, Tinevez J-Y, White DJ, Hartenstein V, Eliceiri K, Tomancak P, Cardona A. 2012. Fiji: an open-source platform for biological-image analysis. *Nat Methods* 9:676–82.

Schöder H, Gönen M. 2007. Screening for cancer with PET and PET/CT: potential and limitations. *J Nucl Med* 48 Suppl 1:4S–18S.

Scholle A, Vreemann J, Blank V, Nold A, Boos W, Manson MD. 1987. Sequence of the mglB gene from Escherichia coli K12: comparison of wild-type and mutant galactose chemoreceptors. *Mol Gen Genet* 208:247–53.

Sperandio V, Mellies JL, Nguyen W, Shin S, Kaper JB. 1999. Quorum sensing controls expression of the type III secretion gene transcription and protein secretion in enterohemorrhagic and enteropathogenic *Escherichia coli*. *Proc Natl Acad Sci U S A* 96:15196–201.

St Jean AT, Swofford CA, Panteli JT, Brentzel ZJ, Forbes NS. 2014. Bacterial Delivery of Staphylococcus aureus alpha-Hemolysin Causes Tumor Regression and Necrosis in Murine Tumors. *Mol Ther* 22(7):1266–74.

Stritzker J, Weibel S, Hill PJ, Oelschlaeger TA, Goebel W, Szalay AA. 2007. Tumor-specific colonization, tissue distribution, and gene induction by probiotic Escherichia coli Nissle 1917 in live mice. *Int J Med Microbiol* 297:151–62.

Surette MG, Bassler BL. 1998. Quorum sensing in *Escherichia coli* and *Salmonella typhimurium*. *Proc Natl Acad Sci U S A* 95:7046–50.

Surette MG, Miller MB, Bassler BL. 1999. Quorum sensing in *Escherichia coli*, *Salmonella typhimurium*, and *Vibrio harveyi*: a new family of genes responsible for autoinducer production. *Proc Natl Acad Sci U S A* 96:1639–44.

Sutcliffe JG. 1979. Complete nucleotide sequence of the Escherichia coli plasmid pBR322. *Cold Spring Harb Symp Quant Biol* 43 Pt 1:77–90.

Sutherland RM, Durand RE. 1984. Growth and cellular characteristics of multicell spheroids. *Recent Results Cancer Res* 95:24–49.

Swofford C a, St Jean AT, Panteli JT, Brentzel ZJ, Forbes NS. 2014. Identification of *Staphylococcus aureus* α-hemolysin as a protein drug that is secreted by anticancer bacteria and rapidly kills cancer cells. *Biotechnol Bioeng:*1–32.

Takalkar A, El-Haddad G, Lilien D. 2008. FDG-PET and PET/CT - Part II. *Indian J Radiol Imaging* 18:17.

Thamm DH, Kurzman ID, King I, Li Z, Sznol M, Dubielzig RR, Vail DM, MacEwen EG. 2005. Systemic administration of an attenuated, tumor-targeting *Salmonella typhimurium* to dogs with spontaneous neoplasia: phase I evaluation. *Clin Cancer Res* 11:4827–34.

Thanassi DG, Hultgren SJ. 2000. Multiple pathways allow protein secretion across the bacterial outer membrane. *Curr Opin Cell Biol* 12:420–30.

Thompson IM, Ankerst DP, Chi C, Lucia MS, Goodman PJ, Crowley JJ, Parnes HL, Coltman CA. 2005. Operating characteristics of prostate-specific antigen in men with an initial PSA level of 3.0 ng/ml or lower. *JAMA* 294:66–70.

Thompson JR, Cronin B, Bayley H, Wallace MI. 2011. Rapid assembly of a multimeric membrane protein pore. *Biophys J* 101:2679–83.

Toley BJ, Forbes NS. 2012. Motility is critical for effective distribution and accumulation of bacteria in tumor tissue. *Integr Biol (Camb)* 4:165–76.

Toso BJF, Gill VJ, Hwu P, Marincola FM, Restifo NP, Schwartzentruber DJ, Sherry RM, Topalian SL, Yang JC, Stock F, Freezer LJ, Morton KE, Seipp C, Haworth L, Mavroukakis S, White D, Macdonald S, Mao J, Sznol M, Rosenberg SA. 2002. Phase I Study of the Intravenous Administration of Attenuated *Salmonella typhimurium* to Patients With Metastatic Melanoma 20:142–152.

Trédan O, Galmarini CM, Patel K, Tannock IF. 2007. Drug Resistance and the Solid Tumor Microenvironment. *October:*1441–1454.

Tseng T-T, Tyler BM, Setubal JC. 2009. Protein secretion systems in bacterial-host associations, and their description in the Gene Ontology. *BMC Microbiol* 9 Suppl 1:S2.

Vansteenkiste J, Dooms C, Mascaux C, Nackaerts K. 2012. Screening and early--detection of lung cancer. *Ann Oncol* 23 Suppl 1:x320–x327.

Veronesi G, Bellomi M, Veronesi U, Paganelli G, Maisonneuve P, Scanagatta P, Leo F, Pelosi G, Travaini L, Rampinelli C, Trifirò G, Sonzogni A, Spaggiari L. 2007. Role of positron emission tomography scanning in the management of lung nodules detected at baseline computed tomography screening. *Ann Thorac Surg* 84:959–65; discussion 965–6.

Walsh CL, Babin BM, Kasinskas RW, Foster J a, McGarry MJ, Forbes NS. 2009. A multipurpose microfluidic device designed to mimic microenvironment gradients and develop targeted cancer therapeutics. *Lab Chip* 9:545–54.

Waukau J, Forst S. 1992. Molecular analysis of the signaling pathway between EnvZ and OmpR in Escherichia coli. *J Bacteriol* 174:1522–7.

Weibel S, Stritzker J, Eck M, Goebel W, Szalay A a. 2008. Colonization of experimental murine breast tumours by Escherichia coli K-12 significantly alters the tumour microenvironment. *Cell Microbiol* 10:1235–48.

Wellen KE, Lu C, Mancuso A, Lemons JMS, Ryczko M, Dennis JW, Rabinowitz JD, Coller HA, Thompson CB. 2010. The hexosamine biosynthetic pathway couples growth factor-induced glutamine uptake to glucose metabolism. *Genes Dev* 24:2784–99.

Wybranietz WA, Gross CD, Phelan A, O'Hare P, Spiegel M, Graepler F, Bitzer M, Stähler P, Gregor M, Lauer UM. 2001. Enhanced suicide gene effect by adenoviral transduction of a VP22-cytosine deaminase (CD) fusion gene. *Gene Ther* 8:1654–64.

Xu MJ, Cooke M, Steinmetz D, Karakousis G, Saxena D, Bartlett E, Xu X, Hahn SM, Dorsey JF, Kao GD. 2015. A novel approach for the detection and genetic analysis of live melanoma circulating tumor cells. *PLoS One* 10:e0123376.

Xue H, Lu B, Zhang J, Wu M, Huang Q, Wu Q, Sheng H, Wu D, Hu J, Lai M. 2010. Identification of Serum Biomarkers for Colorectal Cancer Metastasis Using a Differential Secretome Approach research articles:545–555.

Yasuda S, Kubota M, Tajima T, Umemura S, Fujii H, Takahashi W, Ide M, Shohtsu A. 1999. A Small Breast Cancer Detected by PET. *Jpn J Clin Oncol* 29:387–389.

Yu YA, Shabahang S, Timiryasova TM, Zhang Q, Beltz R, Gentschev I, Goebel W, Szalay AA. 2004. Visualization of tumors and metastases in live animals with bacteria and vaccinia virus encoding light-emitting proteins. *Nat Biotechnol* 22:313–321.

Zhang M, Swofford CA, Forbes NS. 2014. Lipid A controls the robustness of intratumoral accumulation of attenuated *Salmonella* in mice. *Int J Cancer* 135:647–57.

Zhang T, He Y, Wei J, Que L. 2012. Nanostructured optical microchips for cancer biomarker detection. *Biosens Bioelectron* 38:382–8.

Zheng LM, Luo X, Feng M, Li Z, Le T, Ittensohn M, Trailsmith M, Bermudes D, Lin SL, King IC. 2000. Tumor amplified protein expression therapy: *Salmonella* as a tumor-selective protein delivery vector. *Oncol Res* 12:127–35.

Zwietering MH, Jongenburger I, Rombouts FM, van 't Riet K. 1990. Modeling of the bacterial growth curve. *Appl Environ Microbiol* 56:1875–81.